

LA-UR-20-25982

Approved for public release; distribution is unlimited.

Title: MCNP6 High-energy Event Generators

Author(s): Mashnik, Stepan G.

Intended for: Report

Issued: 2020-08-05

Disclaimer:

Los Alamos National Laboratory, an affirmative action/equal opportunity employer, is operated by Triad National Security, LLC for the National Nuclear Security Administration of U.S. Department of Energy under contract 89233218CNA000001. By approving this article, the publisher recognizes that the U.S. Government retains nonexclusive, royalty-free license to publish or reproduce the published form of this contribution, or to allow others to do so, for U.S. Government purposes. Los Alamos National Laboratory requests that the publisher identify this article as work performed under the auspices of the U.S. Department of Energy. Los Alamos National Laboratory strongly supports academic freedom and a researcher's right to publish; as an institution, however, the Laboratory does not endorse the viewpoint of a publication or guarantee its technical correctness.

MCNP6 High-energy Event Generators

Stepan G. Mashnik

Monte Carlo Methods, Codes, and Applications Group (XCP-3)

Los Alamos National Laboratory

Los Alamos, NM 87545, USA

May 2016

Abstract

This report presents a brief description of all high-energy event generators used by MCNP6, namely, of the intranuclear cascade models (INC); Fermi breakup models; coalescence models; preequilibrium nuclear reactions; evaporation reactions; and of the fission reaction models.

Foreword

This document represents the best available and reproducible copy of work that Stepan G. Mashnik documented in the May 2016 timeframe. It is posthumously archived to ensure that the knowledge captured within is not lost for the benefit of all future readers.

To create this document from Stepan's files, figures are converted from PostScript (.ps) to Adobe PDF format, layout customization to control DVI output is removed, and hyperlinks are added (to improve navigability). As a result of making these changes, no technical differences are introduced and this document compiles using the `pdflatex` command distributed with TeXLive 2019.

Comments, questions, or concerns about this work can be directed to the MCNP development team at mcnp_help@lanl.gov.

Joel A. Kulesza
Monte Carlo Codes Group (XCP-3)
Los Alamos National Laboratory
May 2020

Contents

1	Event Generators Overview	3
2	The Intra-Nuclear Cascade (INC) Models	3
2.1	The INC of CEM03.03	6
2.2	The INC of LAQGSM	13
2.3	The INC of the Bertini Model	15
2.4	The INC of ISABEL	22
2.5	The INC of INCL4.2	26
3	Preequilibrium Reactions	31
3.1	Preequilibrium Reactions in CEM03.03 and LAQGSM03.03	32
3.2	Preequilibrium Reactions Simulated with the Bertini INC and ISABEL	37
4	Evaporation Reactions	41
4.1	Evaporation Reactions in CEM03.03 and LAQGSM03.03	41
4.2	Evaporation Reactions with the Bertini INC and ISABEL	48
4.3	Evaporation Reactions Simulated with INCL4.2	49
4.4	Emission of Low-Energy Photons with the PHT Model	51
5	Fission Reactions	53
5.1	Fission Reactions in CEM03.03 and LAQGSM03.03	54
5.1.1	Fission Probability	54
5.1.2	Mass Distribution	55
5.1.3	Charge Distribution	57
5.1.4	Kinetic Energy Distribution	58
5.1.5	Modifications to GEM2 in CEM03.03 and LAQGSM03.03	58
5.2	Fission Reactions Simulated with the Bertini INC and ISABEL	60
5.2.1	The RAL Fission Model	60
5.2.2	The ORNL Fission Model	61
5.3	Fission Reactions Simulated with INCL4.2	62
6	Fermi Break-up Reactions	66
6.1	Fermi Breakup Reactions in CEM03.03 and LAQGSM03.03	66
6.2	Fermi Breakup Reactions Simulated with the Bertini INC, ISABEL, or INCL4.2	69
7	Coalescence Reactions	70

1 Event Generators Overview

MCNP6 uses by default the latest version of the cascade-exciton model (CEM) [1, 2, 3] as incorporated in its event generator CEM03.03 [1] to simulate reactions induced by nucleons, pions, and photons at energies up to 4.5 GeV and the Los Alamos version of the quark-gluon string model (LAQGSM) [3, 4, 5] as implemented in the code LAQGSM03.03 [5] to simulate such reactions at higher energies, as well as reactions induced by other elementary particles and nuclei with energies up to ~ 1 TeV/nucleon. MCNP6 also can use the intra-nuclear cascade (INC) developed at Liege (INCL), version 4.2 [6], merged with the evaporation/fission models ABLA [7] to describe reactions induced by nucleons, pions, and d, t, ^3He , and ^4He at energies up to ~ 1 GeV. MCNP6 uses also by default the Bertini INC [8] to simulate reactions on light nuclei with $A < 12$ and reactions induced by elementary particles at energies below ~ 4.5 GeV (at higher energies, it uses LAQGSM03.03), as well as the INC from ISABEL [9] to simulate by default reactions induced by antinucleons and d, t, ^3He , and ^4He at energies below ~ 940 MeV (at higher energies, it uses LAQGSM03.03).

After the INC stage of reactions, CEM and LAQGSM simulate the second stage of reactions with their own exciton model of pre-equilibrium reactions, namely using the latest version of the Modified Exciton Model (MEM) [10, 11]. as implemented in CEM03.03 [1]. Bertini INC and ISABEL simulate this second stage of reactions with the Multistage Preequilibrium Model (MPM) version of the exciton model [12], or, may neglect of this stage of reactions, if required so in the MCNP6 input file. INCL does not use any preequilibrium models.

CEM and LAQGSM have their own evaporation and fission models, while Bertini INC and ISABEL use the EVAP [13]–[17] evaporation model as it was implemented in LAHET [18], merged with the ORNL [19] and the RAL [20] fission models.

If the mass number, A , of the residual nucleus after the INC (or after any other stages of reactions, in the case of CEM and LAQGSM) is $A \leq 12$, then all event generators use the Fermi break-up model [21] (slightly different in different event generators) to simulate the remaining of nuclear reaction instead of using the preequilibrium and evaporation models.

CEM and LAQGSM event generators use also the coalescence model [22] to simulate production of energetic d, t, ^3He , and ^4He from coalescence of INC-emitted nucleons.

The following sections present briefly all these nuclear reaction models.

2 The Intra-Nuclear Cascade (INC) Models

The inelastic interaction of a high-energy particle with a nucleus, and even more the collisions of two nuclei, is a very complex and multi-faceted phenomenon whose analytical description encounters considerable difficulties [23, 24].

The INC approach was apparently first developed by Goldberger [25], who in turn based his work on the ideas of Serber [26], who regarded intranuclear cascades as a series of successive quasi-free collisions of the fast primary particle with the individual nucleons of the nucleus.

Let us recall here the main basic assumptions of the INC, following [23, 24]. The main condition for the applicability of the intranuclear-cascade model is that the DeBroglie wave-

length λ of the particles participating in the interaction be sufficiently small: It is necessary that for most of these particles λ be less than the average distance between the intranuclear nucleons $\Delta \sim 10^{-13}$ cm. Only in this case does the particle acquire quasi-classical features and can we speak approximately of particle trajectory and two-particle collisions inside the nucleus. It is clear that for this to be the case the primary particle kinetic energy T must be greater than several tens of MeV.

Another important condition for applicability of the INC is the requirement that the time in which an individual two-particle intranuclear collision occurs on the average, $\tau \sim 10^{-23}$ sec, be less than the time interval between two such consecutive interactions

$$\Delta t = l/c \gtrsim 4\pi R^3/3A\sigma c \gtrsim 3 \cdot 10^{-22}/\sigma \text{ (mb) sec,}$$

where l is the mean range of the cascade particle before the interaction, c is the velocity of light, $R = r_0 A^{1/3}$ is the mean radius of the nucleus, and σ is the cross section for interaction with an intranuclear nucleon. This permits the interaction of the incident particle with the nucleus to be reduced to a set of individual statistically independent intranuclear collisions.

The requirement $\tau < \Delta t$ is equivalent to the requirement that the intranuclear interaction cross section be sufficient small: $\sigma \lesssim 100\xi$ mb, where the coefficient $\xi \sim 1$.

Since the energy of the particles participating in the cascade is rather large, as a rule significantly greater than the binding energy of the intranuclear nucleons, the same characteristics can be used for interaction of cascade particles inside the nucleus as for the interaction of free particles. The effect of other intranuclear nucleons is taken into account by introduction of some average potential V , and also by the action of the Pauli principle.¹

We can say that a high-energy particle which has entered the nucleus passes through a gas of free nucleons, producing a cascade (avalanche) of secondary particles. A fraction of these secondary particles leaves the nucleus, and the remaining fraction is absorbed, exciting the nucleus to some energy E^* .

Following [23, 24], after the choice of a nuclear model and an algorithm for determination of the elementary particles involved in the INC with the intranuclear nucleons (for this purpose it is necessary to store in the computer memory the values of the integrated cross sections for elastic and inelastic interactions $\sigma_{el}(T)$ and $\sigma_{in}(T)$), calculation of the intranuclear cascade can be carried out according to the scheme shown in Fig. 1. The turquoise boxes 1, 2, 4, 5, 8–10, 12, and 14 in the diagram denote operations which are definite logically closed parts of the INC code. The yellow boxes 3, 6, 7, 11, and 13 denote logical operations which control the various branchings of the code (transfer conditions).

Box 1 takes into account the change in primary-particle momentum due to the effect of the intranuclear potential and to refraction and reflection of the DeBroglie wave of the particle at the nuclear boundary.

In box 2 is chosen the momentum and isospin (proton or neutron) of the intranuclear nucleon with which the interaction occurs (for brevity we will call this nucleon the “partner”), and from the given elementary cross section $\sigma_{tot}(t) = \sigma_{el}(t) + \sigma_{in}(t)$ (where t is the relative

¹The nucleus is considered to be a degenerate Fermi gas of nucleons enclosed in the nuclear volume. According to the Pauli principle the nucleons, after an intranuclear collision, must have energy above the Fermi energy; otherwise such an interaction is forbidden. The action of the Pauli principle leads in effect to an increase of the mean free path of fast particles inside the nucleus.

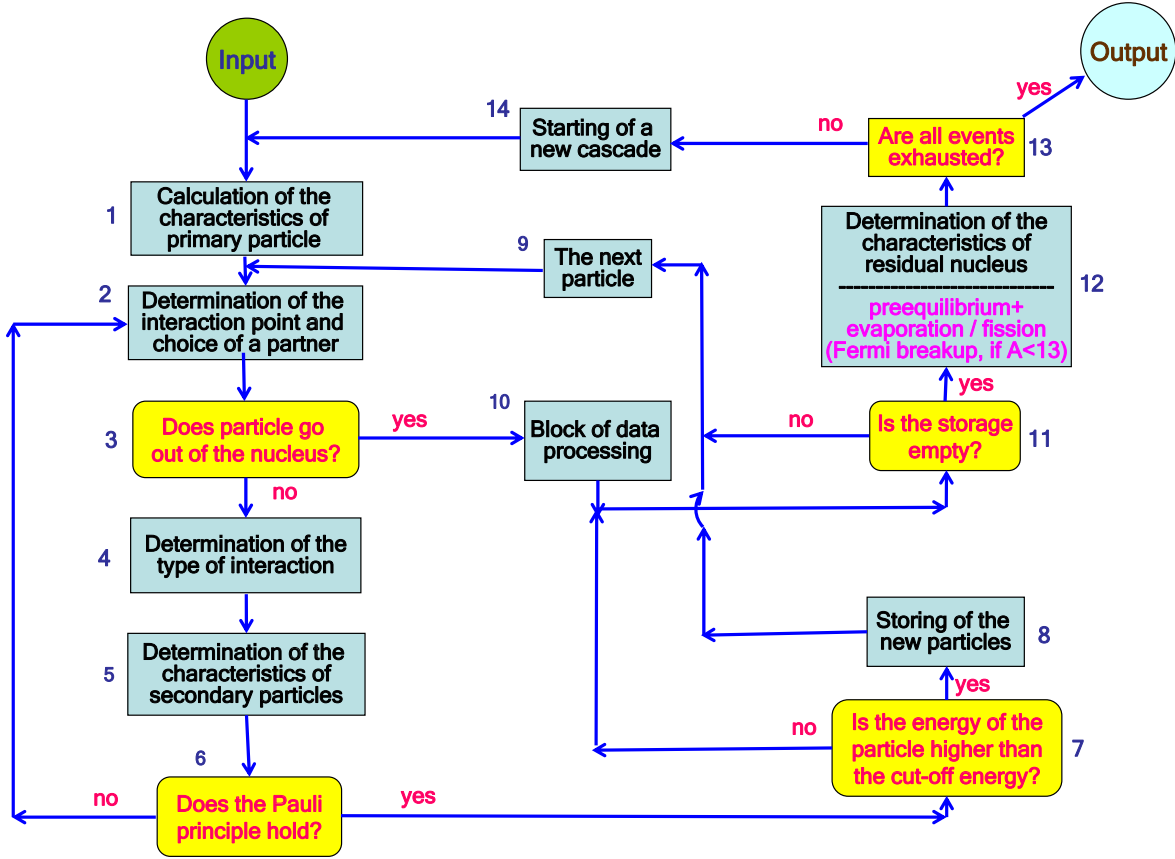


Figure 1: Flow chart for the intranuclear cascade calculation.

energy of the primary particle and the partner taking part in the intranuclear motion) the mean free path of the particle in nuclear matter $L = L(\sigma_{tot})$ is calculated and the point of interaction is determined.

Box 3 tests whether this point of interaction is inside the nucleus. If it is not, then the particle is assumed to have passed through the nucleus without interaction. The ratio of the number of such particles to the total number of interactions considered with the nucleus N_{tot} obviously characterizes the reaction cross section $\sigma_{in}(t)$.

If the point of interaction is inside the nucleus, then the type of interaction: elastic or inelastic, is determined from the known cross sections $\sigma_{el}(t)$ and $\sigma_{in}(t)$ in box 4.

In box 5 the secondary-particle characteristics are determined in accordance with the type of interaction selected (the nature, number, energy, and the emission angle).

Box 6 is a test of whether the Pauli principle is satisfied. Interactions which do not satisfy this principle are considered forbidden and the particle trajectory is followed beyond the point of the forbidden interaction.

In box 7 the particle energy T is compared with some initially specified cutoff energy T_{cut} which determinates whether this particle is sufficiently energetic ($T > T_{cut}$) to take further part in development of the intranuclear cascade or whether its energy is so small ($T \leq T_{cut}$) that the particle is simply absorbed by the nucleus. In the first case the particle is followed further as was described above. (For this the parameters of all cascade particles with energy $T > T_{cut}$ are stored in the memory in box 8 and later the cascade calculation is repeated for each of them in turn by going to boxes 9 and 2.) In the second case the INC treatment of this particle is terminated; if this particle is a nucleon, in box 10 it contributes to the energy of the residual nucleus and become an exciton to be further treated by a preequilibrium model of nuclear reactions in box 12.

The calculation is carried out until all particles are absorbed or leave the nucleus. The operations in boxes 8, 9, and 11 are responsible for this. If the history of one particle which entered the nucleus had been completed (*i.e.*, if the computer memory is empty; see box 11), a possible preequilibrium, followed by evaporation/fission, or/and Fermi breakup stage of this event is simulated in box 12 until the excitation energy of the residual nucleus is below the binding energy of a neutron or other particles that could be emitted from this nucleus, then, the history of the next particle (*i.e.*, next “event”) is simulated (boxes 13 and 14), and so forth, until all events are simulated and we get the needed statistics.

Any cascade calculation at not very high energies where it is still possible to neglect many-particle interactions and the change in density of the intranuclear nucleons can be fitted into the general scheme shown in Fig. 2. The specific form of the box operations and their complexity are determined by the choice of the nuclear model and by the number and variety of elementary processes which it is considered necessary to take into account in a given calculation. The individual boxes can be studied in more detail in Refs. [27, 28], as well as in the already old, but still one of the best monographs on the INC and other nuclear reaction models [23], we highly recommend to readers interested in details of high-energy nuclear reactions. Many specific details on the INC of CEM03.03, LAQGSM03.03, Bertini model, ISABEL, and INCL4.2 are provided in the following subsections.

2.1 The INC of CEM03.03

The intranuclear cascade model in CEM03.03 is based on the standard (non-time-dependent) version of the Dubna cascade model [23, 24, 27, 28]. All the cascade calculations are carried out in a three-dimensional geometry. The nuclear matter density $\rho(r)$ is described by a Fermi distribution with two parameters taken from the analysis of electron-nucleus scattering, namely

$$\rho(r) = \rho_p(r) + \rho_n(r) = \rho_0 \{1 + \exp[(r - c)/a]\} , \quad (1)$$

where $c = 1.07A^{1/3}$ fm, A is the mass number of the target, and $a = 0.545$ fm. For simplicity, the target nucleus is divided by concentric spheres into seven zones in which the nuclear density is considered to be constant. The energy spectrum of the target nucleons is estimated in the perfect Fermi-gas approximation with the local Fermi energy $T_F(r) = \hbar^2 [3\pi^2 \rho(r)]^{2/3} / (2m_N)$, where m_N is the nucleon mass. An example of the nucleon density and the Fermi energy used by CEM03.03 to calculate nuclear reactions on ^{208}Pb can be find in Fig. 3 of Ref. [3].

The influence of intranuclear nucleons on the incoming projectile is taken into account by adding to its laboratory kinetic energy an effective real potential V , as well as by considering the Pauli principle which forbids a number of intranuclear collisions and effectively increases the mean free path of cascade particles inside the target. For incident nucleons $V \equiv V_N(r) = T_F(r) + \epsilon$, where $T_F(r)$ is the corresponding Fermi energy and ϵ is the binding energy of the nucleons. For pions, CEM03.03 uses a square-well nuclear potential with the depth $V_\pi \simeq 25$ MeV, independently of the nucleus and pion energy, as was done in the initial Dubna INC [23, 24].

The interaction of the incident particle with the nucleus is approximated as a series of successive quasi-free collisions of the fast cascade particles (N , π , or γ) with intranuclear nucleons:

$$NN \rightarrow NN, \quad NN \rightarrow \pi NN, \quad NN \rightarrow \pi_1, \dots, \pi_i NN, \quad (2)$$

$$\pi N \rightarrow \pi N, \quad \pi N \rightarrow \pi_1, \dots, \pi_i N \quad (i \geq 2). \quad (3)$$

In the case of pions, besides the elementary processes (3), CEM03.03 also takes into account pion absorption on nucleon pairs

$$\pi NN \rightarrow NN. \quad (4)$$

The momenta of the two nucleons participating in the absorption are chosen randomly from the Fermi distribution, and the pion energy is distributed equally between these nucleons in the center-of-mass system of the three particles participating in the absorption. The direction of motion of the resultant nucleons in this system is taken as isotropically distributed in space. The effective cross section for absorption is related (but not equal) to the experimental cross sections for pion absorption by deuterons.

In the case of photonuclear reactions [29], CEM03.03 follows the ideas of the photonuclear version of the Dubna INC proposed initially in Ref. [30] to describe photonuclear reactions at energies above the Giant Dipole Resonance (GDR) region [31]. [At photon energies $T_\gamma = 10\text{--}40$ MeV, the DeBroglie wavelength λ is of the order of 20–5 fm, greater than the average inter-nucleonic distance in the nucleus; the photons interact with the nuclear dipole resonance as a whole, thus the INC is not applicable.] Below the pion-production threshold, the Dubna INC considers absorption of photons on only “quasi-deuteron” pairs according to the Levinger model [32]:

$$\sigma_{\gamma A} = L \frac{Z(A-Z)}{A} \sigma_{\gamma d}, \quad (5)$$

where A and Z are the mass and charge numbers of the nucleus, $L \approx 10$, and $\sigma_{\gamma d}$ is the total photo-absorption cross section on deuterons as defined from experimental data.

At photon energies above the pion-production threshold, the Dubna INC considers production of one or two pions; the specific mode of the reaction is chosen by the Monte-Carlo method according to the partial cross sections (defined from available experimental data):

$$\gamma + p \rightarrow p + \pi^0, \quad (6)$$

$$\rightarrow n + \pi^+, \quad (7)$$

$$\rightarrow p + \pi^+ + \pi^-, \quad (8)$$

$$\rightarrow p + \pi^0 + \pi^0, \quad (9)$$

$$\rightarrow n + \pi^+ + \pi^0. \quad (10)$$

The cross sections of $\gamma + n$ interactions are derived from consideration of isotopic invariance, *i.e.* it is assumed that $\sigma(\gamma + n) = \sigma(\gamma + p)$. The Compton effect on intranuclear nucleons is neglected, as its cross section is less than $\approx 2\%$ of other reaction modes (see, *e.g.* Fig. 6.13 in Ref. [33]). The Dubna INC does not consider processes involving production of three and more pions; this limits the model's applicability to photon energies $T_\gamma \lesssim 1.5$ GeV [for T_γ higher than the threshold for three-pion production, the sum of the cross sections (8)–(10) is assumed to be equal to the difference between the total inelastic $\gamma + p$ cross section and the sum of the cross sections of the two-body reactions (6)–(7)].

The integral cross sections for the free NN , πN , and γN interactions (2)–(10) are approximated in the Dubna INC model [23] used in the CEM95 [34] version of CEM and its predecessors using a special algorithm of interpolation/extrapolation through a number of picked points, mapping as well as possible the experimental data. This was done very accurately by the group of Prof. Barashenkov using all experimental data available at that time. Currently the experimental data on cross sections is much more complete than at that time; therefore, for CEM03.03, revised approximations of all the integral elementary cross sections have been developed (see details in [35, 29]). So far, for CEM03.03, new approximations for 34 different types of elementary cross sections induced by nucleons, pions, and gammas have been developed. Integral cross sections for other types of interactions taken into account in CEM03.03 are calculated from isospin considerations using the former as input.

Examples of several compiled experimental cross sections together with the new approximations used in CEM03.03 and the old approximations from CEM95 [34] are shown in Fig. 2. More similar results can be found in Refs. [3, 35].

The kinematics of two-body elementary interactions and absorption of photons and pions by a pair of nucleons is completely defined by a given direction of emission of one of the secondary particles. The cosine of the angle of emission of secondary particles in the c.m. system is calculated by the Dubna INC [23] as a function of a random number ξ , distributed uniformly in the interval $[0,1]$ as

$$\cos \Theta = 2\xi^{1/2} \left[\sum_{n=0}^N a_n \xi^n + \left(1 - \sum_{n=0}^N a_n\right) \xi^{N+1} \right] - 1, \quad (11)$$

where $N = M = 3$,

$$a_n = \sum_{k=0}^M a_{nk} T_i^k. \quad (12)$$

The coefficients a_{nk} were fitted to the then available experimental data at a number of incident kinetic energies T_i , then interpolated and extrapolated to other energies (see details in [23, 30, 31] and references therein). The distribution of secondary particles over the azimuthal angle φ is assumed isotropic. For elementary interactions with more than two particles in the final state, the Dubna INC uses the statistical model to simulate the angles and energies of products (see details in [23]).

For the improved version of the INC in CEM03.03, currently available experimental data and recently published systematics proposed by other authors have been used and new approximations have been developed for the angular and energy distributions of particles produced in nucleon-nucleon and photon-proton interactions.

So, for pp , np , and nn interactions at energies up to 2 GeV, the authors of CEM03.03 did not have to develop their own approximations analogous to the ones described by Eqs. (11) and (12), since reliable systematics have been developed recently by Cugnon *et al.* for the Liege INC [6], then improved still further by Duarte for the BRIC code [36]; they simply incorporated into CEM03.03 the systematics by Duarte [36].

Examples of angular distributions of secondary particles from np reactions at several energies are shown in Fig. 3. The new approximations reproduce the experimental data much better than the old Dubna INC used in the previous CEM code versions (and in several other codes developed from the Dubna INC).

In the case of γp reactions (6) and (7), CEM03.03 choses another way: Instead of fitting the parameters a_n from Eq. (11) at different E_γ where measured data were found (see, *e.g.*, Fig. 4) and finding the energy dependence of parameters a_{nk} in Eq. (12) using the values obtained for a_n , CEM took advantage of the event generator for γp and γn reactions from the Moscow INC [38] kindly sent by Dr. Igor Pshenichnov to the authors of CEM.

That event generator includes a data file with smooth approximations through presently available experimental data at 50 different gamma energies from 117.65 to 6054 MeV (in the system where the p or n interacting with γ is at rest) for the c.m. angular distributions $d\sigma/d\Omega$ of secondary particles as functions of Θ tabulated for values of Θ from 0 to 180 deg., with the step $\Delta\Theta = 10$ deg., for 60 different channels of γp and γn reactions considered by the Moscow INC (see details in [38]). The authors of CEM use part of that data file with data for reactions (6) and (7), and have written an algorithm to simulate unambiguously $d\sigma/d\Omega$ and to choose the corresponding value of Θ for any E_γ , using a single random number ξ uniformly distributed in the interval [0,1]. This is straightforward due to the fact that the function $\xi(\cos \Theta)$

$$\xi(\cos \Theta) = \frac{\int_{-1}^{\cos \Theta} d\sigma/d\Omega d \cos \Theta}{\int_{-1}^1 d\sigma/d\Omega d \cos \Theta}$$

is a smooth monotonic function increasing from 0 to 1 as $\cos \Theta$ varies from -1 to 1. Naturally, when E_γ differs from the values tabulated in the data file, CEM performs first the needed interpolation in energy. This procedure is used to describe in CEM03.03 angular distributions of secondary particles from reactions (6) and (7), as well as for isotopically symmetric reactions $\gamma + n \rightarrow n + \pi^0$ and $\gamma + n \rightarrow p + \pi^-$.

Examples of eight angular distributions of π^+ from $\gamma p \rightarrow \pi^+ n$ as functions of $\Theta_{c.m.s}^\pi$ are presented in Fig. 4. It can be seen that the approximations developed in CEM03.03 (solid histograms) agree much better with the available experimental data than the old Dubna INC approximations (11)–(12) used in all predecessors of CEM03 (dashed histograms).

The analysis of experimental data has shown that the channel (8) of two-pion photo-production proceeds mainly through the decay of the Δ^{++} isobar listed in the last Review of Particle Physics by the Particle Data Group as having the mass $M = 1232$ MeV



whereas the production cross section of other isobar components ($\frac{3}{2}, \frac{3}{2}$) are small and can be neglected. The Dubna INC uses the Lindenbaum-Sternheimer resonance model [39] to simulate the reaction (13). In this model, the mass of the isobar M is determined from the distribution

$$\frac{dW}{dM} \sim F(E, M)\sigma(M) , \quad (14)$$

where E is the total energy of the system, F is the two-body phase space of the isobar and π^- meson, and σ is the isobar production cross section which is assumed to be equal to the cross section for elastic $\pi^+ p$ scattering.

The c.m. emission angle of the isobar is approximated using Eqs. (11) and (12) with the coefficients a_{nk} listed in Tab. 3 of Ref. [31]; isotropy of the decay of the isobar in its c.m. system is assumed.

In order to calculate the kinematics of the non-resonant part of the reaction (8) and the two remaining three-body channels (9) and (10), the Dubna INC uses the statistical model. The total energies of the two particles (pions) in the c.m. system are determined from the

distribution

$$\frac{dW}{dE_{\pi_1} dE_{\pi_2}} \sim (E - E_{\pi_1} - E_{\pi_2}) E_{\pi_1} E_{\pi_2} / E, \quad (15)$$

and that of the third particle (nucleon, N) from conservation of energy. The actual simulation of such reactions is done as follows: Using a random number ξ , the energy of the first pion is simulated in the beginning using

$$E_{\pi_1} = m_{\pi_1} + \xi(E_{\pi_1}^{max} - m_{\pi_1}),$$

where

$$E_{\pi_1}^{max} = [E^2 + m_{\pi_1}^2 - (m_{\pi_2} + m_N)^2] / 2E.$$

Then, energy of the second pion E_{π_2} is simulated the according to Eq. (15) using the Monte-Carlo rejection method. The energy of the nucleon is calculated as $E_N = E - E_{\pi_1} - E_{\pi_2}$, following which a checking is performed to make sure that the ‘‘triangle law’’ for momenta

$$|p_{\pi_1} - p_{\pi_2}| \leq p_N \leq |p_{\pi_1} + p_{\pi_2}|$$

is fulfilled, otherwise this sampling is rejected and the procedure is repeated. The angles Θ and φ of the pions are sampled assuming an isotropic distribution of particles in the c.m. system,

$$\cos \Theta_{\pi_1} = 2\xi_1 - 1, \quad \cos \Theta_{\pi_2} = 2\xi_2 - 1, \quad \varphi_{\pi_1} = 2\pi\xi_3, \quad \varphi_{\pi_2} = 2\pi\xi_4,$$

and the angles of the nucleon are defined from momentum conservation, $\vec{p}_N = -(\vec{p}_{\pi_1} + \vec{p}_{\pi_2})$. More details on the new CEM approximations for differential elementary cross sections may be found in [29, 37].

The Pauli exclusion principle at the cascade stage of the reaction is handled by assuming that nucleons of the target occupy all the energy levels up to the Fermi energy. Each simulated elastic or inelastic interaction of the projectile (or of a cascade particle) with a nucleon of the target is considered forbidden if the ‘‘secondary’’ nucleons have energies smaller than the Fermi energy. If they do, the trajectory of the particle is traced further from the forbidden point and a new interaction point, a new partner and a new interaction mode are simulated for the traced particle, *etc.*, until the Pauli principle is satisfied or the particle leaves the nucleus.

In this version of the INC, the kinetic energy of the cascade particles is increased or decreased as they move from one of the seven potential regions (zones) to another, but their directions remain unchanged. That is, in such calculations, refraction or reflection of cascade nucleons at potential boundaries is neglected. CEM03.03 allows to take into account refractions and reflections of cascade nucleons at potential boundaries; for this, one needs to change the value of the parameter **irefrac** from 0 to 1 in the subroutine **initial**. But this option provides somewhat worse overall agreement of calculations with some experimental data, therefore the option of no refractions/reflections was chosen as the default in CEM03.03.

The INC in CEM does not take into account the so-called ‘‘trawling’’ effect [23]. That is, in the beginning of the simulation of each event, the nuclear density distributions for the protons and neutrons of the target are calculated according to Eq. (1) and a subsequent

decrease of the nuclear density with the emission of cascade particles is not taken into account. Detailed analyses of different characteristics of nucleon- and pion-induced reactions for targets from C to Am have shown that this effect may be neglected at incident energies below about 5 GeV in the case of heavy targets like actinides and below about 1 GeV for light targets like carbon. At higher incident energies the progressive decrease of nuclear density with the development of the intranuclear cascade has a strong influence on the calculated characteristics and this effect has to be taken into account [23]. Therefore, MCNP6 uses as default CEM03.03 only at projectile energies below 4.5 GeV (for incident nucleons) and switches to simulations using LAQGSM03.03, which considers the “trawling” effect, at higher energies of transported particles.

An important ingredient of the CEM is the criterion for transition from the intranuclear cascade to the preequilibrium model. In conventional cascade-evaporation models (like the Bertini INC [8]), fast particles are traced down to some minimal energy, the cutoff energy T_{cut} (or one compares the duration of the cascade stage of a reaction with a cutoff time, in “time-like” INC models, such as the Liege INC [6]). This cutoff is usually less than $\simeq 10$ MeV above the Fermi energy, below which particles are considered to be absorbed by the nucleus. The CEM uses a different criterion to decide when a primary particle is considered to have left the cascade.

An effective local optical absorptive potential $W_{opt. mod.}(r)$ is defined from the local interaction cross section of the particle, including Pauli-blocking effects. This imaginary potential is compared to one defined by a phenomenological global optical model $W_{opt. exp.}(r)$. CEM characterizes the degree of similarity or difference of these imaginary potentials by the parameter

$$\mathcal{P} = |(W_{opt. mod.} - W_{opt. exp.})/W_{opt. exp.}|. \quad (16)$$

When \mathcal{P} increases above an empirically chosen value, the particle leaves the cascade, and is then considered to be an exciton. From a physical point of view, such a smooth transition from the cascade stage of the reaction seems to be more attractive than the “sharp cut-off” method. In addition, as was shown in Ref. [2], this improves the agreement between the calculated and experimental spectra of secondary nucleons, especially at low incident energies and backward angles of the detected nucleons (see *e.g.*, Figs. 3 and 11 of Ref. [2]). More details about this feature in the CEM03.03 INC can be found in Refs. [2, 3].

Beside the changes to the Dubna INC mentioned above, a number of other improvements and refinements have been made in the INC of CEM03.03, such as imposing momentum-energy conservation for each simulated event (the Monte-Carlo algorithm used in several initial versions of CEM provided momentum-energy conservation only statistically, on the average, but not exactly for each simulated event) and using real binding energies for nucleons in the cascade instead of the approximation of a constant separation energy of 7 MeV used in early versions of the CEM.

In addition, in CEM03.03, many algorithms used in the Monte-Carlo simulations in many subroutines have also been improved, decreasing the computing time by up to a factor of 6 for heavy targets, which is very important when performing practical simulations with MCNP6 for complex applications.

It should be mentioned that in the CEM the initial configuration for the preequilibrium decay (number of excited particles and holes, *i.e.* excitons $n_0 = p_0 + h_0$, excitation energy

E_0^* , linear momentum \mathbf{P}_0 , and angular momentum \mathbf{L}_0 of the nucleus) differs significantly from that usually postulated in other exciton models. Many calculations have shown that the distributions of residual nuclei remaining after the cascade stage of the reaction, *i.e.* before the preequilibrium emission, with respect to n_0 , p_0 , h_0 , E_0^* , \mathbf{P}_0 , and \mathbf{L}_0 are rather broad (see Ref. [3] and references therein for more details) .

2.2 The INC of LAQGSM

The INC of LAQGSM03.03 is described with a recently improved version [5, 40] of the time-dependent intranuclear cascade model developed initially at JINR in Dubna, often referred to in the literature as the Dubna intranuclear Cascade Model, DCM (see [41] and references therein). The DCM models interactions of fast cascade particles (“participants”) with nucleon spectators of both the target and projectile nuclei and includes as well interactions of two participants (cascade particles). It uses experimental cross sections at energies below 4.5 GeV/nucleon, or those calculated by the Quark-Gluon String Model, QGSM (see Refs. [42, 43, 44, 45] and references therein) at higher energies to simulate angular and energy distributions of cascade particles, and also considers the Pauli exclusion principle.

In contrast to the CEM03.03 version of the INC described above, DCM uses a continuous nuclear density distribution (instead of the approximation of several concentric zones, where inside each the nuclear density is considered to be constant); therefore, it does not need to consider refraction and reflection of cascade particles inside or on the border of a nucleus. It also keeps track of the time of an intranuclear collision and of the depletion of the nuclear density during the development of the cascade (the so-called “trawling effect” mentioned above) and takes into account the hadron formation time (see Fig. 5).

In the INC used in LAQGSM03.03, all the new approximations developed recently for the INC of CEM03.03 to describe total cross sections and elementary energy and angular distributions of secondary particles from hadron-hadron interactions have been incorporated. Then, a new high-energy photonuclear reaction model based of the event generators for γp and γn reactions from the Moscow INC [38] kindly provided by Dr. Igor Pshenichnov to the authors of LAQGSM, and on the latest photonuclear version of CEM [29] was developed and incorporated [40] into the INC of LAQGSM, which allows to calculate reactions induced by photons with energies of up to tens of GeV.

The 56 channels to consider γp elementary interactions during the cascade stage of reactions, and 56 channels for γn interactions incorporated in LAQGSM03.03 are listed in Table 1.

To describe the two-body channels #1–14, LAQGSM03.03 uses part of a file containing smooth approximations through presently available experimental data sent by Dr. Pshenichnov to the authors of LAQGSM. However, in LAQGSM, its own algorithms have been developed and its own routines were written to simulate unambiguously $d\sigma/d\Omega$ and to choose the corresponding value of Θ for any E_γ , using a single random number ξ uniformly distributed in the interval [0,1], as described in [29] and in previous subsection. Fig. 6 shows examples of angular distributions of π^0 from $\gamma p \rightarrow \pi^0 p$ interactions as functions of $\Theta_{c.m.s}^\pi$ at eight different photon energies as simulated by the LAQGSM routines compared with available experimental data.

To describe the channels #15–21 with two and three pions in the final state, LAQGSM

uses the γp and γn event generators provided by Dr. Pshenichnov, but uses its own interpolation for integral cross sections. No examples of cross sections for these channels are shown here, as LAQGSM03.03 reproduces all the results by Pshenichnov *et al.* shown in Figs. 6 and 8 of Ref. [38].

Finally, to describe the multi-pion channels #22–56, LAQGSM03.03 uses the isospin statistical model as realized in the γp and γn event generators provided by Dr. Pshenichnov and described in details in [38], without any changes. For channels #22–56, LAQGSM03.03 reproduces exactly the results by Pshenichnov *et al.* as published in Ref. [38], therefore no examples of such results are shown here.

After the bombarding photon is absorbed by two nucleons or interacts inelastically with a nucleon according the channels #1–56, LAQGSM gets inside the nucleus several “secondary” cascade nucleons, pions, or other mesons and resonances listed in Table 1, depending on which channel is simulated from the corresponding cross sections at the given photon energy to actually occur. These “secondary” cascade particles interact further with intranuclear nucleons or leave the nucleus, depending on their coordinates and momenta. The further behavior of the reaction starting from this stage, after the photon had “disappeared”, is described by LAQGSM03.03 exactly the same way as for any other types of reactions, induced, *e.g.*, by nucleons or heavy ions.

In the latest version of LAQGSM, LAQGSM03.03 [5], the INC was modified for a better description of nuclear reactions at very high energies (above 20 GeV/nucleon), namely:

1) The latest fits to currently available evaluated experimental databases for the total and elastic $\pi^+ p$, $\pi^- p$, pp , and pn cross sections (see the last edition of the Review of Particle Physics (Particle Data Group) and references therein) have been incorporated into LAQGSM. LAQGSM03.03 uses now these approximations at energies above 20–30 GeV, and its own approximations developed for CEM03.03 [1] at lower energies.

2) Initially, LAQGSM was used only at energies below ~ 800 GeV. In [5], the possibility of using LAQGSM03.03 at ultra-relativistic energies, above 1 TeV, was studied. It was found that to describe ultra-high energy reactions, the value of the parameter $\sigma_{\perp} = 0.51$ GeV/c in the transverse momentum distribution of the constituent quarks of QGSM (see Eq. (12) in [4] or Eq. (10) in Ref. [45]) has to be increased. As shown in Fig. 7, to describe properly $p + p$ interactions at $\sqrt{s} = 200$ GeV, which corresponds to $T_p \simeq 21314$ GeV, we need to use $\sigma_{\perp} = 2.0$ GeV/c. In other words, to be able to describe well with LAQGSM reactions induced by intermediate and high energy projectiles as well as reactions induced by ultra-relativistic energy projectiles, we need to use an energy dependent average transverse momentum parameter σ_{\perp} increasing with the projectile energy from 0.51 GeV/c at $T_p \leq 200$ GeV [4] to $\sigma_{\perp} \simeq 2$ GeV/c at $T_p \simeq 21$ TeV.

Finally, the algorithms of many LAQGSM INC routines were changed and some INC routines were rewritten, which speeded up the code significantly; some preexisting bugs in the DCM were fixed; many useful comments were added [5].

More details on the INC of LAQGSM03.03 may be found in Refs. [5, 4, 40, 42, 43, 44, 45]. Many examples of results by LAQGSM03.03 are presented in Refs. [3, 5, 40, 47, 48, 49, 50, 51].

2.3 The INC of the Bertini Model

It should be noted that there are several, and quite different, versions of the INC developed by Dr. Hugo Bertini at ORNL. A good review on this point and the corresponding references may be found in the *Handbook of Spallation Research* by Filges and Goldenbaum [52].

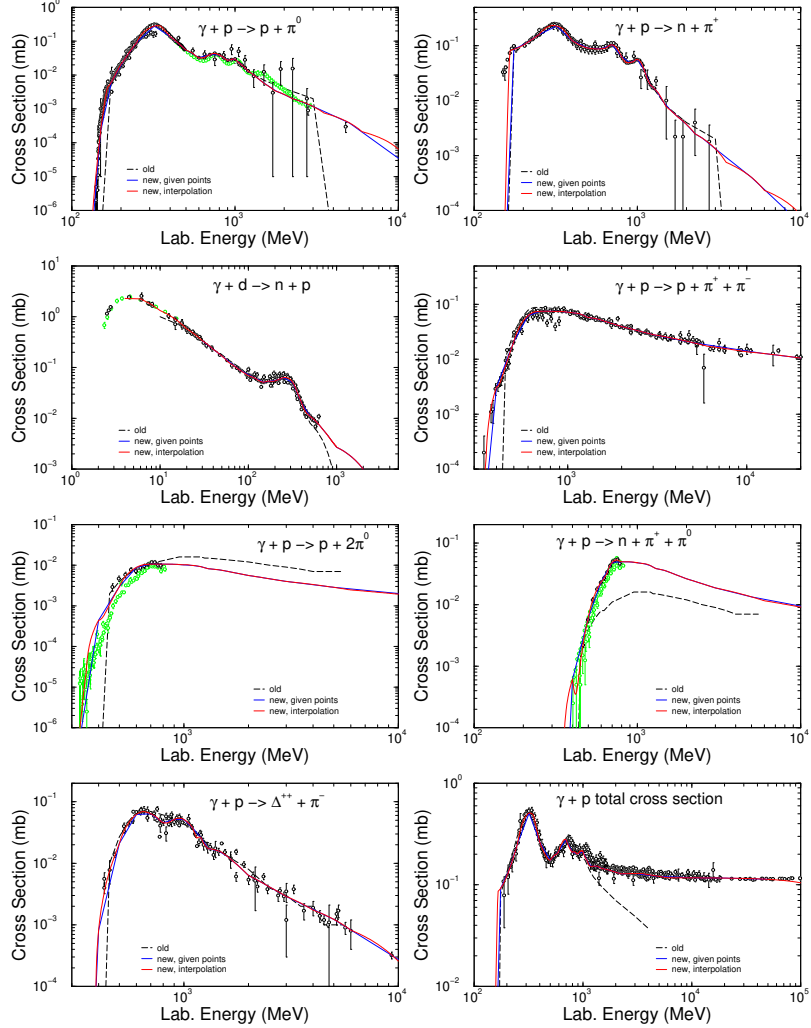


Figure 2: Comparison of eight experimental total $\gamma + p(d)$ cross sections with the old approximations used in the Dubna INC [23] and with the approximations incorporated into the CEM03.03 code. The red curve gives the code results using parabolic interpolation, while the blue solid curve uses linear interpolation between our tabulated points. Where no blue curve is visible, it is coincident with the red curve. References to experimental data shown by black and green circles may be found in Ref. [29]. The green circles show recent experimental data that became available to the authors of CEM03.03 after the fit published in Ref. [29] was completed; Although these recent data agree reasonably well with the CEM03.03 approximations, a refitting would slightly improve the agreement.

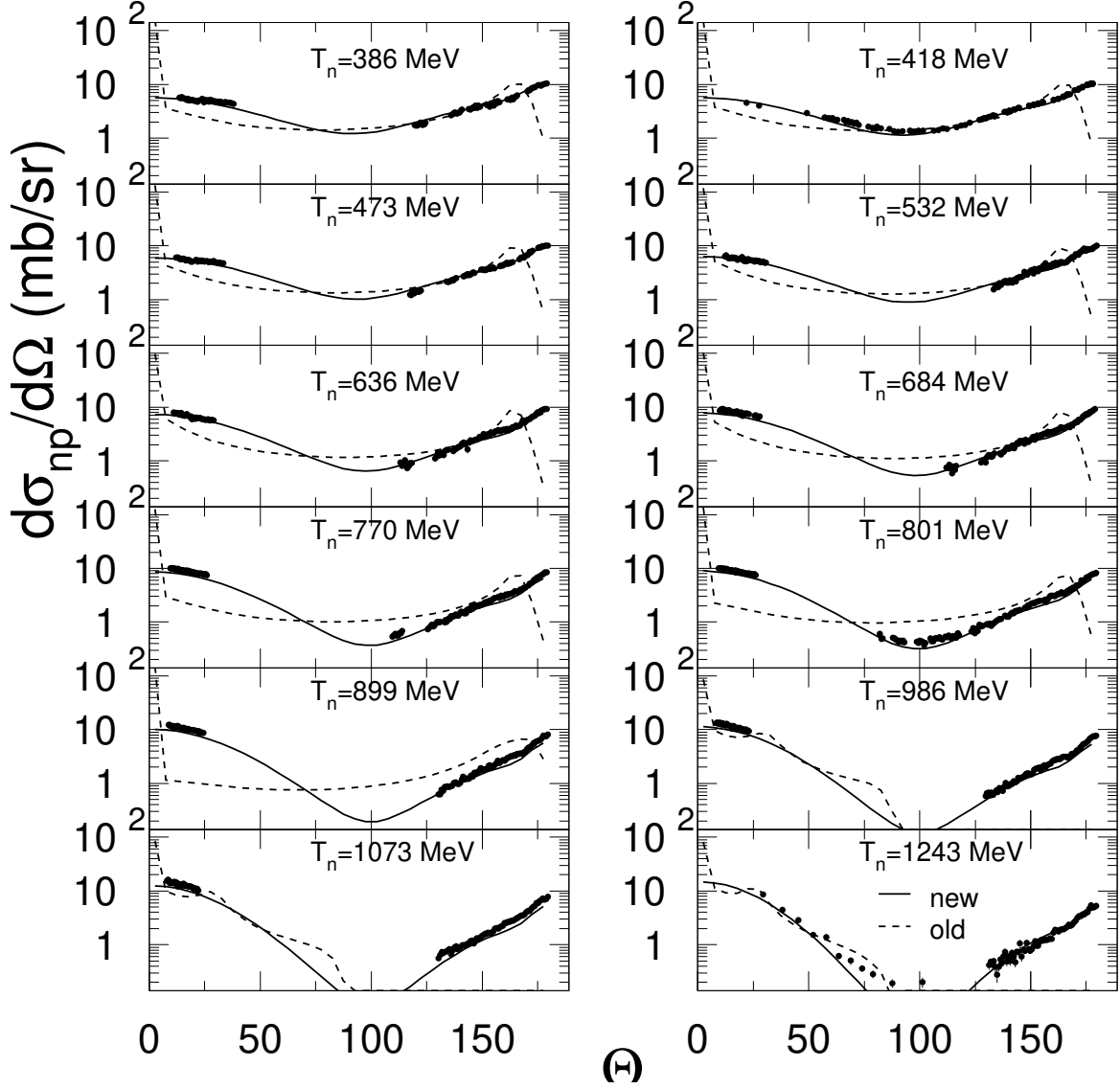


Figure 3: Example of twelve angular distributions of n from np elastic interactions as functions of $\Theta_{c.m.}^n$ at T_n from 386 to 1243 MeV. The dashed lines show the old approximations from the Dubna INC while the solid lines are the new approximations incorporated into CEM03.03 (and LAQGSM03.03). References to experimental data shown here by black circles may be found in Ref. [37].

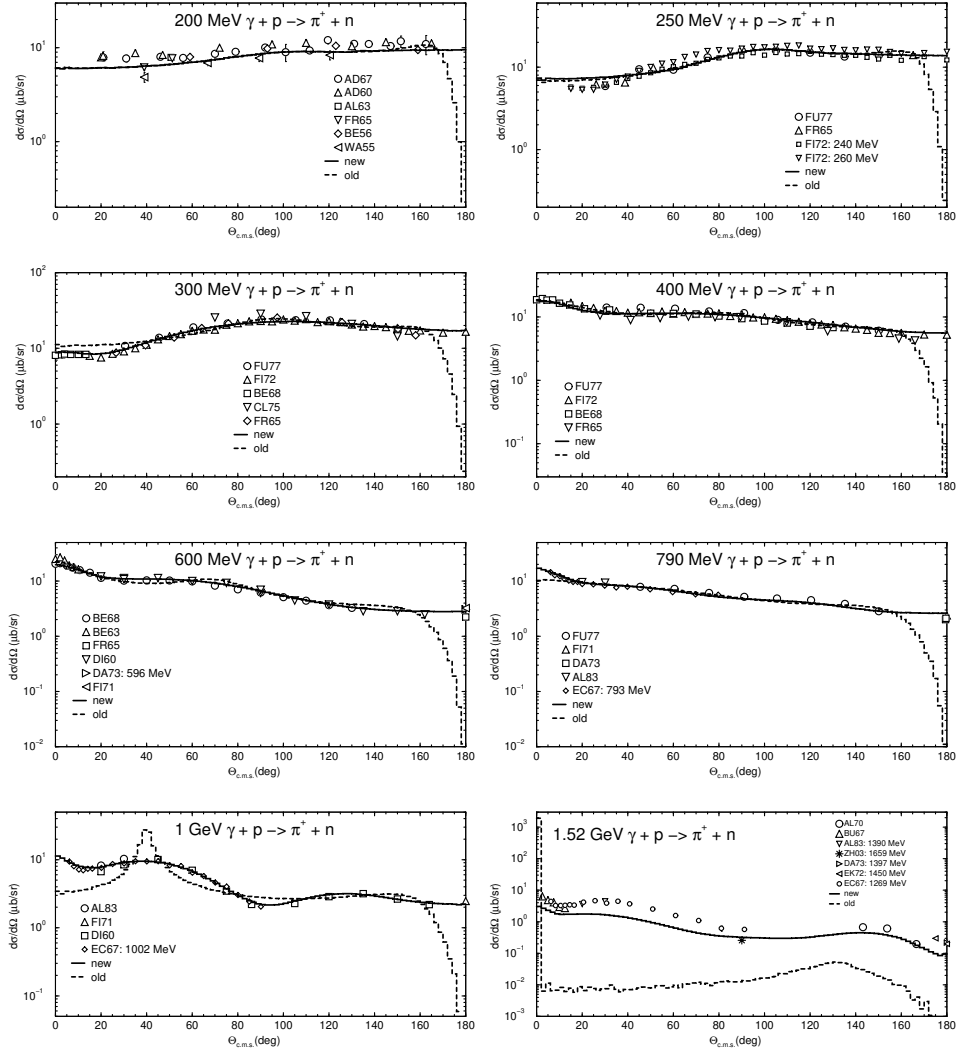


Figure 4: Example of eight angular distributions of π^+ from $\gamma p \rightarrow \pi^+ n$ as functions of $\Theta_{c.m.s.}^\pi$ at photon energies from 200 MeV to 1.52 GeV. The dashed lines show the old approximations used in the Dubna INC while the solid lines are the new approximations incorporated into the CEM03.03 and LAQGSM03.03 codes. References to experimental data shown by symbols may be found in Ref. [29].

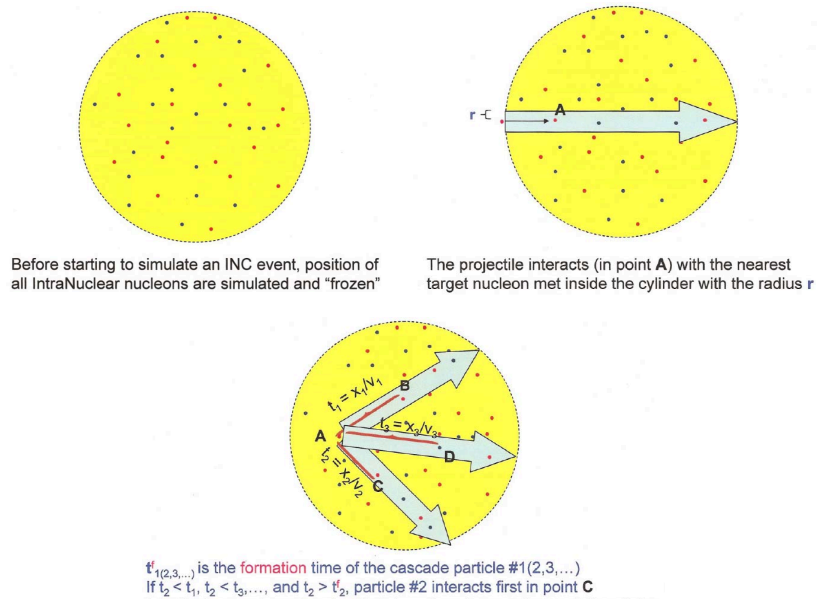


Figure 5: An illustrative scheme of a target nucleus, of interaction points of cascade particles (participants) with intranuclear nucleons (spectators), and of selection of the corresponding time of such interactions, as performed in the INC used in LAQGSM.

Table 1: Channels of elementary γN interactions taken into account in LAQGSM03.03

#	γp -interactions	γn -interactions
1	$\gamma p \rightarrow \pi^+ n$	$\gamma n \rightarrow \pi^- p$
2	$\gamma p \rightarrow \pi^0 p$	$\gamma n \rightarrow \pi^0 n$
3	$\gamma p \rightarrow \Delta^{++} \pi^-$	$\gamma n \rightarrow \Delta^+ \pi^-$
4	$\gamma p \rightarrow \Delta^+ \pi^0$	$\gamma n \rightarrow \Delta^0 \pi^0$
5	$\gamma p \rightarrow \Delta^0 \pi^+$	$\gamma n \rightarrow \Delta^- \pi^+$
6	$\gamma p \rightarrow \rho^0 p$	$\gamma n \rightarrow \rho^0 n$
7	$\gamma p \rightarrow \rho^+ n$	$\gamma n \rightarrow \rho^- p$
8	$\gamma p \rightarrow \eta p$	$\gamma n \rightarrow \eta n$
9	$\gamma p \rightarrow \omega p$	$\gamma n \rightarrow \omega n$
10	$\gamma p \rightarrow \Lambda K^+$	$\gamma n \rightarrow \Lambda K^0$
11	$\gamma p \rightarrow \Sigma^0 K^+$	$\gamma n \rightarrow \Sigma^0 K^0$
12	$\gamma p \rightarrow \Sigma^+ K^0$	$\gamma n \rightarrow \Sigma^- K^+$
13	$\gamma p \rightarrow \eta' p$	$\gamma n \rightarrow \eta' n$
14	$\gamma p \rightarrow \phi p$	$\gamma n \rightarrow \phi n$
15	$\gamma p \rightarrow \pi^+ \pi^- p$	$\gamma n \rightarrow \pi^+ \pi^- n$
16	$\gamma p \rightarrow \pi^0 \pi^+ n$	$\gamma n \rightarrow \pi^0 \pi^- p$
17	$\gamma p \rightarrow \pi^0 \pi^0 p$	$\gamma n \rightarrow \pi^0 \pi^0 n$
18	$\gamma p \rightarrow \pi^0 \pi^0 \pi^0 p$	$\gamma n \rightarrow \pi^0 \pi^0 \pi^0 n$
19	$\gamma p \rightarrow \pi^+ \pi^- \pi^0 p$	$\gamma n \rightarrow \pi^+ \pi^- \pi^0 n$
20	$\gamma p \rightarrow \pi^+ \pi^0 \pi^0 n$	$\gamma n \rightarrow \pi^- \pi^0 \pi^0 p$
21	$\gamma p \rightarrow \pi^+ \pi^+ \pi^- n$	$\gamma n \rightarrow \pi^+ \pi^- \pi^- p$
22	$\gamma p \rightarrow \pi^0 \pi^0 \pi^0 \pi^0 p$	$\gamma n \rightarrow \pi^0 \pi^0 \pi^0 \pi^0 n$
23	$\gamma p \rightarrow \pi^+ \pi^- \pi^0 \pi^0 p$	$\gamma n \rightarrow \pi^+ \pi^- \pi^0 \pi^0 n$
24	$\gamma p \rightarrow \pi^+ \pi^+ \pi^- \pi^- p$	$\gamma n \rightarrow \pi^+ \pi^+ \pi^- \pi^- n$
25	$\gamma p \rightarrow \pi^+ \pi^0 \pi^0 \pi^0 n$	$\gamma n \rightarrow \pi^- \pi^0 \pi^0 \pi^0 p$
26	$\gamma p \rightarrow \pi^+ \pi^+ \pi^- \pi^0 n$	$\gamma n \rightarrow \pi^+ \pi^- \pi^- \pi^0 p$
27	$\gamma p \rightarrow \pi^0 \pi^0 \pi^0 \pi^0 \pi^0 p$	$\gamma n \rightarrow \pi^0 \pi^0 \pi^0 \pi^0 \pi^0 n$
28	$\gamma p \rightarrow \pi^+ \pi^- \pi^0 \pi^0 \pi^0 p$	$\gamma n \rightarrow \pi^+ \pi^- \pi^0 \pi^0 \pi^0 n$
29	$\gamma p \rightarrow \pi^+ \pi^+ \pi^- \pi^- \pi^0 p$	$\gamma n \rightarrow \pi^+ \pi^+ \pi^- \pi^- \pi^0 n$
30	$\gamma p \rightarrow \pi^+ \pi^0 \pi^0 \pi^0 \pi^0 n$	$\gamma n \rightarrow \pi^- \pi^0 \pi^0 \pi^0 \pi^0 p$
31	$\gamma p \rightarrow \pi^+ \pi^+ \pi^- \pi^0 \pi^0 n$	$\gamma n \rightarrow \pi^+ \pi^- \pi^- \pi^0 \pi^0 p$
32	$\gamma p \rightarrow \pi^+ \pi^+ \pi^+ \pi^- \pi^- n$	$\gamma n \rightarrow \pi^+ \pi^+ \pi^- \pi^- \pi^- p$
33	$\gamma p \rightarrow \pi^0 \pi^0 \pi^0 \pi^0 \pi^0 \pi^0 p$	$\gamma n \rightarrow \pi^0 \pi^0 \pi^0 \pi^0 \pi^0 \pi^0 n$
34	$\gamma p \rightarrow \pi^+ \pi^- \pi^0 \pi^0 \pi^0 \pi^0 p$	$\gamma n \rightarrow \pi^+ \pi^- \pi^0 \pi^0 \pi^0 \pi^0 n$
35	$\gamma p \rightarrow \pi^+ \pi^+ \pi^- \pi^- \pi^0 \pi^0 p$	$\gamma n \rightarrow \pi^+ \pi^+ \pi^- \pi^- \pi^0 \pi^0 n$
36	$\gamma p \rightarrow \pi^+ \pi^+ \pi^+ \pi^- \pi^- \pi^- p$	$\gamma n \rightarrow \pi^+ \pi^+ \pi^+ \pi^- \pi^- \pi^- n$
37	$\gamma p \rightarrow \pi^+ \pi^0 \pi^0 \pi^0 \pi^0 \pi^0 n$	$\gamma n \rightarrow \pi^- \pi^0 \pi^0 \pi^0 \pi^0 \pi^0 p$
38	$\gamma p \rightarrow \pi^+ \pi^+ \pi^- \pi^0 \pi^0 \pi^0 n$	$\gamma n \rightarrow \pi^+ \pi^- \pi^- \pi^0 \pi^0 \pi^0 p$
39	$\gamma p \rightarrow \pi^+ \pi^+ \pi^+ \pi^- \pi^- \pi^0 n$	$\gamma n \rightarrow \pi^+ \pi^+ \pi^- \pi^- \pi^- \pi^0 p$

Table 1: (continuation). Channels of elementary γN interactions taken into account in LAQGSM03.03

#	γp -interactions	γn -interactions
40	$\gamma p \rightarrow \pi^0 \pi^0 \pi^0 \pi^0 \pi^0 \pi^0 p$	$\gamma n \rightarrow \pi^0 \pi^0 \pi^0 \pi^0 \pi^0 \pi^0 n$
41	$\gamma p \rightarrow \pi^+ \pi^- \pi^0 \pi^0 \pi^0 \pi^0 p$	$\gamma n \rightarrow \pi^+ \pi^- \pi^0 \pi^0 \pi^0 \pi^0 n$
42	$\gamma p \rightarrow \pi^+ \pi^+ \pi^- \pi^- \pi^0 \pi^0 p$	$\gamma n \rightarrow \pi^+ \pi^+ \pi^- \pi^- \pi^0 \pi^0 n$
43	$\gamma p \rightarrow \pi^+ \pi^+ \pi^+ \pi^- \pi^- \pi^- p$	$\gamma n \rightarrow \pi^+ \pi^+ \pi^+ \pi^- \pi^- \pi^- n$
44	$\gamma p \rightarrow \pi^+ \pi^0 \pi^0 \pi^0 \pi^0 \pi^0 n$	$\gamma n \rightarrow \pi^- \pi^0 \pi^0 \pi^0 \pi^0 \pi^0 p$
45	$\gamma p \rightarrow \pi^+ \pi^+ \pi^- \pi^0 \pi^0 \pi^0 n$	$\gamma n \rightarrow \pi^+ \pi^- \pi^- \pi^0 \pi^0 \pi^0 p$
46	$\gamma p \rightarrow \pi^+ \pi^+ \pi^+ \pi^- \pi^- \pi^0 n$	$\gamma n \rightarrow \pi^+ \pi^+ \pi^- \pi^- \pi^- \pi^0 p$
47	$\gamma p \rightarrow \pi^+ \pi^+ \pi^+ \pi^+ \pi^- \pi^- n$	$\gamma n \rightarrow \pi^+ \pi^+ \pi^+ \pi^- \pi^- \pi^- n$
48	$\gamma p \rightarrow \pi^0 \pi^0 \pi^0 \pi^0 \pi^0 \pi^0 p$	$\gamma n \rightarrow \pi^0 \pi^0 \pi^0 \pi^0 \pi^0 \pi^0 n$
49	$\gamma p \rightarrow \pi^+ \pi^- \pi^0 \pi^0 \pi^0 \pi^0 p$	$\gamma n \rightarrow \pi^+ \pi^- \pi^0 \pi^0 \pi^0 \pi^0 n$
50	$\gamma p \rightarrow \pi^+ \pi^+ \pi^- \pi^- \pi^0 \pi^0 p$	$\gamma n \rightarrow \pi^+ \pi^+ \pi^- \pi^- \pi^0 \pi^0 n$
51	$\gamma p \rightarrow \pi^+ \pi^+ \pi^+ \pi^- \pi^- \pi^0 p$	$\gamma n \rightarrow \pi^+ \pi^+ \pi^+ \pi^- \pi^- \pi^0 n$
52	$\gamma p \rightarrow \pi^+ \pi^+ \pi^+ \pi^+ \pi^- \pi^- \pi^- p$	$\gamma n \rightarrow \pi^+ \pi^+ \pi^+ \pi^+ \pi^- \pi^- \pi^- n$
53	$\gamma p \rightarrow \pi^+ \pi^0 \pi^0 \pi^0 \pi^0 \pi^0 n$	$\gamma n \rightarrow \pi^- \pi^0 \pi^0 \pi^0 \pi^0 \pi^0 p$
54	$\gamma p \rightarrow \pi^+ \pi^+ \pi^- \pi^0 \pi^0 \pi^0 n$	$\gamma n \rightarrow \pi^+ \pi^- \pi^- \pi^0 \pi^0 \pi^0 p$
55	$\gamma p \rightarrow \pi^+ \pi^+ \pi^+ \pi^- \pi^- \pi^0 n$	$\gamma n \rightarrow \pi^+ \pi^+ \pi^- \pi^- \pi^- \pi^0 p$
56	$\gamma p \rightarrow \pi^+ \pi^+ \pi^+ \pi^+ \pi^- \pi^- \pi^- n$	$\gamma n \rightarrow \pi^+ \pi^+ \pi^+ \pi^- \pi^- \pi^- n$

MCNP6 does not use the latest version in the Bertini INC as published by Hugo Bertini or its extension to higher energies and to handle reactions induced by projectiles not considered by the original Bertini INC developed recently by younger authors for GEANT4 in C++ (see, *e.g.*, [53] and references therein). Instead, just like its precursors MCNPX [54] and LAHET [18], MCNP6 uses an “intermediate” version of the Bertini INC as implemented initially in the FORTRAN code MECC-7 [55, 56] and used in the transport code HETC [57].

The MECC-7 version of the Bertini INC is based mostly on the original publications by Hugo Bertini [8, 58, 59] and is described also in Ref. [17]. The Bertini INC describes interactions induced by nucleons below 3.5 GeV and the pion interactions up to 2.5 GeV; a scaling law approximation is used to continue the interaction energy to arbitrarily high energies, although a reasonable upper limit is about 10 GeV. In the version of the Bertini INC as implemented in LAHET, and later in MCNPX, and, finally, in MCNP6, a special care was taken by Dick Prael to make sure that it does not crash the code even when it is used for very light target-nuclei and/or at incident energies where the assumptions of the model are not well grounded. Although we can not expect very good predictions from such “difficult” simulations, it was proved that Bertini INC handles them without crashes, providing still reasonable results. For this reason, Bertini INC is set as the default option in MCNP6 to simulate reactions on very light nuclei, like H, d, t, ^3He , and ^4He at arbitrary energies (particle-nucleon interactions at energies above 4.5 GeV are simulated by default in MCNP6 with LAQGSM).

In a way, MECC-7 is similar to the initial Dubna INC [23, 24] used by the early versions of CEM and discussed above. More than this, these two INC models were compared by their authors and developers in Ref. [60]. The most important differences are in details of how the nuclear density and Fermi momenta are described, how the free particle-particle cross sections are approximated, and when the INC stage of reactions is assumed to be completed. So, Bertini INC models the target nucleus as consisting of three concentric spheres (“three zones”). The Fermi gas model is used to describe the Fermi momenta of intranuclear nucleons; the Pauli exclusion principle is taken into account. The INC process starts when a nucleon or pion projectile hits a nucleon in the target-nucleus and produces “secondary particles”. The history of each particle is followed until it either escapes from the nucleus or its energy becomes below a “cutoff energy”, which, in general, is taken to be half of the Coulomb barrier of the surface of the nucleus. The energy is different for different types of projectiles and can be found, *e.g.*, in Ref. [17]. At this point the energy conservation of the cascade process is verified. The binding energy of the most loosely bound nucleon is taken to be 8 MeV in the Bertini INC and is assumed to be the same for all three zones and for all nuclei. Relativistic kinematics is used throughout the Bertini INC. More details on the Bertini INC can be found in Refs. [8, 17, 52, 58, 59, 60].

2.4 The INC of ISABEL

The second model, from a historical point of view, migrated to MCNP6 via MCNPX [54] from LAHET [18] is the ISABEL INC [9, 61]. ISABEL is the default option in MCNP6 for reactions induced by d, t, ^3He , ^4He , and antinucleons at energies up to about 1 GeV per nucleon. If specified in the MCNP6 input file, ISABEL can be used to also simulate reactions induced by nucleons, pions, kaons, and light-ions at energies below 1 GeV/nucleon. Just like Bertini INC [8], ISABEL can be used in MCNP6 with or without taking into account the preequilibrium reactions as described by MPM [12]. By default, after MPM, ISABEL is followed by the evaporation model EVAP [14]-[17] and the fission model RAL [20] (or the ORNL fission code HETFIS [19], if required so in the MCNP6 input file).

The ISABEL INC model [9, 61] is an extension by Yariv and Frankel [9] of the VEGAS code [62]. It has the capability of treating nucleus-nucleus as well as particle-nucleus interactions. It allows for interactions (“cascade-cascade”) between particles both of which are excited above the Fermi sea [63]. The nuclear density is represented by up to 16 density steps, rather than three as is in the Bertini INC [8] or seven in CEM03.03 [1]. It also allows antiproton annihilation [64], with emission of kaons and pions. In MCNP6, just like in its precursors MCNPX and LAHET, only projectiles with $A \leq 4$ are allowed for ISABEL.

Below, we provide a little more information about the physical assumptions and actual implementation of ISABEL, following mainly Ref. [61].

ISABEL is a “time-like-basis” Monte Carlo realization of an INC model for hadron-nucleus and nucleus-nucleus collisions. Hadrons included are nucleons, pions, anti-nucleons, and kaons. ISABEL is a direct generalization of the VEGAS [62] and ISOBAR [65] INC codes. As in ISOBAR [65], pion production and absorption modes are included in ISABEL via the Δ_{33} resonance (pion-nucleon isobar) formation in nucleon-nucleon scattering

$$N_1 + N_2 \iff \Delta_{33} , \tag{17}$$

$$\Delta_{33} \iff \pi + N . \quad (18)$$

As does CEM03.03, the original VEGAS [62] code uses the nuclear charge distribution obtained from the analysis of electron-nucleus scattering data, described by Eq. 1, with the same values for parameters c and a .

A step-function distribution is used to approximate the nuclear charge distribution. The nucleus is divided into several (usually 8 or 16) concentric regions, each of constant density. The ratio of proton to neutron density is assumed to be $Z/(A - Z)$ in all the regions.

The momentum distribution of nucleons in the nucleus is assumed to be that of degenerate Fermi gas with the same Fermi energy as discussed above for CEM03.03.

Due to the variation of the Fermi energy, the nuclear potentials of the protons and neutrons differ in the various density regions:

$$V_i = T_{F_i} + (\textit{Separation Energy}) . \quad (19)$$

The average pion potential is uncertain, and may be set to a constant, but because of the short pion mean free path, is generally ignored in ISABEL calculations. The average potential that the Δ feels is even more uncertain, and is taken after [66] as:

$$V_{\Delta^{++}} = V_p; V_{\Delta^+} = V_p + \frac{(V_p + V_n)}{3}; V_{\Delta^0} + \frac{(V_p + V_n)}{3} = V_n; V_{\Delta^-} = V_n . \quad (20)$$

Conservation of energy and momentum requires that the kinetic energy of the particles and their direction change as they cross density region boundary (refraction). If the impact angle at the region boundary is greater than the critical angle the particle is reflected. However, as pointed out in [62], “full” refraction gives generally worse results than particle kinetic energy correction without direction change, just as discussed above for CEM03.03. It was speculated [62] that in order to treat properly the refraction one should introduce energy dependence of the nuclear potential, as indicated by optical potential models. ISABEL may be used with the option of “full refraction” or just proper kinetic energy corrections on region boundaries. There is no option for energy dependent potential.

The Coulomb interactions between the target nucleus and the incident or emitted charged particle is explicitly considered in one way only: The refraction, or simple energy correction, of the particles entering or leaving the nuclear boundary is calculated taking into account the Coulomb potential there.

The nucleon-nucleon cross sections used in ISABEL are the on-mass-shell free nucleon-nucleon cross sections. Parameterization of [65] is used for the total, σ_{tot} , elastic, σ_{el} , and inelastic (pion production), σ_{inel} , cross sections. Parameterization of [67] is used for the elastic scattering angular distribution, $d\sigma_{el}/d\Omega$.

The types of outgoing nucleon and Δ in inelastic scattering, Eq. (17), are determined by isotopic spin considerations [68]. The mass of the $\Delta_{3,3}$ is chosen, according to Ref. [66], from the (normalized) distribution:

$$\begin{aligned} P(m_\Delta, E_{cm}^{N+N}) &= \textit{const.} \times \sigma_{tot}^{\pi^+ + p}(E_{cm}^{N+N}) \times F(m_\Delta, E_{cm}^{N+N}) , \\ m_\pi + m_N &< m_\Delta < m_\pi + m_N + 500 \text{ MeV} , \end{aligned} \quad (21)$$

where F is the two body phase factor for the produced $N + \Delta$. The angular distribution of the outgoing (N, Δ) is uncertain, and is taken, tentatively, from the distribution $P(\cos_{cm}) = 0.25 + 0.75 \times (\cos_{cm})^2$.

The types of outgoing nucleons in “pion capture” scattering, Eq. (18), are determined by isotopic spin considerations [68]. The capture cross sections used were calculated from the inverse process with the aid of the principle of detailed balance [68], using the one-pion-exchange model for Δ production process [39].

The Δ charge exchange process, $\Delta + N \rightarrow \Delta' + N'$, is considered as a two step process: first Δ decays into pion and nucleon and another nucleon absorbs the pion to become a “charge exchanged” Δ as shown schematically in Fig. 8.

The types of outgoing particles, are determined by isotopic spin considerations and the cross sections were calculated using the experimental π - N cross sections [39, 68]. Though, in principle, both the mass and charge of the Δ may change in this process, the assumption is made that the mass of the Δ does not change.

For processes involving intermediate Δ , $\pi + N \rightarrow \Delta \rightarrow \pi' + N'$, the relevant cross sections were calculated from the experimental πN scattering data [69]. If, after being created, Δ “charge exchanges” – it decays isotropically. However, if the Δ decays without intermediate interaction – the code calculates correctly the $\pi + N \rightarrow \pi' + N'$ kinematics.

The energy dependant Δ width is parameterized according to [66].

A pictorial example of an event simulated by ISABEL is shown on Fig. 9.

As mentioned above, ISABEL is a “time-like” type of INC. The most important advantage of the time-like basis Monte Carlo procedure is the possibility of changing the global properties of the system as the interaction proceeds. As a cascade develops, the density in the participating Fermi seas is depleted. Since the detailed nature of the density rearrangement is unknown, ISABEL adopted two extreme prescriptions:

Fast rearrangement. After each collision with a target partner, the density distribution ρ_i of the “partner type” (i denotes proton or neutron) in the target is instantaneously and uniformly reduced for the whole nucleus. In addition “distance restriction” is usually applied — any given particle is not allowed to interact within a distance smaller than some $r_{min,i}$ from its last interaction. There are few options for $r_{min,i}$, that should be close to d_i , the average (local) interparticle distance in the Fermi sea, and may depend on the local density of protons or neutrons.

Slow rearrangement. After each collision, a hole of radius r_{min} is punched in the density distribution configuration space around the position of the interaction. No more interactions are allowed in this hole. The holes may be either isospin dependant or isospin independent, *i.e.* ISABEL may punch them for protons and neutrons independently, with possibly different $r_{min,i}$ or punch holes for nucleons using common r_{min} . The slow rearrangement prescription with isospin dependant holes and $r_{min,i} = 1.1$ fm was found to be the best and was adopted as the default option in ISABEL.

The depletion of the Fermi seas affects the Pauli blocking. Two options for dealing with Pauli blocking are included in ISABEL:

Full Pauli blocking. After each interaction cascade nucleons are tested for Pauli principle violation. If cascade nucleon energy is lower than the target Fermi energy – the interaction is forbidden.

Partial Pauli blocking. After each interaction proton and neutron Fermi sea depletion

factors (ratio of actual to original number of particles in the Fermi sea) is calculated. If the energy of a cascade proton (neutron) generated in an interaction is lower than the target Fermi energy, a random number is compared to the depletion factor, and only if it is smaller – the reaction is forbidden. Intuitively, as the Fermi sea is depleted, cascade particles are allowed to fill the “empty” states below the Fermi energy. In such approximation, this depletion of the Fermi sea is “global” – it does not depend on position or energies of the particles lifted from the Fermi sea or those trying to fall into it. Pauli blocking contributes to extension of the mean free path, Λ , of nucleons and to prolongation of the lifetime of Δ in the nucleus (since it is forbidden to decay into a nucleon violating the Pauli principle).

In the *particle-nucleus* collision the Fermi sea of the target nucleus is treated as a continuous density distribution, whereas the incoming and the “cascade” particles are discrete particles of well defined position and momentum. In the *nucleus-nucleus* collision one has two Fermi seas interacting with each other and hence the following prescription is used: For the purpose of calculating the interactions between nucleons of the *projectile* Fermi sea and the nucleons in the *target* Fermi sea the *projectile* Fermi sea is assumed to consist of a gas of *discrete particles* whose positions in space and momenta are randomly chosen from the appropriate distribution. However for the purpose of calculating interaction between the (discrete) “cascade” particles and the Fermi sea of the projectile or target, the latter two distributions are considered *continuous*. This procedure was chosen in order to calculate the collision in the same manner as was done in the particle-nucleus INC calculation. It ensures the equal treatment of projectile and target, *i.e.* the Lorentz invariance of the calculation.

The INC model of *nucleus-nucleus* collisions involves a large number of “cascade” particles. The evolving particle density outside the target and projectile Fermi seas in such an interaction is high, and the relative distances between the energetic particles are quite small. The scattering between pairs of “cascade” particles, neglected in the VEGAS model [62] and early version of ISABEL, cannot be justified, and may lead to disagreement with experiments. The introduction of “cascade-cascade” interactions [63] led to significant improvement of the model.

The “cascade-cascade” interactions are treated, once again, as interactions of a discrete particle with continuous density. Each cascade particle is represented, in its rest-frame, by a spherical Gaussian density distribution $\rho(r)$ centered at its discrete position with standard deviation of 1 fm. Each cascade particle may thus interact with the continuous Fermi sea of the target and projectile and the continuous distribution of its fellow cascade particles. The only restriction is that two given cascade particles cannot interact more than once, until at least one of them interacted with a third particle. The interacting cascade particles are brought to common position and the reaction kinematics is calculated with “zero range.” This procedure conserves energy and momentum in each cascade-cascade interaction, but only “on the average” conserves angular momentum in cascade-cascade interactions.

In ISABEL, the projectile and target nucleons are initially bound in their respective nuclei by real potential wells (approximated by step-function distributions) that are uniquely determined for a degenerate Fermi gas by the nuclear density. Since the potential energy of a particle can not be transformed covariantly from one Lorentz frame to another, the *projectile nucleons* (*i.e.* projectile Fermi sea nucleons and cascade nucleons with momentum lower in the projectile frame of reference than in the target frame of reference) are assumed to feel the *projectile potential* while they are in the projectile volume and are treated as

free nucleons outside this volume. They do not feel the target potential. Similarly, the *target nucleons* feel the target potential while they are in the target volume and are treated as free nucleons outside this volume. After an interaction between target and projectile nucleons, the identity of the outgoing nucleons is determined according to their momentum relative to the projectile and the target frames. This procedure might be considered a crude approximation to a velocity dependent potential that vanishes for high velocities.

The residual excitation energies, linear and angular momenta of the target and projectile are calculated summing the hole and “below cutoff particle” energies and momenta and may be processed by a deexcitation code. The projectile velocity is kept constant during the collision, the recoil being calculated at the end.

More details on ISABEL can be found in [9, 61, 63, 64] and references therein.

2.5 The INC of INCL4.2

At present, MCNP6 uses the “standard” INCL4.2 version [6, 70] of the INC model developed at the university of Liege (INCL) by Prof. Joseph Cugnon and his students in collaboration with colleagues from CEA Saclay, France. INCL4.2 can describe successfully reactions induced by nucleons, pions, and complex particles d, t, ^3He , and ^4He at energies up to several GeV. In MCNP6, INCL4.2 is always followed by the ABLA code developed at GSI [7] to describe the evaporation and fission (if the nucleus is heavy enough to fission) stages of reactions, independently of what users would choose for the evaporation and fission models in their MCNP6 input files. INCL4.2 does not consider explicitly preequilibrium reactions after the INC stage of reactions. Newer and better versions of both INCL and ABLA are planned for incorporating in future versions of MCNP6.

Below, we provide a little more information about the physical assumptions and actual implementation of INCL4.2, following mainly Ref. [70].

The basic premises of the INCL model are schematically illustrated in Fig. 10. Particles are moving freely between instantaneous events and are called “avatars” (to distinguish from the usual meaning of “event,” namely a complete simulation or “realization” of the reaction). These avatars can be of three types: two-body collision, decay and transmission or reflection at the nuclear periphery. In INCL4.2, only three types of particles are considered: nucleons (n , p), Δ -isobars (4 charge states) and pions (3 charge states). The target is composed of pointlike particles. All particles are followed in space-time and are propagated in single steps between avatars, on a manner described below. The simulation is stopped according to a selfconsistent criterion, which constitutes a unique feature of INCL4.2. The properties of the exit channel are recorded and are transferred to an evaporation/fission module (ABLA).

In INCL4.2, before starting simulation of a reaction, the nucleons of the target are positioned at random, according to a distribution $f(r)$ which follows nuclear density (*i.e.* with the same shape), taken from electron scattering measurements. For target mass $A > 27$, a Woods-Saxon distribution is used up to a maximum distance R_{max} , fixed to $R_0 + 8a$. For $6 < A < 27$, a “modified harmonic oscillator” distribution is adopted and for $A < 6$, Gaussian density distributions are used. The values of R_0 and a are taken from electron scattering measurements and parametrized, for convenience, from Al to U, as $R_0 = (2.745 \times 10^{-4} A_T + 1.063) A_T^{1/3}$ fm, $a = 0.510 + 1.63 \times 10^{-4} A_T$ fm, and A_T is the target mass number.

Nucleon momenta are taken at random in a sphere of radius p_F , the Fermi momentum, equal to 270 MeV/c, a value corresponding to normal nuclear matter. The same distribution is used for protons and neutrons.

Actually, momentum and position are not taken independently. Momentum p is generated first at random and the position is taken at random inside a sphere of radius $R(p)$, which is implicitly given by:

$$\left(\frac{p}{p_F}\right)^3 = -\frac{1}{3N} \int_0^{R_{max}} \frac{df(r)}{dr} r^3 dr, \quad (22)$$

where N is a normalization constant

$$N = \int_0^{R_{max}} f(r) r^2 dr. \quad (23)$$

$R(p)$ is an increasing function going from 0 at $p = 0$ to R_{max} at $p = p_F$. It is shown in Ref. [6] that this procedure amounts to requiring that the nucleons with momentum contained in the interval $[p, p + dp]$ are contributing to the density profile by a horizontal slab corresponding to the vertical coordinates $R(p)$ and $R(p + dp)$, as shown in Fig. 11, or equivalently that nucleons with momentum p do not propagate farther than $R(p)$. The procedure is also equivalent to a phase space joint distribution function of the form

$$\frac{dn}{d^3\vec{r}d^3\vec{p}} \sim \frac{\theta(R(p) - r)\theta(p_F - p)}{R(p)^3}, \quad (24)$$

where $\theta(x)$ is the Heaviside function. Although this distribution obviously generates correlations between r and p coordinates, it nevertheless yields the constant Fermi gas distribution and the r -space distribution $f(r)$ after integration over \vec{r} and \vec{p} , respectively, as demonstrated in Ref. [6]. There are no other correlations. There is no attempt to have zero total momentum ($\sum \vec{p} = 0$) location of the barycenter at the origin ($\sum \vec{r} = 0$) nor zero total angular momentum ($\sum \vec{r} \times \vec{p} = 0$).

All target particles are sitting in a (fixed and constant) attractive square potential well, with a momentum-dependent radius $R(p)$ and a depth V_0 . The function $R(p)$ is such that, in absence of collisions, nucleons are moving while the average (over events) spatial and momentum distributions remain unaffected. It is clear from Fig. 11 that nucleons can be divided into groups of particles with the same momentum occupying given spheres in r -space. In absence of collisions, the distribution in r - and p -space remains the same on the average (this is a well-known property of a system of billiard board particles with initial momentum and directions at random bouncing elastically on the interior surface of a sphere). In other words, this indicates that particles with momentum larger than p_F experience a potential well with radius R_{max} (as for $p = p_F$).

The $r - p$ correlations introduced in INCL4.2 are not of the conventional type. They comply with the fact that high (kinetic) energy particles can propagate farther out than low energy particles, as they should, in accordance with the standard shell-model. In contrast

with the latter, particles keep the same momentum, be they in the center or in the (allowed) surface region of the nucleus.

The projectile-nucleon is incoming along the z -direction and is given at random in the xy -plane an impact parameter b inside a circle of radius $R_{max} = R_0 + 8a$. A sphere of the same radius centered on the middle of the target is defined as the “volume of calculation.” Nothing happens to the particles outside this volume. At $t = 0$ (beginning of the calculation), the incoming nucleon is positioned at the surface of the volume of calculation. As described above, this is also the surface of the potential well felt by this particle. It is considered that at $t = 0$, the incident nucleon has just entered the well. Therefore its total energy has increased by the value of the potential depth V_0 and its momentum has been increased accordingly (direction is not changed; no reflection, no refraction in the entrance channel). The choice of b_{max} guarantees a good compromise between computational efficiency and accurate evaluation of the total reaction cross section. Indeed only a small fraction (10^{-4}) of the interacting events beyond b_{max} is missed.

For an incident pion, the procedure is the same, except that the pion does not experience any average potential. For an incident light ion (d , t , ${}^3\text{He}$, and ${}^4\text{He}$), the procedure is more involved. First the incident ion has to be generated. In the rest frame of the latter, nucleons are given positions and momenta at random according to Gaussian laws, with *rms* values given in Table 1 of Ref. [6]. The values of the Gaussian parameters are either taken from the Paris potential for the deuteron, and from experiment or from realistic wave functions, for the other ions. In this case, $\sum \vec{r} = 0$ and $\sum \vec{p} = 0$ are imposed, simply by choosing the values for the last nucleon appropriately, possibly after a renewed generation of the first ones. The maximum impact parameter is taken as b_{max} defined above plus the *rms* radius of the ion. The transverse position of the ion center of mass is taken randomly in a circle of radius equal to this new value. The ion is then Lorentz-contracted along the collision axis and the longitudinal position of the ion is chosen in such a way that one of the nucleons is just touching the “interaction volume,” the other ones being outside. The ion is then “boosted”: 4-momenta undergo the Lorentz transformation corresponding to the velocity of the incident ion. They are finally corrected in order to comply with the energy content of the incoming ion.

At $t = 0$, all nucleons are set in motion with their initial velocity and are assumed to follow straight-line trajectories until an avatar occurs, *i.e.* until two of them achieve their minimum distance of approach, or until one of them hits the nuclear surface, or until a Δ -resonance decays. Due to the straight-line trajectories, the times at which these events occur can be predicted. The smallest of these times is selected and the particles are propagated in a single step. The simplicity of this propagation is a particular feature of the INCL model. After the occurrence of an avatar, straight-line motion is resumed until the next avatar, and so on. The process is followed up and terminated according to a criterion explained below.

Inelastic nucleon-nucleon collisions are dominated by the production of pions. At incident energies $T \leq 2$ GeV, there are good indications that pion production results from the production of a Δ -resonance followed by its decay. Although the Δ -resonance is short-lived, it has a good chance to interact with another nucleon before decaying. The philosophy of the standard INCL model is to propagate the Δ -isobars (instead of describing the NN inelastic collisions by the asymptotic channels in free space). Therefore, the following possible reactions are considered

$$NN \rightarrow NN, NN \rightarrow N\Delta, N\Delta \rightarrow N\Delta, \Delta\Delta \rightarrow \Delta\Delta, \pi N \rightarrow \Delta . \quad (25)$$

For any of the incident channels (NN , $N\Delta$, $\Delta\Delta$), the final channel is selected at random, by the standard method of comparing a random number with the ratio between elastic and inelastic cross sections. The relevant cross sections, as parameterized in INCL4.2, as well as the angular distributions, are given in Refs. [6, 71]. Elastic NN cross sections are of course taken directly from experiment. The $NN \rightarrow N\Delta$ cross section is taken as equal to the experimental inelastic NN cross section (pp and np , the nn cross section is taken equal to the pp cross section). The $N\Delta \rightarrow NN$ cross section is taken from the previous one by detailed balance:

$$\sigma_{N\Delta \rightarrow NN}(s) = f_{corr} \frac{1}{2} \left(\frac{p_{NN}}{p_{N\Delta}} \right)^2 \frac{1}{1 + \delta_{NN}} \sigma_{NN \rightarrow N\Delta}(s) . \quad (26)$$

In this equation, valid for definite charge states of the particles, p_{ab} is the momentum of the particles in the $c.m.$

$$p_{ab} = p_{ab}(s) = \frac{[(s - (m_a + m_b)^2)(s - (m_a - m_b)^2)]^{1/2}}{2\sqrt{s}} , \quad (27)$$

the $1/2$ factor comes from the spin degeneracies and the Kronecker symbol applies to the isospin states of the nucleons.

The $N\Delta \rightarrow N\Delta$ and $\Delta\Delta \rightarrow \Delta\Delta$ cross sections are taken as equal to the NN elastic cross section at the same $c.m.$ energy.

Due to the fermionic nature of the particles, the collision probability may be diminished as a consequence of the Pauli principle. Although it is a purely quantum effect, the reduction may fortunately be expressed in terms of phase space density. In INCL4, Pauli blocking is implemented in this spirit.

Let consider as an example the case of two body collisions $a + b \rightarrow c + d$ with two nucleons in the final state and let \vec{r}_i and \vec{p}_i ($i = c, d$) denote the positions and momenta of the nucleons just after the realization of the collision (the avatar). Phase space occupation probabilities f_i are estimated by counting the nucleons lying in phase space in a small test volume centered of the representative point of nucleon i in phase space. They are given by:

$$f_i = \frac{1}{2} \frac{(2\pi\hbar)^3}{\frac{4\pi}{3} r_{PB}^3 \frac{4\pi}{3} p_{PB}^3} \sum_{k \neq i} \theta(r_{PB} - |\vec{r}_k - \vec{r}_i|) \theta(p_{PB} - |\vec{p}_k - \vec{p}_i|) , \quad (28)$$

where the summation runs over nucleons of the same isospin state as nucleon i and where θ is the Heaviside function. The factor $1/2$ stands for spin degeneracy (nucleon spin is not considered). The parameters r_{PB} and p_{PB} define the size of the test volume (an hypersphere) in phase space. They should not be too small, otherwise the estimated occupation probability can be vanishing almost all the time and they should not be too large, otherwise the variations of the occupation probability in the occupied phase space can be missed. In INCL4, r_{PB} and p_{PB} have been taken just large enough for results (in typical cases) to be more or less insensitive to moderate modifications on these parameters: $r_{PB} = 3.18$ fm and $p_{PB} = 200$ MeV/c, which corresponds to ~ 2.3 natural units of phase space. We remind that in the

ground state of normal nuclear matter there is one nucleon (of given spin and isospin) per natural unit. It is generally considered that there cannot be more than one particle per unit phase space in any circumstance and that this density is more or less achieved in the ground state of actual (at least heavy) nuclei.

The collision will be allowed stochastically with a probability $P = (1 - f_c)(1 - f_d)$. Pauli blocking is not applied to Δ -isobars (for a collision with a Δ and a nucleon in the final state, there is only one blocking factor). On the other hand, it is enforced for nucleons issued from Δ -decays.

An original feature of INCL4.2 is the consistent determination of the stopping time, *i.e.* the time at which the cascade should be stopped. A criterion has been adopted which is based on physical results concerning the time-dependence of several key physical quantities when averaged over events. Examples are given in Fig. 12 below. One can see that both the excitation energy of the target nucleus and the average kinetic energy of the ejectiles assume large values at early times, decrease rapidly until some time, after which they vary much more slowly. The time derivative of the excitation energy and the anisotropy of the momentum distribution of the participants sitting inside the target, offer a similar pattern with a rapid variation followed by a much slower one. For all of them, the change of regime occurs *at the same time*, defined within a few fm/c. This observation suggests that the regime of fast variation, typical of a cascade, gives place at a rather well defined time to a regime of softer variation, typical of an evaporation. In INCL4.2, the cascade is stopped at this common time, called the stopping time t_{stop} . It has been sampled once for all and parameterized as

$$t_{stop} = f_{stop} t_c \left(\frac{A_T}{208} \right)^{0.16}, \quad (29)$$

with $f_{stop} = 1$ and $t_c = 70$ fm/c. This parametric form seems reasonable for the range of energy and target mass under interest, but may be improved at the border of this range, by using another value for f_{stop} .

An event is stopped when the clock for a foreseen avatar gives a time larger than t_{stop} . Some events may be stopped earlier. An event may be stopped at the very beginning, if the initial time list for the collision avatars is empty. This happens mainly for peripheral events. Such an event is named a *void event*. An event may also terminate at a time earlier than t_{stop} if the list of times becomes empty when it is updated. In a no-void event, it may happen that no collision has taken place (due to Pauli blocking for instance) and that the incident particle has left the interaction volume with its incident energy. Such events, together with the void events are named “transparent event.” The other events are called “interacting events.” Transparent events are just disregarded (but they are counted for cross section evaluation, see later). The other events, after they are stopped, may possibly be completed by the decay of the remaining Δ -isobars, if any. The Pauli blocking is not applied in this case and the resulting nucleons are considered as belonging to the remnant.

It is instructive to detail how INCL4.2 handles conservation laws. The most important conservation laws can in general be formulated as follows:

$$A_P + A_T = A_{ej} + A_{rem}, \quad (30)$$

$$Z_P + Z_T = Z_{ej} + Z_\pi + Z_{rem}, \quad (31)$$

$$\vec{p}_P + \vec{p}_T = \vec{p}_{ej} + \vec{p}_\pi + \vec{p}_{rem} , \quad (32)$$

$$T_P = K_{ej} + W_\pi + T_{rec} + E^* + S , \quad (33)$$

$$\vec{l}_P = \vec{l}_{ej} + \vec{l}_\pi + \vec{l}_{rem} + \vec{l}^* , \quad (34)$$

for baryon number, charge, momentum, energy and angular momentum, respectively. Let consider a projectile P colliding with a target T and generating baryonic ejectiles, pions and a remnant (the remaining nucleus at the end of the cascade). In Eq. (33), K_{ej} is the kinetic energy of the ejectiles, W_π is the total energy of the pions, T_{rec} is the recoil energy of the remnant, E^* is the excitation energy of the remnant, and S is the separation energy (*i.e.* minus the Q -value of the reaction). Strictly speaking, energy conservation law should include rest mass energies. They have been eliminated from Eq. (33) owing to the use of Eq. (30). The other notations are self-explanatory.

In INCL4.2, conservation laws (30), (31), and (33) are exactly fulfilled. On the contrary, momentum (Eq. (32)) and angular momentum (Eq. (34)) are not conserved. Momentum is conserved during collisions but not at the entrance or exit of particles. Angular momentum is not conserved, even at the level of the collisions. However, the results of the cascade can be used to evaluate with reasonable accuracy the momentum, angular momentum and recoil energy of the remnant.

More details on INCL4.2 can be found in [6, 52, 70, 71] and references therein.

3 Preequilibrium Reactions

As discussed in the previous section, the intranuclear cascade models are used to describe the so-called “fast”, or “energetic”, or “direct” stages of nuclear reactions. It is believed that such processes occur during the first $\sim 10^{-23} - 10^{-20}$ seconds of reactions, during which only “direct” interactions of the projectile or of “secondary” cascade particles with intranuclear nucleons take place. Such a treatment of reactions is well grounded at bombarding energies of the order of ~ 100 MeV and higher and is not expected to work well at lower energies.

At the other extreme, at low energies of only a few tens of MeV and lower, it is usually assumed that the projectile is captured by the target nucleus, and that the resulting “compound nucleus” attains statistical equilibrium without prior particle emission. The decay of the long-lived ($\sim 10^{-18} - 10^{-16}$ sec) compound nucleus may then be treated by equilibrium statistical mechanics. The deexcitation of compound nuclei is believed to take place via “evaporation” of particles and light fragments, or via fission, if the nucleus is heavy enough to fission. Such reactions are discussed in the next sections.

From a general logical point of view, it is hard to understand that we may have only “fast” or “energetic” and “slow” or “low-energy” interactions, and nothing in between them. It is natural to expect that an intermediate stage, both from the point of view of the time of interaction and of the energy involved, should exist. Such intermediate reactions should occur before the equilibrium compound nucleus is created, therefore, can be called as “preequilibrium” reactions.

Most important, from an experimental point of view, in many spectra, continuous high energy components were observed that were consistent neither with predictions of the compound nucleus (evaporation/fission) model nor with existing direct reaction (or INC) models.

In recent decades, these phenomena have been treated by classical or quantum preequilibrium models that formulate the decay into the continuum of a system with an initial partition of projectile energy between relatively few (intrinsic) degrees of freedom, progressing through more complicated configurations until an equilibrium distribution of energy is attained (see, *e.g.* Refs. [72] – [75] for good reviews of preequilibrium models).

MCNP6 considers only two classical preequilibrium reaction models, namely: 1) the latest version of the Modified Exciton Model (MEM) [10, 11] used (always) with the CEM03.03 and LAQGSM03.03 event generators, and 2) the Multistage Preequilibrium Model (MPM) version of the exciton model [12], used “by default” after the Bertini INC and ISABEL, but can be omitted, if required so in the MCNP6 input file. INCL4.2 does not use any preequilibrium models. Below we discuss briefly both MEM and MPM.

3.1 Preequilibrium Reactions in CEM03.03 and LAQGSM03.03

The preequilibrium interaction stage of nuclear reactions is considered by the current CEM and LAQGSM in the framework of the latest version of the Modified Exciton Model (MEM) [10, 11] as implemented in CEM03.03 [1]. At the preequilibrium stage of a reaction, all possible nuclear transitions changing the number of excitons n with $\Delta n = +2, -2$, and 0, as well as all possible multiple subsequent emissions of $n, p, d, t, {}^3\text{He}$, and ${}^4\text{He}$ are taken into account. The corresponding system of master equations describing the behavior of a nucleus at the preequilibrium stage is solved by the Monte-Carlo technique [2].

For a preequilibrium nucleus with excitation energy E and number of excitons $n = p + h$, the partial transition probabilities changing the exciton number by Δn are

$$\lambda_{\Delta n}(p, h, E) = \frac{2\pi}{\hbar} |M_{\Delta n}|^2 \omega_{\Delta n}(p, h, E) . \quad (35)$$

The emission rate of a nucleon of type j into the continuum is estimated according to the detailed balance principle

$$\begin{aligned} \Gamma_j(p, h, E) &= \int_{V_j^c}^{E-B_j} \lambda_c^j(p, h, E, T) dT , \\ \lambda_c^j(p, h, E, T) &= \frac{2s_j + 1}{\pi^2 \hbar^3} \mu_j \mathfrak{R}_j(p, h) \frac{\omega(p-1, h, E - B_j - T)}{\omega(p, h, E)} T \sigma_{inv}(T) , \end{aligned} \quad (36)$$

where s_j, B_j, V_j^c , and μ_j are the spin, binding energy, Coulomb barrier, and reduced mass of the emitted particle, respectively. The factor $\mathfrak{R}_j(p, h)$ ensures the condition for the exciton chosen to be the particle of type j and can easily be calculated by the Monte-Carlo technique.

For the inverse cross section, σ_{inv} , MEM uses the Dostrovsky’s formula [13] for all emitted nucleons and complex particles ($d, t, {}^3\text{He}$, and ${}^4\text{He}$):

$$\sigma_{inv}(\epsilon) = \sigma_g \alpha \left(1 + \frac{\beta}{\epsilon} \right) , \quad (37)$$

which is often written as

$$\sigma_{inv}(\epsilon) = \begin{cases} \sigma_g c_n (1 + b/\epsilon) & \text{for neutrons} \\ \sigma_g c_j (1 - V/\epsilon) & \text{for charged particles ,} \end{cases}$$

where $\sigma_g = \pi R_d^2$ [fm²] is the geometrical cross section. “*d*” denotes the “daughter” nucleus with mass and charge numbers A_d and Z_d produced from the “parent” nucleus “*i*” with mass and charge numbers A_i and Z_i after the emission of the particle “*j*” with mass and charge numbers A_j and Z_j and kinetic energy ϵ ; $R_d = r_0 A_d^{1/3}$, and $r_0 = 1.5$ fm. α and β are defined as:

$$\alpha = 0.76 + 2.2A_d \text{ MeV},$$

$$\beta = \frac{2.12A_d^{-2/3} - 0.05}{0.76 + 2.2A_d^{-1/3}} \text{ MeV},$$

and c_j is estimated by interpolation of the tabulated values published in Ref. [13].

The Coulomb barrier (in MeV) is estimated as:

$$V = k_j Z_j Z_d e^2 / R_c, \quad (38)$$

where $R_c = r_0(A_d^{1/3} + A_j^{1/3})$, $r_0 = 1.5$ fm, and the penetrability coefficients k_j are calculated via interpolation of the tabulated values published in Ref. [13].

Assuming an equidistant level scheme with the single-particle density g , the level density of the n -exciton state can be calculated as [76]

$$\omega(p, h, E) = \frac{g(gE)^{p+h-1}}{p!h!(p+h-1)!}. \quad (39)$$

This expression should be substituted into Eq. (36). For the transition rates (35), one needs the number of states taking into account the selection rules for intranuclear exciton-exciton scattering. The appropriate formulae have been derived by Williams [77] and later corrected for the exclusion principle and indistinguishability of identical excitons in Refs. [78, 79]:

$$\begin{aligned} \omega_+(p, h, E) &= \frac{1}{2}g \frac{[gE - \mathcal{A}(p+1, h+1)]^2}{n+1} \left[\frac{gE - \mathcal{A}(p+1, h+1)}{gE - \mathcal{A}(p, h)} \right]^{n-1}, \\ \omega_0(p, h, E) &= \frac{1}{2}g \frac{[gE - \mathcal{A}(p, h)]}{n} [p(p-1) + 4ph + h(h-1)], \\ \omega_-(p, h, E) &= \frac{1}{2}gph(n-2), \end{aligned} \quad (40)$$

where $\mathcal{A}(p, h) = (p^2 + h^2 + p - h)/4 - h/2$. By neglecting the difference of matrix elements with different Δn , $M_+ = M_- = M_0 = M$, the value of M for a given nuclear state is estimated by associating the $\lambda_+(p, h, E)$ transition with the probability for quasi-free scattering of a nucleon above the Fermi level on a nucleon of the target nucleus:

$$\frac{\langle \sigma(v_{rel})v_{rel} \rangle}{V_{int}} = \frac{\pi}{\hbar} |M|^2 \frac{g[gE - \mathcal{A}(p+1, h+1)]}{n+1} \left[\frac{gE - \mathcal{A}(p+1, h+1)}{gE - \mathcal{A}(p, h)} \right]^{n-1}. \quad (41)$$

Here, V_{int} is the interaction volume estimated as $V_{int} = \frac{4}{3}\pi(2r_c + \lambda/2\pi)^3$, with the de Broglie wave length $\lambda/2\pi$ corresponding to the relative velocity $v_{rel} = \sqrt{2T_{rel}/m_N}$. A value of the order of the nucleon radius is used for r_c in the CEM: $r_c = 0.6$ fm.

The averaging in the left-hand side of Eq. (41) is carried out over all excited states taking into account the Pauli principle in the approximation

$$\langle \sigma(v_{rel})v_{rel} \rangle \simeq \langle \sigma(v_{rel}) \rangle \langle v_{rel} \rangle . \quad (42)$$

The averaged cross section $\langle \sigma(v_{rel}) \rangle$ is calculated by the Monte-Carlo simulation method and by introducing a factor η effectively taking into account the Pauli principle exactly as is done in the Fermi-gas model.

$$\sigma(v_{rel}) = \frac{1}{2}[\sigma_{pp}(v_{rel}) + \sigma_{pn}(v_{rel})]\eta(T_F/T) , \text{ where} \quad (43)$$

$$\eta(x) = \begin{cases} 1 - \frac{7}{5}x, & \text{if } x \leq 0.5 , \\ 1 - \frac{7}{5}x + \frac{2}{5}x(2 - \frac{1}{x})^{5/2}, & \text{if } x > 0.5 . \end{cases} \quad (44)$$

Here, v_{rel} is the relative velocity of the excited nucleon (exciton) and the target nucleon in units of the speed of light and T is the kinetic energy of the exciton. The free-particle interaction cross sections $\sigma_{pp}(v_{rel})$ and $\sigma_{pn}(v_{rel})$ in Eq. (43) are estimated using the relations suggested by Metropolis *et al.* [80]

$$\begin{aligned} \sigma_{pp}(v_{rel}) &= \frac{10.63}{v_{rel}^2} - \frac{29.92}{v_{rel}} + 42.9 , \\ \sigma_{pn}(v_{rel}) &= \frac{34.10}{v_{rel}^2} - \frac{82.2}{v_{rel}} + 82.2 , \end{aligned} \quad (45)$$

where the cross sections are given in mb.

The relative kinetic energy of colliding particles necessary to calculate $\langle v_{rel} \rangle$ and the factor η in Eqs. (43, 44) are estimated in the so-called “right-angle-collision” approximation [10], *i.e.* as a sum of the mean kinetic energy of an excited particle (exciton) measured from the bottom of the potential well $T_p = T_F + E/n$ plus the mean kinetic energy of an intranuclear nucleon partner $T_N = 3T_F/5$, that is $T_{rel} = T_p + T_N = 8T_F/5 + E/n$.

Combining (35), (39), and (41), the transition rates can be written as:

$$\begin{aligned} \lambda_+(p, h, E) &= \frac{\langle \sigma(v_{rel})v_{rel} \rangle}{V_{int}} , \\ \lambda_0(p, h, E) &= \frac{\langle \sigma(v_{rel})v_{rel} \rangle}{V_{int}} \frac{n+1}{n} \left[\frac{gE - \mathcal{A}(p, h)}{gE - \mathcal{A}(p+1, h+1)} \right]^{n+1} \frac{p(p-1) + 4ph + h(h-1)}{gE - \mathcal{A}(p, h)} , \\ \lambda_-(p, h, E) &= \frac{\langle \sigma(v_{rel})v_{rel} \rangle}{V_{int}} \left[\frac{gE - \mathcal{A}(p, h)}{gE - \mathcal{A}(p+1, h+1)} \right]^{n+1} \frac{ph(n+1)(n-2)}{[gE - \mathcal{A}(p, h)]^2} . \end{aligned} \quad (46)$$

CEM considers the possibility of fast d , t , ${}^3\text{He}$, and ${}^4\text{He}$ emission at the preequilibrium stage of a reaction in addition to the emission of nucleons. It is assumed that in the course of a reaction p_j excited nucleons (excitons) are able to condense with probability γ_j forming a complex particle which can be emitted during the preequilibrium state. A modification of Eq. (36) for the complex-particle emission rates is described in detail in Refs. [2]. The “condensation” probability γ_j is estimated in those references as the overlap integral of the wave function of independent nucleons with that of the complex particle (cluster)

$$\gamma_j \simeq p_j^3 (V_j/V)^{p_j-1} = p_j^3 (p_j/A)^{p_j-1} . \quad (47)$$

This is a rather crude estimate. In the usual way the values γ_j are taken from fitting the theoretical preequilibrium spectra to the experimental ones, which gives rise to an additional, as compared to (47), dependence of the factor γ_j on p_j and excitation energy (see more details and proper references in [1]).

The single-particle density g_j for complex-particle states is found in the CEM by assuming the complex particles move freely in a uniform potential well whose depth is equal to the binding energy of this particle in a nucleus [2]

$$g_j(T) = \frac{V(2s_j + 1)(2\mu_j)^{3/2}}{4\pi^2\hbar^3} (T + B_j)^{1/2} . \quad (48)$$

This is a rather crude approximation and it does not provide a good prediction of emission of preequilibrium α particles. In CEM03.03, to improve the description of preequilibrium complex-particle emission, γ_j is calculated by multiplying the estimate provided by Eq. (47) by an empirical coefficient $M_j(A, Z, T_0)$ whose values are fitted to available nucleon-induced experimental complex-particle spectra. More details and proper references on this feature of CEM03.03 can be found in Refs. [1, 3].

CEM and LAQGSM predict forward-peaked (in the laboratory system) angular distributions for preequilibrium particles. For instance, CEM03.03 assumes that a nuclear state with a given excitation energy E^* should be specified not only by the exciton number n but also by the momentum direction Ω . Following Ref. [81], the master equation (11) from Ref. [2] can be generalized for this case provided that the angular dependence for the transition rates λ_+ , λ_0 , and λ_- (Eq. (46) is factorized. In accordance with Eqs. (41) and (42), in the CEM it is assumed that

$$\langle \sigma \rangle \rightarrow \langle \sigma \rangle F(\Omega) , \quad (49)$$

where

$$F(\Omega) = \frac{d\sigma^{free}/d\Omega}{\int d\Omega' d\sigma^{free}/d\Omega'} . \quad (50)$$

The scattering cross section $d\sigma^{free}/d\Omega$ is assumed to be isotropic in the reference frame of the interacting excitons, thus resulting in an asymmetry in both the nucleus center-of-mass and laboratory frames. The angular distributions of preequilibrium complex particles are assumed [2] to be similar to those for the nucleons in each nuclear state.

This calculation scheme is easily realized by the Monte-Carlo technique. It provides a good description of double differential spectra of preequilibrium nucleons and a not-so-good but still satisfactory description of complex-particle spectra from different types of nuclear reactions at incident energies from tens of MeV to several GeV. For incident energies below about 200 MeV, Kalbach [82] has developed a phenomenological systematics for preequilibrium-particle angular distributions by fitting available measured spectra of nucleons and complex particles. As the Kalbach systematics are based on measured spectra, they describe very well the double-differential spectra of preequilibrium particles and generally provide a better agreement of calculated preequilibrium complex-particle spectra with data than does the CEM approach based on Eqs. (49, 50). This is why in CEM03.03 and LAQGSM03.03, the Kalbach systematics [82] have been incorporated to describe angular distributions of both preequilibrium nucleons and complex particles at incident energies up to 210 MeV. At higher energies, we use the CEM approach based on Eqs. (49, 50).

By “preequilibrium particles” particles which are emitted after the cascade stage of a reaction but before achieving statistical equilibrium at a time t_{eq} are meant, which is fixed by the condition $\lambda_+(n_{eq}, E) = \lambda_-(n_{eq}, E)$ from which one can get

$$n_{eq} \simeq \sqrt{2gE} . \quad (51)$$

At $t \geq t_{eq}$ (or $n \geq n_{eq}$), the behavior of the remaining excited compound nucleus is described in the framework of both the Weisskopf-Ewing statistical theory of particle evaporation [83] and fission competition according to Bohr-Wheeler theory [84].

The parameter g entering into Eqs. (46) and (51) is related to the level-density parameter of single-particle states $a = \pi^2 g/6$. At the preequilibrium stage, the level-density parameter a is calculated with the approximation derived in Ref. [85] in the form proposed initially by Ignatyuk *et al.* [86], following the method by Iljinov *et al.* [87]:

$$a(Z, N, E^*) = \tilde{a}(A) \left\{ 1 + \delta W_{gs}(Z, N) \frac{f(E^* - \Delta)}{E^* - \Delta} \right\} , \quad (52)$$

where

$$\tilde{a}(A) = \alpha A + \beta A^{2/3} B_s \quad (53)$$

is the asymptotic Fermi-gas value of the level-density parameter at high excitation energies. Here, B_s is the ratio of the surface area of the nucleus to the surface area of a sphere of the same volume (for the ground state of a nucleus, $B_s \approx 1$), and

$$f(E) = 1 - \exp(-\gamma E) . \quad (54)$$

E^* is the total excitation energy of the nucleus, related to the “thermal” energy U by: $U = E^* - E_R - \Delta$, where E_R and Δ are the rotational and pairing energies, respectively.

CEM03.03 uses the shell correction $\delta W_{gs}(Z, N)$ by Möller *et al.* [88] and the pairing energy shifts from Möller, Nix, and Kratz [89]. The values of the parameters α , β , and γ were derived in Ref. [85] by fitting the the same data analyzed by Iljinov *et al.* [87] (in Ref. [85] it was discovered that Iljinov *et al.* used $11/\sqrt{A}$ for the pairing energies Δ in deriving their level-density systematics instead of the value of $12/\sqrt{A}$ stated in Ref. [87]; it was also found several misprints in the nuclear level-density data shown in their Tables. 1 and 2 used in the fit):

$$\alpha = 0.1463, \beta = -0.0716, \text{ and } \gamma = 0.0542 .$$

Several investigations have shown that the standard version of the CEM [2] provides an overestimation of preequilibrium particle emission from different reactions we have analyzed (see more details in [90, 91]). One way to solve this problem suggested in Ref. [90] is to change the criterion for the transition from the cascade stage to the preequilibrium one, as described in previous section. Another easy way suggested in Ref. [90] to shorten the preequilibrium stage of a reaction is to arbitrarily allow only transitions that increase the number of excitons, $\Delta n = +2$, *i.e.*, only allow the evolution of a nucleus toward the compound nucleus. In this case, the time of the equilibration will be shorter and fewer preequilibrium particles will be emitted, leaving more excitation energy for the evaporation. Such a “never-come-back” approach is used by some other exciton models, for instance, by

the Multistage Preequilibrium Model (MPM) [12] presented in the following subsection. This approach was used in the CEM2k [90] version of the CEM and it allowed the authors of Ref. [90] to describe much better the p+A reactions measured at GSI in inverse kinematics at energies around 1 GeV/nucleon. Nevertheless, the “never-come-back” approach seems unphysical, therefore CEM and LAQGSM no longer use it at present. The problem of emitting fewer preequilibrium particles in the CEM is addressed now following Veselský [92]. It is assumed that the ratio of the number of quasi-particles (excitons) n at each preequilibrium reaction stage to the number of excitons in the equilibrium configuration n_{eq} , corresponding to the same excitation energy, to be a crucial parameter for determining the probability of preequilibrium emission P_{pre} . This probability for a given preequilibrium reaction stage is evaluated using the formula

$$P_{pre}(n/n_{eq}) = 1 - \exp\left(-\frac{(n/n_{eq} - 1)}{2\sigma_{pre}^2}\right) \quad (55)$$

for $n \leq n_{eq}$ and equal to zero for $n > n_{eq}$. The basic assumption leading to Eq. (55) is that P_{pre} depends exclusively on the ratio n/n_{eq} . The parameter σ_{pre} is a free parameter and it is assumed no dependence on excitation energy [92]. Test-calculations of several reactions using different values of σ_{pre} show that an overall reasonable agreement with available data can be obtained using $\sigma_{pre} = 0.4$ – 0.5 (see Fig. 11 in Ref. [91]). In CEM03.03, the fixed value $\sigma_{pre} = 0.4$ was chosen and Eqs. (51, 55) are used as criteria for the transition from the preequilibrium stage of reactions to evaporation, instead of using the “never-come-back” approach along with Eq. (51), as was done in CEM2k.

Algorithms of many preequilibrium routines are changed in CEM03.03 and almost all these routines are rewritten, which has speeded up the code significantly. Finally, some bugs were fixed as previously mentioned.

3.2 Preequilibrium Reactions Simulated with the Bertini INC and ISABEL

The Multistage Preequilibrium Model (MPM) [12] was developed at LANL as a Monte Carlo implementation of the exciton preequilibrium model which may be used in transport codes to replace the intranuclear cascade at low energies and, at higher energies, to supplement the intranuclear cascade as a subsequent preequilibrium emission model before application of the evaporation model. Initially, MPM was developed in a stand-alone code called PREEQ1; later, it was implemented in LAHET [18], MCNPX [54], and, finally, in MCNP6. In order to develop MPM, models and methods used in the well known “analytical” preequilibrium codes GNASH [93], PRECO [94], and GRYPHON [95] have been supplemented by techniques peculiar to the Monte Carlo method or dictated by considerations of computing efficiency when using the Monte Carlo method.

Like MEM [10, 11] discussed in the previous subsection, MPM considers at each preequilibrium stage a possibility of emission of a neutron, proton, deuteron, triton, ^3He , or ^4He ; alternatively, the nuclear configuration may evolve toward an equilibrated compound nucleus. Actually, from a general physics idea point of view, MPM is quite similar to MEM. However, these two preequilibrium models differ in several details, the most important differences being in:

- 1) the master equation describing the evolution of the system;
- 2) approximation of the transaction matrix element;
- 3) calculation of the inverse cross sections;
- 4) level density parameter used in calculations;
- 5) angular distribution of preequilibrium particles;
- 6) initial number of excitons after INC.

Below we address briefly all these points as implemented in MPM.

1) In both MEM and MPM, the probability of finding the system at time t in the $E\alpha$ state, $P(E, \alpha, t)$, is given by the differential equation:

$$\frac{\delta P(E, \alpha, t)}{\delta t} = \sum_{\alpha \neq \alpha'} [\lambda(E\alpha, E\alpha')P(E, \alpha', t) - \lambda(E\alpha', E\alpha)P(E, \alpha, t)]. \quad (56)$$

Here $\lambda(E\alpha, E\alpha')$ is the energy-conserving probability rate, defined in the first-order time-dependent perturbation theory as

$$\lambda(E\alpha, E\alpha') = \frac{2\pi}{\hbar} |\langle E\alpha | V | E\alpha' \rangle|^2 \omega_\alpha(E). \quad (57)$$

The matrix element $\langle E\alpha | V | E\alpha' \rangle$ is believed to be a smooth function of energy, and $\omega_\alpha(E)$ is the density of the final states of the system.

As long as the transition probabilities $\lambda(E\alpha, E\alpha')$ are time-independent, the waiting time for the system in the $E\alpha$ state has an exponential distribution (Poisson flow) with the average lifetime $\hbar/\Lambda(\alpha, E) = \hbar/\sum'_\alpha \lambda(E\alpha, E\alpha')$. This prompts a simple method of solving the related system of Eq. (56): simulation of the random process by the Monte-Carlo technique. In this treatment, it is possible to generalize the exciton model to all nuclear transitions with $\Delta n = 0, \pm 2$, and the multiple emission of particles and to depletion of nuclear states due to particle emission. In this case the system (56) becomes [2]:

$$\begin{aligned} \frac{\delta P(E, \alpha, t)}{\delta t} &= -\Lambda(n, E)P(E, n, t) \\ &+ \lambda_+(n-2, E)P(E, n-2, t) + \lambda_0(n, E)P(E, n, t) + \lambda_-(n+2, E)P(E, n+2, t) \quad (58) \\ &+ \sum_j \int dT \int dE' \lambda_j(n, E, T) \times P(E', n+n_j, t) \delta(E' - E - B_j - T). \end{aligned}$$

This master equation is written in its general form, as used in MEM. However, in MPM, it is assumed [12] that:

$$\lambda_+(n, E) \gg \lambda_-(n, E) \text{ and that: } \lambda_-(n, E) \approx \lambda_0(n, E) \approx 0. \quad (59)$$

In other words, in contrast to MEM, MPM considers only transactions towards the equilibration, with $\Delta n = +2$, and neglects all transactions with $\Delta n = -2$ and $\Delta n = 0$. Note that this “never-come-back” approach is used also by other preequilibrium models, like in FLUKA [96], and was used in an older version of CEM, CEM2k [90].

2) As noted above, by neglecting the difference of matrix elements with different Δn , $M_+ = M_- = M_0 = M$, the transaction matrices elements M in MEM is estimated by

associating the $\lambda_+(p, h, E)$ transition with the probability for quasi-free scattering of a nucleon above the Fermi level on a nucleon of the target nucleus, as defined by Eq. (41). On the other hand, MPM considers only $\Delta n = +2$ transactions and their matrix elements are parameterized following Refs. [93, 94] as:

$$\begin{aligned}
|M^2| &= \frac{kn}{A^3 E} \left[\frac{E/n}{7 \text{ MeV}} \frac{E/n}{2 \text{ MeV}} \right]^{1/2} \quad \text{for } E/n < 2 \text{ MeV}, \\
&= \frac{kn}{A^3 E} \left[\frac{E/n}{7 \text{ MeV}} \right]^{1/2} \quad \text{for } 2 \text{ MeV} \leq E/n < 7 \text{ MeV}, \\
&= \frac{kn}{A^3 E} \quad \text{for } 7 \text{ MeV} \leq E/n < 15 \text{ MeV}, \\
&= \frac{kn}{A^3 E} \left[\frac{15 \text{ MeV}}{E/n} \right]^{1/2} \quad \text{for } 15 \text{ MeV} \leq E/n,
\end{aligned}$$

where A , E , and n are the mass number of the nucleus, its excitation energy, and the number of excitons, respectively. The constant k is taken to be 135 MeV^3 [94].

3) For the inverse cross section $\sigma_{inv}(\epsilon) \equiv \sigma_b(\epsilon)$, MPM employs the geometric cross section of reference [94] with a Coulomb barrier penetration factor $T_b(\epsilon)$:

$$\sigma_b(\epsilon) = \pi(\mathfrak{R}A_r^{1/3} + R_b + \lambda(\epsilon)/(2\pi))^2 T_b(\epsilon), \quad (60)$$

where:

A_r is the mass number of the potential residual nucleus;

$\mathfrak{R} = 1.23 \text{ fm}$;

$R_b = 0$ for $b = n$ and p ;

$R_b = 0.8 \text{ fm}$ for $b = d, t$, and ${}^3\text{He}$;

$R_b = 1.2 \text{ fm}$ for $b = {}^4\text{He}$;

$\lambda(\epsilon)/(2\pi)$ is the (non relativistic) reduced channel wavelength;

$T_n(\epsilon) = 1$ for neutrons. The Coulomb barrier penetration factor is given by

$$T_b(\epsilon) = (1 - k_b V_b/\epsilon), \quad (61)$$

with the Coulomb energy V_b given by

$$V_b = \frac{z_b(Z - z_b)e^2}{\mathfrak{R}_c A_r^{1/3} + R_b}$$

for $\mathfrak{R}_c = 1.70 \text{ fm}$. The factors $k_b < 1$ reflect barrier penetration and are obtained from a parameterization of the s-wave Coulomb barrier transmission factor at the condition $\epsilon = V_b$.

4) Like in MEM [10, 11], the level density formulation employed in MPM is that of Williams [77, 78] (see Eqs. (39) and (40)). But in contrast to MEM, to obtain the single-particle level density parameter g , MPM uses the energy dependent formulation of Ignatyuk [86] as implemented in GNASH [93] with the provision that

$$\lim_{E \rightarrow 0} g(E) = g_0$$

where g_0 is the level density parameter obtained from Gilbert and Cameron [97].

5) In contrast to MEM [10, 11], the emission of the second and subsequent preequilibrium particles from the excited nucleus is treated by MPM as isotropic in the center of mass (COM) system; the assumption is made that memory of the incident particle direction is lost after the emission of one particle. However, this is not the case for first stage emission. For the first stage emission, just like MEM does, MPM uses the parameterization of the angular distribution based on an analysis of experimental data developed by Kalbach [82].

As described in Ref. [82], the probability distribution for $\mu = \cos\theta$ is given by

$$p(\mu) = \frac{a}{2 \sinh a} [\cosh a\mu + F_{msd} \sinh a\mu] , \quad (62)$$

where θ is the emission angle with respect to the direction of the incident particle. The quantity a is determined by the Kalbach parameterization [82]. The parameter F_{msd} is defined [94] as that fraction of the strength of the emitting state which arises only from unbound states in the present and all previous exciton configurations. With the more complex preequilibrium model of reference [94], F_{msd} may be calculated; in the MPM model, it must be supplied. In GNASH [93], $F_{msd} = 1$. In a transport code, the completion of an intranuclear cascade is equivalent to saying that the system has reached a “bound” configuration; a subsequent MPM phase would then have $F_{msd} = 0$. When MPM is used as a stand-alone code, PREEQ1, it is assumed that F_{msd} decreases geometrically from $F_{msd} = 1$ in the initial configuration with exciton number n_0 to $F_{msd} = f = 0.1$ at the equilibrium exciton number n_{max}

$$F_{msd} = f^x , \quad (63)$$

where

$$x = \frac{n - n_0}{n_{max} - n_0} \text{ and } n_{max} = \sqrt{1.6gE} .$$

6) MEM is used after the INC of CEM and LAQGSM, which calculate exactly and provide for MEM the initial number of excited particles p and holes h ($n = p + h$). With MPM, the situation is different. Namely, when MPM is used after ISABEL [9], it is possible to determine explicitly the particle-hole state of the residual nucleus since a count of the valid excitations from the Fermi sea (and the filling of existing holes) is provided. To define the initial condition for the MPM, the number of particle-hole pairs is reduced by one for each intranuclear collision for which both exiting nucleons are below the top of the nuclear potential well. This method is the only option implemented in MCNP6 to link the MPM with the ISABEL INC.

In adapting the MPM to the Bertini INC, it has not been possible yet to extract the same detailed information from the intranuclear cascade history. Consequently, the algorithm which defines the interface between the Bertini INC and the MPM is a rather crude approximation, intended to permit initial evaluation of the MPM but open to further improvement. In this case, the initial condition for the MPM is one particle-hole pair beyond the minimum particle-hole configuration allowed by the outcome of the intranuclear cascade (“normal MPM”). For the initial condition algorithm used with the Bertini INC, the user has a choice of invoking the MPM in one of three optional modes:

a) the MPM continues from the final state of the INC with the initial condition defined as above (“normal MPM” used when the parameter *ipreq* on the **LCA** MCNP6 input card has the **default** value of 1);

b) the INC is used only to determine that an interaction has occurred and the MPM proceeds from the excited nucleus formed by the absorption of the incident particle (“pure MPM”) employed when *ipreq* = 3 and *ievisa* = 0 on the **LCA** MCNP6 input card;

c) a random selection is made of one of the above modes at each collision with a probability $P = \min[E_1/E_c, 1.0]$ of choosing the “pure MPM” mode, where E_c is the incident energy in MeV and $E_1 = 25$ MeV (“hybrid MPM”) used when *ipreq* = 2 and *ievisa* = 0 on the **LCA** MCNP6 input card;

d) *ipreq* = 0 on the **LCA** input card tells MCNP6 to not use at all the MPM after INC. More details on MPM can be found in Refs. [12, 18].

4 Evaporation Reactions

After the fast and intermediate stages of nuclear reactions described with a chosen INC and preequilibrium model, as a rule, we get an excited compound nucleus and its further deexcitation is calculated with an evaporation model. MCNP6 has and uses three different evaporation models: 1) an extension of the Generalized Evaporation Model code GEM2 Furihata [99]–[101] used with the CEM03.03 and LAQGSM03.03 event generators (only); 2) the EVAP [14]–[17] evaporation model used with the Bertini INC [8] and ISABEL [9] models; 3) the ABLA evaporation model [7] merged in MCNP6 with the INCL4.2 intranuclear cascade code [6], which uses only ABLA, independently of what the users choose for the evaporation and fission models in their MCNP6 input files.

In the following subsections, all these three evaporation models are briefly reviewed.

4.1 Evaporation Reactions in CEM03.03 and LAQGSM03.03

CEM03.03 and LAQGSM03.03 use an extension of the Generalized Evaporation Model (GEM) code GEM2 by Furihata [99]–[101] after the preequilibrium stage of reactions to describe evaporation of nucleons, complex particles, and light fragments heavier than ${}^4\text{He}$ (up to ${}^{28}\text{Mg}$) from excited compound nuclei and to describe their fission, if the compound nuclei are heavy enough to fission ($Z \geq 65$). The GEM is an extension by Furihata of the Dostrovsky evaporation model [13] as implemented in LAHET [18] to include up to 66 types of particles and fragments that can be evaporated from an excited compound nucleus plus a modification of the version of Atchison’s fission model [20] used in LAHET. Many of the parameters were adjusted by Furihata for a better description of fission reactions when using it in conjunction with the extended evaporation model.

A very detailed description of the GEM, together with a large amount of results obtained for many reactions using the GEM coupled either with the Bertini or ISABEL INC models may be found in [99, 100]. Therefore, only the main features of the GEM are presented here, following mainly [100] and using as well useful information obtained in private communications with Dr. Furihata.

Furihata did not change in the GEM the general algorithms used in LAHET to simulate evaporation and fission. The decay widths of evaporated particles and fragments are estimated using the classical Weisskopf-Ewing statistical model [83]. In this approach, the decay probability P_j for the emission of a particle j from a parent compound nucleus i with the total kinetic energy in the center-of-mass system between ϵ and $\epsilon + d\epsilon$ is

$$P_j(\epsilon)d\epsilon = g_j\sigma_{inv}(\epsilon)\frac{\rho_d(E - Q - \epsilon)}{\rho_i(E)}\epsilon d\epsilon, \quad (64)$$

where E [MeV] is the excitation energy of the parent nucleus i with mass A_i and charge Z_i , and d denotes a daughter nucleus with mass A_d and charge Z_d produced after the emission of ejectile j with mass A_j and charge Z_j in its ground state. σ_{inv} is the cross section for the inverse reaction, ρ_i and ρ_d are the level densities [MeV]⁻¹ of the parent and the daughter nucleus, respectively. $g_j = (2S_j + 1)m_j/\pi^2\hbar^2$, where S_j is the spin and m_j is the reduced mass of the emitted particle j . The Q -value is calculated using the excess mass $M(A, Z)$ as $Q = M(A_j, Z_j) + M(A_d, Z_d) - M(A_i, Z_i)$. In GEM2, four mass tables are used to calculate Q values, according to the following priorities, where a lower priority table is only used outside the range of validity of the higher priority one: (1) the Audi-Wapstra mass table [102], (2) theoretical masses calculated by Möller *et al.* [88], (3) theoretical masses calculated by Comay *et al.* [103], (4) the mass excess calculated using the old Cameron formula [104]. As does LAHET, GEM2 uses Dostrovsky's formula [13] to calculate the inverse cross section σ_{inv} for all emitted particles and fragments (see Eqs. (37) and (38) above).

One important new ingredient in GEM2 in comparison with LAHET, which considers evaporation of only 6 particles (n, p, d, t, ³He, and ⁴He), is that Furihata includes the possibility of evaporation of up to 66 types of particles and fragments and incorporates into GEM2 several alternative sets of parameters b , c_j , k_j , R_b , and R_c for each particle type.

The 66 ejectiles considered by GEM2 for evaporation are selected to satisfy the following criteria: (1) isotopes with $Z_j \leq 12$; (2) naturally existing isotopes or isotopes near the stability line; (3) isotopes with half-lives longer than 1 ms. All the 66 ejectiles considered by GEM2 are shown in Table 2.

GEM2 includes several options for the parameter set in expressions (37, 38):

1) The “simple” parameter set is given as $c_n = c_j = k_j = 1$, $b = 0$, and $R_b = R_c = r_0(A_j^{1/3} + A_d^{1/3})$ [fm]; users need to input r_0 .

2) The “precise” parameter set is used in GEM2 as the default, and this set is used in CEM03.03.

A) For all light ejectiles up to α ($A_j \leq 4$), the parameters determined by Dostrovsky *et al.* [13] are used in GEM2, namely: $c_n = 0.76 + c_a A_d^{-1/3}$, $b = (b_a A_d^{-2/3} - 0.050)/(0.76 + c_a A_d^{-1/3})$ (and $b = 0$ for $A_d \geq 192$), where $c_a = 1.93$ and $b_a = 1.66$, $c_p = 1 + c$, $c_d = 1 + c/2$, $c_t = 1 + c/3$, $c_{^3\text{He}} = c_\alpha = 0$, $k_p = k$, $k_d = k + 0.06$, $k_t = k + 0.12$, $k_{^3\text{He}} = k_\alpha - 0.06$, where c , k , and k_α are listed in Table 3 for a set of Z_d . Between the Z_d values listed in Table 3, c , k , and k_α are interpolated linearly. The nuclear distances are given by $R_b = 1.5A^{1/3}$ for neutrons and protons, and $1.5(A_d^{1/3} + A_j^{1/3})$ for d, t, ³He, and α .

The nuclear distance for the Coulomb barrier is expressed as $R_c = R_d + R_j$, where $R_d = r_0^c A^{1/3}$, $r_0^c = 1.7$, and $R_j = 0$ for protons, and $R_j = 1.2$ for d, t, ³He, and ⁴He. We note that several of these parameters are similar to the original values published by Dostrovsky

Table 2: The evaporated particles considered by GEM2

Z_j	Ejectiles						
0	n						
1	p	d	t				
2	^3He	^4He	^6He	^8He			
3	^6Li	^7Li	^8Li	^9Li			
4	^7Be	^9Be	^{10}Be	^{11}Be	^{12}Be		
5	^8B	^{10}B	^{11}B	^{12}B	^{13}B		
6	^{10}C	^{11}C	^{12}C	^{13}C	^{14}C	^{15}C	^{16}C
7	^{12}N	^{13}N	^{14}N	^{15}N	^{16}N	^{17}N	
8	^{14}O	^{15}O	^{16}O	^{17}O	^{18}O	^{19}O	^{20}O
9	^{17}F	^{18}F	^{19}F	^{20}F	^{21}F		
10	^{18}Ne	^{19}Ne	^{20}Ne	^{21}Ne	^{22}Ne	^{23}Ne	^{24}Ne
11	^{21}Na	^{22}Na	^{23}Na	^{24}Na	^{25}Na		
12	^{22}Mg	^{23}Mg	^{24}Mg	^{25}Mg	^{26}Mg	^{27}Mg	^{28}Mg

Table 3: k , k_α , and c parameters used in GEM2

Z_d	k	k_α	c
≤ 20	0.51	0.81	0.0
30	0.60	0.85	-0.06
40	0.66	0.89	-0.10
≥ 50	0.68	0.93	-0.10

Table 4: k_p , c_p , k_α , and c_α parameters from Ref. [13]

Z_d	k_p	c_p	k_α	c_α
10	0.42	0.50	0.68	0.10
20	0.58	0.28	0.82	0.10
30	0.68	0.20	0.91	0.10
50	0.77	0.15	0.97	0.08
≥ 70	0.80	0.10	0.98	0.06

et al. [13] but not exactly the same. Dostrovsky *et al.* [13] had $c_a = 2.2$, $b_a = 2.12$, and $r_0^c = 1.5$. Also, for the k , k_α , and c parameters shown in Table 3, they had slightly different values, shown in Table 4.

B) For fragments heavier than α ($A_j \geq 4$), the “precise” parameters of GEM2 use values by Matsuse *et al.* [105], namely: $c_j = k = 1$, $R_b = R_0(A_j) + R_0(A_d) + 2.85$ [fm], $R_c = R_0(A_j) + R_0(A_d) + 3.75$ [fm], where $R_0(A) = 1.12A^{1/3} - 0.86A^{-1/3}$.

3) The code GEM2 contains two other options for the parameters of the inverse cross sections.

A) A set of parameters due to Furihata for light ejectiles in combination with Matsuse’s parameters for fragments heavier than α . Furihata and Nakamura determined k_j for p, d, t, ^3He , and α as follows [101]:

$$k_j = c_1 \log(Z_d) + c_2 \log(A_d) + c_3.$$

The coefficients c_1 , c_2 , and c_3 for each ejectile are shown in Table 5.

Table 5: c_1 , c_2 , and c_3 for p, d, t, ^3He , and α from [101]

Ejectile	c_1	c_2	c_3
p	0.0615	0.0167	0.3227
d	0.0556	0.0135	0.4067
t	0.0530	0.0134	0.4374
^3He	0.0484	0.0122	0.4938
α	0.0468	0.0122	0.5120

When these parameters are chosen in GEM2, the following nuclear radius R is used in the calculation of V and σ_g :

$$R = \begin{cases} 0 & \text{for } A = 1, \\ 1.2 & \text{for } 2 \leq A \leq 4, \\ 2.02 & \text{for } 5 \leq A \leq 6, \\ 2.42 & \text{for } A = 7, \\ 2.83 & \text{for } A = 8, \\ 3.25 & \text{for } A = 9, \\ 1.414A_d^{1/3} + 1 & \text{for } A \geq 10. \end{cases}$$

B) The second new option in GEM2 is to use Furihata’s parameters for light ejectiles up to α and the Botvina *et al.* [106] parameterization for inverse cross sections for heavier ejectiles. Botvina *et al.* [106] found that σ_{inv} can be expressed as

$$\sigma_{inv} = \sigma_g \begin{cases} (1 - V/\epsilon) & \text{for } \epsilon \geq V + 1 \text{ [MeV]}, \\ \exp[\alpha(\epsilon - V - 1)]/(V + 1) & \text{for } \epsilon < V + 1 \text{ [MeV]}, \end{cases} \quad (65)$$

where

$$\alpha = 0.869 + 9.91/Z_j,$$

$$V = \frac{Z_j Z_d}{r_0^b (A_j^{1/3} + A_d^{1/3})},$$

$$r_0^b = 2.173 \frac{1 + 6.103 \times 10^{-3} Z_j Z_d}{1 + 9.443 \times 10^{-3} Z_j Z_d} \text{ [fm]}.$$

The expression of σ_{inv} for $\epsilon < V + 1$ shows the fusion reaction in the sub-barrier region. When using Eq. (65) instead of Eq. (37), the total decay width for a fragment emission can not be calculated analytically. Therefore, the total decay width must be calculated numerically and takes much CPU time.

The total decay width Γ_j is calculated by integrating Eq. (64) with respect to the total kinetic energy ϵ from the Coulomb barrier V up to the maximum possible value, $(E - Q)$. The good feature of Dostrovsky's approximation for the inverse cross sections, Eq. (37), is its simple energy dependence that allows the analytic integration of Eq. (64). By using Eq. (37) for σ_{inv} , the total decay width for the particle emission is

$$\Gamma_j = \frac{g_j \sigma_g \alpha}{\rho_i(E)} \int_V^{E-Q} \epsilon \left(1 + \frac{\beta}{\epsilon}\right) \rho_d(E - Q - \epsilon) d\epsilon. \quad (66)$$

The level density $\rho(E)$ is calculated in GEM2 according to the Fermi-gas model using the expression [97]

$$\rho(E) = \frac{\sqrt{\pi}}{12} \frac{\exp(2\sqrt{a(E - \delta)})}{a^{1/4}(E - \delta)^{5/4}}, \quad (67)$$

where a is the level-density parameter and δ is the pairing energy in MeV. As does LAHET, GEM2 uses the δ values evaluated by Cook *et al.* [107]. For those values not evaluated by Cook *et al.*, δ 's from Gilbert and Cameron [97] are used instead. The simplest option for the level-density parameter in GEM2 is $a = A_d/8$ [MeV⁻¹], but the default is the Gilbert-Cameron-Cook-Ignatyuk (GCCCI) parameterization from LAHET [18]:

$$a = \tilde{a} \frac{1 - e^{-u}}{u} + a_I \left(1 - \frac{1 - e^{-u}}{u}\right), \quad (68)$$

where $u = 0.05(E - \delta)$, and

$$a_I = (0.1375 - 8.36 \times 10^{-5} A_d) \times A_d,$$

$$\tilde{a} = \begin{cases} A_d/8 & \text{for } Z_d < 9 \text{ or } N_d < 9, \\ A_d(a' + 0.00917S) & \text{for others.} \end{cases}$$

For deformed nuclei with $54 \leq Z_d \leq 78$, $86 \leq Z_d \leq 98$, $86 \leq N_d \leq 122$, or $130 \leq N_d \leq 150$, $a' = 0.12$ while $a' = 0.142$ for other nuclei. The shell corrections S is expressed as a sum of separate contributions from neutrons and protons, *i.e.* $S = S(Z_d) + S(N_d)$ from [97, 107] and are tabulated in [99].

The level density is calculated using Eq. (67) only for high excitation energies, $E \geq E_x$, where $E_x = U_x + \delta$ and $U_x = 2.5 + 150/A_d$ (all energies are in MeV). At lower excitation energies, the following [97] is used for the level density:

$$\rho(E) = \frac{\pi}{12} \frac{1}{T} \exp((E - E_0)/T), \quad (69)$$

where T is the nuclear temperature defined as $1/T = \sqrt{a/U_x} - 1.5/U_x$. To provide a smooth connection of Eqs. (67) and (69) at $E = E_x$, E_0 is defined as $E_0 = E_x - T(\log T - 0.25 \log a - 1.25 \log U_x + 2\sqrt{aU_x})$.

For $E - Q - V < E_x$, substituting Eq. (69) into Eq. (67) we can calculate the integral analytically, if we neglect the dependence of the level-density parameter a on E :

$$\Gamma_j = \frac{\pi g_j \sigma_g \alpha}{12 \rho_i(E)} \{I_1(t, t) + (\beta + V)I_0(t)\}, \quad (70)$$

where $I_0(t)$ and $I_1(t, t_x)$ are expressed as

$$\begin{aligned} I_0(t) &= e^{-E_0/T} (e^t - 1), \\ I_1(t, t_x) &= e^{-E_0/T} T \{(t - t_x + 1)e^{t_x} - t - 1\}, \end{aligned}$$

where $t = (E - Q - V)/T$ and $t_x = E_x/T$. For $E - Q - V \geq E_x$, the integral of Eq. (66) cannot be solved analytically because of the denominator in Eq. (67). However, it is approximated as

$$\Gamma_j = \frac{\pi g_j \sigma_g \alpha}{12 \rho_i(E)} [I_1(t, t_x) + I_3(s, s_x)e^s + (\beta + V)\{I_0(t_x) - I_2(s, s_x)e^s\}], \quad (71)$$

where $I_2(s, s_x)$ and $I_3(s, s_x)$ are given by

$$I_2(s, s_x) = 2\sqrt{2}\{s^{-3/2} + 1.5s^{-5/2} + 3.75s^{-7/2} - (s_x^{-3/2} + 1.5s_x^{-5/2} + 3.75s_x^{-7/2})e^{s_x-s}\},$$

$$\begin{aligned} I_3(s, s_x) &= (\sqrt{2}a)^{-1} [2s^{-1/2} + 4s^{-3/2} + 13.5s^{-5/2} + 60.0s^{-7/2} + 325.125s^{-9/2} \\ &- \{(s^2 - s_x^2)s_x^{-3/2} + (1.5s^2 + 0.5s_x^2)s_x^{-5/2} + (3.75s^2 + 0.25s_x^2)s_x^{-7/2} + (12.875s^2 \\ &+ 0.625s_x^2)s_x^{-9/2} + (59.0625s^2 + 0.9375s_x^2)s_x^{-11/2} + (324.8s_x^2 + 3.28s_x^2)s_x^{-13/2}\}e^{s_x-s}], \end{aligned}$$

with $s = 2\sqrt{a(E - Q - V - \delta)}$ and $s_x = 2\sqrt{a(E_x - \delta)}$.

The particle type j to be evaporated is selected in GEM2 by the Monte-Carlo method according to the probability distribution calculated as $P_j = \Gamma_j / \sum_j \Gamma_j$, where Γ_j is given by Eqs. (70) or (71). The total kinetic energy ϵ of the emitted particle j and the recoil energy of the daughter nucleus is chosen according to the probability distribution given by Eq. (64). The angular distribution of ejectiles is simulated to be isotropic in the center-of-mass system.

According to Friedman and Lynch [108], it is important to include excited states in the particle emitted via the evaporation process along with evaporation of particles in their ground states, because it greatly enhances the yield of heavy particles. Taking this into consideration, GEM2 includes evaporation of complex particles and light fragments both in the ground states and excited states. An excited state of a fragment is included in calculations if its half-life $T_{1/2}(s)$ satisfies the following condition:

$$\frac{T_{1/2}}{\ln 2} > \frac{\hbar}{\Gamma_j^*}, \quad (72)$$

where Γ_j^* is the decay width of the excited particle (resonance). GEM2 calculates Γ_j^* in the same manner as for a ground-state particle emission. The Q -value for the resonance emission

is expressed as $Q^* = Q + E_j^*$, where E_j^* is the excitation energy of the resonance. The spin state of the resonance S_j^* is used in the calculation of g_j , instead of the spin of the ground state S_j . GEM2 uses the ground state masses m_j for excited states because the difference between the masses is negligible.

Instead of treating a resonance as an independent particle, GEM2 simply enhances the decay width Γ_j of the ground state particle emission as follows:

$$\Gamma_j = \Gamma_j^0 + \sum_n \Gamma_j^n, \quad (73)$$

where Γ_j^0 is the decay width of the ground state particle emission, and Γ_j^n is that of the n th excited state of the particle j emission which satisfies Eq. (72).

The total-kinetic-energy distribution of the excited particles is assumed to be the same as that of the ground-state particle. S_j^* , E_j^* , and $T_{1/2}$ used in GEM2 are extracted from the Evaluated Nuclear Structure Data File (ENSDF) database maintained by the National Nuclear Data Center at Brookhaven National Laboratory [109].

Note that when including evaporation of up to 66 particles in GEM2, its running time increases significantly compared to the case when evaporating only 6 particles, up to ${}^4\text{He}$. The major particles emitted from an excited nucleus are n, p, d, t, ${}^3\text{He}$, and ${}^4\text{He}$. For most cases, the total emission probability of particles heavier than α is negligible compared to those for the emission of light ejectiles. Detailed studies of different reactions (see, *e.g.*, [110] and references therein) shows that if we need only nucleon and complex-particle spectra or only spallation and fission products and are not interested at all in light fragments, we can consider evaporation of only 6 types of particles in GEM2 and save much time, getting results very close to the ones calculated with the more time consuming “66” option. In CEM03.03 and LAQGSM03.03, an input parameter called **nevtype** was introduced that defines the number of types of particles to be considered at the evaporation stage. The index of each type of particle that can be evaporated corresponds to the particle arrangement in Table 2, with values, *e.g.*, of 1, 2, 3, 4, 5, and 6 for n, p, d, t, ${}^3\text{He}$, and ${}^4\text{He}$, with succeeding values up to 66 for ${}^{28}\text{Mg}$. For all ten examples of inputs and outputs of CEM03.03 included in Appendices 1 and 2 of the CEM03.03 User Manual [1], whose results are plotted in the figures in Appendix 3 of [1], calculations have been performed taking into account only 6 types of evaporated particles (**nevtype** = **6**) as well as with the “66” option (**nevtype** = **66**) and the corresponding computing time is provided for these examples in the captions to the appropriate figures shown in Appendix 3 of Ref. [1]. The “6” option can be up to several times faster than the “66” option, providing meanwhile almost the same results.

MCNP6 uses as default **nevtype** = **66**. When MCNP6 users have powerful computers and do not care much about the computing time needed to complete their simulations, they may not pay any attention to **nevtype** and MCNP6 will use its default value of 66. But if/when MCNP6 users have to simulate very complex systems requiring a huge statistics and their materials contain a good portion of preactinide nuclei like Au, Pb, or/and Bi, they can save much computing time by changing the value of **nevtype** from its default value of 66 to a smaller value provided on the 11th entry of the **LCA** card of the MCNP6 input file. In such cases, it is recommended that users of CEM03.03 and LAQGSM03.03 event generators of MCNP6 employ the default value of 66 for **nevtype** only when they are interested in all fragments heavier than ${}^4\text{He}$; otherwise, it is recommended to use for the 11th parameter of

the **LCA** MCNP6 input file card a value of 6, saving much computing time. Alternatively, users may choose intermediate values of **nevtype**, for example 9 if one wants to calculate the production of ${}^6\text{Li}$, or 14 for modeling the production of ${}^9\text{Be}$ and lighter fragments and nucleons only, while still saving computing time compared to running the code with the maximum value of 66.

4.2 Evaporation Reactions with the Bertini INC and ISABEL

When using the Bertini INC [8] or ISABEL [9], MCNP6 employs after MPM [12] (or after INC, if no preequilibrium reactions are choosing to be simulated, by using the option *iprec* = 0 on the **LCA** MCNP6 input card) the EVAP [14]-[17] evaporation model as it was implemented in LAHET [18], merged with the RAL [20] and the ORNL [19] fission models. (Note that Bertini INC and ISABEL can be also used in MCNP6 with the ABLA evaporation/fission model [7], if users chose *ievap* = 2 on the 7th entry of the **LEA** MCNP6 input card. However, this option is not used often, ABLA is merged by default in MCNP6 with INCL4.2 [6]; ABLA is discussed separately, in the next subsection.)

The EVAP model is used also in the case of incident protons with energies below or of the order of only several tens of MeV, when the MCNP6 users do not like to use data libraries (*e.g.*, when the 3rd entry on the **phys:h** MCNP6 input card is set to 0, *i.e.*, requiring to use data libraries at energies up to 0 MeV, in other words, to not use them at all) and choose to start the simulation directly with MPM, without any INC (*i.e.*, when *ipreq* = 3 and *ixaxis* = 0 is specified on the **LCA** MCNP6 input card).

The EVAP evaporation code adopted and modified by Dr. Richard Prael for LAHET [18] is based on the theory of emission of particles from excited compound nuclei originally due to Weisskopf and Ewing [83] and implemented in the first Monte Carlo evaporation code by Dostrovsky et al. [13]. EVAP is often cited in the literature as “the Dresner’s evaporation model,” because of its implementation in the EVAP code by Dresner in Ref. [14]. However, it needs to be mentioned that MCNP6 actually does not use the original EVAP code by Dresner [14], which considers the possibility of evaporation up to 19 types of particles and light fragments, from n to ${}^{10}\text{Be}$ (see details in [14]). After the initial implementation by Dresner [14], EVAP was further revised and improved in Refs. [15, 16, 17, 18]; it considers now emission of only 6 types of ejectiles, namely: n , p , d , t , ${}^3\text{He}$, and ${}^4\text{He}$.

MCNP6 uses the latest version of EVAP. It was described in good detail in the previous subsection, when discussing the GEM2 code by Furihata [99]–[101] adopted by the CEM03.03 and LAQGSM03.03 event generators of MCNP6, therefore this is not repeated here.

As discussed in the previous subsection, Dr. Shiori Furihata added many additional options for the calculation of nuclear masses, shell and pairing corrections, inverse cross sections, Coulomb barriers, and level density parameters in her GEM2 extension of the EVAP code taken from LAHET. The version of EVAP used in MCNP6 employs only the “standard” options available in LAHET for these quantities. Namely, it evaluates nuclear masses using the Audi and Wabstra [102] or Wabstra and Bos [111] mass tables. For nuclei with Z or $N < 13$, it uses the shell plus pairing energy corrections by Peele and Aebersold [112]. The inverse cross sections in EVAP are calculated using the Dostrovsky approximation [13]. The level density parameter a is calculated in EVAP using the Gilbert-Cameron-Cook-Ignatyuk (GCCCI) parameterization from LAHET [18] defined by Eq. (68).

More details on the latest version of EVAP used in MCNP6 can be found in Refs. [14, 15, 16, 17, 18, 52].

4.3 Evaporation Reactions Simulated with INCL4.2

The INCL4.2 intranuclear cascade code is merged in MCNP6 only with the ABLA evaporation/fission model [7] and will use only it, independently of what the users choose for the evaporation and fission models in their MCNP6 input files.

ABLA is similar to many other evaporation/fission codes, but considers evaporation of only n , p , and α . For many applications, such an approach is good enough, especially if to consider that ABLA has a reliable fission model. The evaporation of particles is calculated by ABLA using the Weisskopf and Ewing theory [83].

The emission of a particle j in an evaporation process from the excited nucleus with neutron number N , proton number Z , angular momentum J , and excitation energy E is characterized by the emission width Γ_j which is calculated by the statistical model. The emission probability of the particle j is determined [7] by:

$$W_j(N, Z, E) = \frac{\Gamma_j(N, Z, E)}{\sum_k \Gamma_k(N, Z, E)}, \quad (74)$$

whereby the angular momentum is not considered explicitly.

The Fermi-gas state density is used in ABLA with shell and pairing corrections as described in Refs. [7, 113].

The intrinsic state density is expressed by:

$$\rho_{intr} = \frac{\sqrt{\pi} \exp(S)}{12\tilde{a}^{1/4} E^{5/4}}, \quad (75)$$

with the entropy S

$$S = 2\sqrt{\tilde{a}(E + \delta U k(E) + \delta P h(E))},$$

and the asymptotic level-density parameter \tilde{a} as given in Ref. [86]

$$\tilde{a} = 0.073A \text{ MeV}^{-1} + 0.095B_S A^{2/3} \text{ MeV}^{-1},$$

where B_S is the dimensionless surface area of a deformed nucleus. For saddle-point shapes, B_S is a function of the fissility parameter [114], while for a spherical ground state $B_S = 1$. δU is the shell correction as calculated in the finite-range liquid-drop model [88]. $k(E) = 1 - \exp(-\gamma E)$ with $1/\gamma = 0.4A^{4/3}/\tilde{a}$ describes the damping of the shell effects with excitation energy. The function $k(E)$ has been adapted to give close agreement with microscopic calculations of the level density of heavy nuclei [86, 113].

$$\delta P = -\frac{1}{4}\Delta^2 g + 2\Delta$$

is the effective pairing energy shift with an average pairing gap $\Delta = 12/\sqrt{A}$ MeV, and $g = \tilde{a}6/\pi$ is the single-particle level density at the Fermi energy.

$$h(E) = \begin{cases} 1 - \left(1 - \frac{E}{E_{crit}}\right)^2 & \text{for } E < E_{crit}, \\ 1 & \text{for } E \geq E_{crit}, \end{cases}$$

$h(E)$ describes the washing out of the pairing correlations with the critical energy $E_{crit} = 10$ MeV. The effective energy E is shifted with respect to the excitation energy E^* to accommodate for the different condensation energies of even-even, odd-mass, and odd-odd nuclei [7]:

$$E = \begin{cases} E^* & \text{for odd-odd nuclei,} \\ E^* - \Delta & \text{for odd-mass nuclei,} \\ E^* - 2\Delta & \text{for even-even nuclei.} \end{cases}$$

Collective excitations can contribute considerably to the nuclear level density. The total level density including collective and intrinsic excitations $\rho(E)$ can be expressed by the level density of intrinsic excitations $\rho_{intr}(E)$ multiplied by a collective enhancement factor $K_{coll}(E)$:

$$\rho(E) = K_{coll}(E)\rho_{intr}(E) . \quad (76)$$

In deformed nuclei the most important contribution to the collective enhancement of the level density originates from rotational bands, in spherical nuclei the collective enhancement is caused by vibrational excitations.

For nuclei with a quadrupole deformation $|\beta_2| > 0.15$, ABLA calculates the rotational enhancement factor in terms of the spin-cutoff parameter σ_{\perp} :

$$\begin{aligned} K_{rot} &= \begin{cases} (\sigma_{\perp}^2 - 1)f(E) + 1 & \text{for } \sigma_{\perp}^2 > 1 , \\ 1 & \text{for } \sigma_{\perp}^2 \leq 1 , \end{cases} \\ \sigma_{\perp}^2 &= \frac{\mathfrak{S}_{\perp}T}{\hbar^2} , \\ f(E) &= \left(1 + \exp\left(\frac{E - E_{cr}}{d_{cr}}\right) \right)^{-1} . \end{aligned} \quad (77)$$

Here $\mathfrak{S}_{\perp} = \frac{2}{5}m_0AR^2(1 + \beta_2/3)$ is the rigid-body moment of inertia perpendicular to the symmetry axis, with A the nuclear mass number, $R = 1.2 \text{ fm } A^{1/3}$ the nuclear radius, and m_0 the mass unit. T denotes the nuclear temperature. The ground-state quadrupole deformation β_2 is taken from the finite-range liquid-drop model including microscopic corrections [88] while the saddle-point deformation is taken from the liquid-drop model as given in Ref. [115].

Eq. (77) is valid for nuclei which are both axially- and mirror-symmetric. For other symmetry classes (*e.g.* triaxial shapes), different rotational enhancement factors should be applied [7], but as the actual ground-state shape of most of the neutron-deficient nuclei is not known, ABLA uses the expression for axially- and mirror-symmetric shapes as an approximation. The same symmetry class is used to describe the saddle-point deformations. The damping of the collective modes with increasing excitation energy is described in ABLA by a Fermi function with parameters $E_{cr} = 40$ MeV, $d_{cr} = 10$ MeV.

The vibrational enhancement for spherical nuclei is generally smaller than the rotational enhancement for deformed nuclei. For nuclei with ground-state quadrupole deformation of $|\beta_2| < 0.15$, an effective vibrational enhancement factor $K_{vib}(E)$ is formulated in ABLA on the basis of the functional dependence of $K_{rot}(E)$:

$$K_{vib} = 25\beta_{eff}^2 K_{rot}(E) , \quad (78)$$

where the dynamical deformation parameter β_{eff} is defined as:

$$\beta_{eff} = 0.022 + 0.003\Delta N + 0.005\Delta Z ,$$

where $\Delta N(\Delta Z)$ are the absolute values of the number of neutrons (protons) above or below the nearest shell closure.

A newer and much better version of ABLA, ABLA07, has been developed recently [116]. It is not implemented yet in MCNP6, but it is planned to be used in the future.

More details about the collective enhancement and about ABLA can be found in Refs. [7, 52, 113, 116].

4.4 Emission of Low-Energy Photons with the PHT Model

It should be noted that none of the INC, Fermi break-up, preequilibrium, or/and evaporation/fission models of the event generators used in MCNP6 accounts directly for the production of photons. (We do not mean here production of gammas from the decays of neutral pions emitted during INC: such gammas are not “direct” and are produced only during the MCNP6 transport of radiation through the matter.) This is because at high and intermediate energies the probability of the production of gammas during the INC, Fermi break-up, preequilibrium, or/and the evaporation/fission stages of a reaction is much lower than the probability of emission of particles and light fragments, and, as a rule, production of gammas can be neglected at these stages of reactions (the little possible excitation energy of residual nuclei after these stages of reaction, below the binding energy of evaporation particles - of only several MeV, is accounted by MCNP6 as “energy deposition,” so that there are no problems with the conservation of the energy).

However, there are applications where production of gammas is important and must be accounted explicitly, especially at not very high incident energies. To address this problem, MCNP6 uses the PHT model from LAHET [18].

Dr. Richard Prael developed the PHT model and incorporated it in LAHET so that it accounts production of photons both from the decay of neutral pions and from the deexcitation of residual nuclei produced after the evaporation/fission stages of reactions calculated with the EVAP [14]-[17] evaporation and RAL [20] or ORNL [19] fission models. From LAHET, the same procedure migrated later to MCNPX [54], and finally, to MCNP6.

Dr. Franz Gallmeier incorporated [117] an early version of the CEM model into an early version of MCNPX. By doing so, he merged all subroutines and functions of CEM into a single module, **cemmod.F**, and added the PHT model to the CEM module to account for emission of gammas (let us recall again that the stand-alone CEM03.03 [1] does not account emission of any gammas). This scheme migrated thereafter to later versions of MCNPX, and finally, to MCNP6, for all following versions of CEM developed and used in MCNPX/6 after publication of Ref. [117]. It is needed to be mentioned, however, that at the present time, the PHT model was not merged yet in a similar way with LAQGSM03.03 and with INCL4.2+ABLA. This is, at present, MCNP6 allows us to account explicitly production of photons only when using CEM03.03, Bertini INC, and ISABEL models, but not with LAQGSM03.03 and not with INCL4.2+ABLA.

Bellow, we present a brief description of the production of low energy gammas by the PHT model from deexcitation of residual nuclei (we do not discuss here decay of π^0), following mainly Ref. [18].

For the deexcitation of the residual nuclei, PHT assumes that all particle decay modes have been exhausted; thus gamma emission does not compete with particle emission.

It is assumed that there exists a range of known energy levels, above which there is a continuum of energy levels with level density given by the Gilbert-Cameron formulae [97]. The library of level data is based on the CDRL82 collection [118], with over 50,000 listed levels. If the excitation energy of a residual nucleus lies between two levels, it is assigned randomly to one or the other of the levels with a probability that depends linearly on the distance from the levels. If the excitation is above the maximum known level, it is assumed the level is in the continuum.

The probability of a transition between levels is assumed to be proportional to the Weisskopf single particle estimates [119, 120] unless specified by the library. For levels in the continuum and for known levels with unknown spin and parity, a spin state is randomly assigned using the Gilbert-Cameron [97] spin densities to generate a sampling distribution; parities, at the present time, are assigned with equal probabilities. For a transition within the continuum to a state of given spin, the transition probability is also proportional to the level density for the final spin state.

The gamma cascade proceeds from the above assumptions. For an excitation energy lying in the continuum, transition to another level in the continuum competes with transitions to known levels. If the initial excitation energy lies within the known levels, or a level has been reached by transition from the the continuum, the probability of a transition to lower levels is obtained from library data if available or from the model otherwise.

The user has the option of selecting the level of the physics model to be used in the PHT calculation. It is possible to ignore the experimental branching ratios and perform a pure model calculation. The user may also choose to treat all transitions as E1 transitions, corresponding to the model previously employed by Troubetzkoy [121].

PHT uses the proper kinematics to obtain the energy and angle distribution for the pion decay gammas. However, at the present time, the emission of deexcitation gammas is assumed to be isotropic in the laboratory frame, ignoring nuclear recoil.

The parameter **icc** of the PHT model defines the level of physics to be applied. Values of 0 through 4 are allowed. The definitions of the physics options chosen by the **icc** parameter are listed below:

1) **icc = 0: The Continuum Model**

When **icc** = 0 is specified, the continuum is assumed to exist at all nuclear excitations above the pairing gap for the residual nucleus. As a consequence, there is no line spectrum but rather only a continuous gamma energy distribution. All transitions, within the continuum or from the continuum to the ground state, are assumed to be E1 transitions.

2) **icc = 1: The Troubetzkoy (E1) Model**

For **icc** = 1, the Troubetzkoy model [121] is used. The nuclear energy levels specified in the data library are used. The continuum is assumed to begin above the highest specified level. However, all transitions, whether continuum-to-continuum, continuum-to-level, or level-to-level, are assumed to be E1 transitions.

3) **icc = 2: The Intermediate Model**

When $icc = 2$, the model employed is really a hybrid between models $icc=0$ and $icc=3$. The nuclear levels, and their spins and parities, are obtained from the data library. The continuum begins above the highest specified level. However, all levels above the lowest that has unknown spin or parity are considered to also have unknown spin. All transitions within or from the continuum, or that involve a level with unknown spin, are treated as El transitions as in model 1 ($icc=0$). All transitions involving only states of known spin and parity utilize the Weisskopf single particle transition model as in option 4 ($icc=3$).

4) **icc = 3: The Spin-dependent Model**

The $icc = 3$ option gives the full model as described above, with the exception that any experimental branching ratios are ignored and a pure model calculation is performed for the transition probabilities using the Weisskopf single particle transition estimates.

5) **icc = 4: The Full Model with Experimental Branching Ratios**

With $icc = 4$, the fill procedure described above is employed, including the use of library specified branching ratios when available.

The default option is $icc = 4$, *i.e.*, the use of the “Full Model.” Users can change the value of the icc parameter with the second entry on the **LEA** card of the MCNP6 input files. With the first entry of the same input card, **ipht**, users can control the use of the PHT model: When $ipht=1$ (default), MCNP6 uses PHT and produces gammas, while if $ipht = 0$, PHT is not used and photons from π^0 decays and from deexcitation of residual nuclei are not produced, at all.

More details about the PHT model can be found in Refs. [18, 52].

5 Fission Reactions

A heavy excited compound nucleus does not only “evaporate” particles and light fragments, but it also can fission. MCNP6 accounts for the possibility of fission of only nuclei with $Z \geq 65$ (when using the CEM03.03 or LAQGSM03.03 event generators; with other event generators, fission is considered only for more heavy nuclei, as described below).

At present, MCNP6 uses with its high-energy event generators four different fission models:

1) An extension of the fission model used in GEM2 [99, 100, 101], based on the Atchison’s model [20, 122], as implemented in LAHET [18]; this fission model is used by CEM03.03 and LAQGSM03.03.

2) The RAL fission model developed by Atchison [20, 122], in its original version, as implemented in LAHET [18]; this model considers a possibility to fission of excited nuclei with $Z \geq 70$ only, and can be used in MCNP6 with the Bertini INC [8] and ISABEL [9].

3) The ORNL fission model working only for nuclei with $Z \geq 91$ and which can be used in MCNP6 also only with the Bertini INC [8] and ISABEL [9].

4) The PROFI fission model [141] (works only for $Z \geq 70$) from the ABLA evaporation/fission code [7] used in MCNP6 only with INCL4.2+ABLA.

All these fission models are briefly reviewed in the following subsections.

5.1 Fission Reactions in CEM03.03 and LAQGSM03.03

The fission model used in GEM2 is based on Atchison's model [20, 122] as implemented in LAHET [18], often referred to in the literature as the Rutherford Appleton Laboratory (RAL) fission model, which is where Atchison developed it. In GEM2, there are two choices of parameters for the fission model: one of them is the original parameter set by Atchison [20, 122] as implemented in LAHET [18], and the other is a parameter set developed by Furihata [99, 100].

5.1.1 Fission Probability

The Atchison fission model is designed to describe only fission of nuclei with $Z \geq 70$. It assumes that fission competes only with neutron emission, *i.e.*, from the widths Γ_j of n, p, d, t, ^3He , and ^4He , the RAL code calculates the probability of evaporation of any particle. When a charged particle is selected to be evaporated, no fission competition is taken into account. When a neutron is selected to be evaporated, the code does not actually simulate its evaporation, instead it considers that fission may compete, and chooses either fission or evaporation of a neutron according to the fission probability P_f . This quantity is treated by the RAL code differently for the elements above and below $Z = 89$. The reasons Atchison split the calculation of the fission probability P_f are: (1) there is very little experimental information on fission in the region $Z = 85$ to 88, (2) the marked rise in the fission barrier for nuclei with Z^2/A below about 34 (see Fig. 2 in [122]) together with the disappearance of asymmetric mass splitting, indicates that a change in the character of the fission process occurs. If experimental information were available, a split between regions around $Z^2/A \approx 34$ would be more sensible [122].

1) $70 \leq Z_i \leq 88$. For fissioning nuclei with $70 \leq Z_i \leq 88$, GEM2 uses the original Atchison calculation of the neutron emission width Γ_n and fission width Γ_f to estimate the fission probability as

$$P_f = \frac{\Gamma_f}{\Gamma_f + \Gamma_n} = \frac{1}{1 + \Gamma_n/\Gamma_f}. \quad (79)$$

Atchison uses [20, 122] the Weisskopf and Ewing statistical model [83] with an energy-independent pre-exponential factor for the level density (see Eq. (67)) and Dostrovsky's [13] inverse cross section for neutrons, and estimates the neutron width Γ_n as

$$\Gamma_n = 0.352(1.68J_0 + 1.93A_i^{1/3}J_1 + A_i^{2/3}(0.76J_1 - 0.05J_0)), \quad (80)$$

where J_0 and J_1 are functions of the level-density parameter a_n and $s_n (= 2\sqrt{a_n(E - Q_n - \delta)})$,

$$J_0 = \frac{(s_n - 1)e^{s_n} + 1}{2a_n},$$

$$J_1 = \frac{(2s_n^2 - 6s_n + 6)e^{s_n} + s_n^2 - 6}{8a_n^2}.$$

Note that the RAL model uses a fixed value for the level-density parameter a_n , namely

$$a_n = (A_i - 1)/8, \quad (81)$$

and this approximation is kept in GEM2 when calculating the fission probability according to Eq. (79), although it differs from the GCCI parameterization (68) used in GEM2 to calculate particle evaporation widths. The fission width for nuclei with $70 \leq Z_i \leq 88$ is calculated in the RAL model and in the GEM as

$$\Gamma_f = \frac{(s_f - 1)e^{s_f} + 1}{a_f}, \quad (82)$$

where $s_f = 2\sqrt{a_f(E - B_f - \delta)}$ and the level-density parameter in the fission mode a_f is fitted by Atchison to describe the measured Γ_f/Γ_n to be [122]:

$$a_f = a_n \left(1.08926 + 0.01098(\chi - 31.08551)^2 \right), \quad (83)$$

and $\chi = Z^2/A$. The fission barriers B_f [MeV] are approximated by

$$B_f = Q_n + 321.2 - 16.7 \frac{Z_i^2}{A_i} + 0.218 \left(\frac{Z_i^2}{A_i} \right)^2. \quad (84)$$

Note that neither the angular momentum nor the excitation energy of the nucleus are taken into account in finding the fission barriers.

2) $Z_i \geq 89$. For heavy fissioning nuclei with $Z_i \geq 89$ GEM2 follows the RAL model [20, 122] and does not calculate at all the fission width Γ_f and does not use Eq. (82) to estimate the fission probability P_f . Instead, the following semi-empirical expression obtained by Atchison [20, 122] by approximating the experimental values of Γ_n/Γ_f published by Vandenbosch and Huizenga [123] is used to calculate the fission probability:

$$\log(\Gamma_n/\Gamma_f) = C(Z_i)(A_i - A_0(Z_i)), \quad (85)$$

where $C(Z)$ and $A_0(Z)$ are constants depending on the nuclear charge Z only. The values of these constants are those used in the current version of LAHET [18] and are tabulated in Table 6 (note that some adjustments of these values have been done since Atchison's papers [20, 122] were published).

In this approach the fission probability P_f is independent of the excitation energy of the fissioning nucleus and its angular momentum.

5.1.2 Mass Distribution

The selection of the mass of the fission fragments depends on whether the fission is symmetric or asymmetric. For a pre-fission nucleus with $Z_i^2/A_i \leq 35$, only symmetric fission is allowed. For $Z_i^2/A_i > 35$, both symmetric and asymmetric fission are allowed, depending on the excitation energy of the fissioning nucleus. No new parameters were determined for asymmetric fission in GEM2.

For nuclei with $Z_i^2/A_i > 35$, whether the fission is symmetric or not is determined by the asymmetric fission probability P_{asy}

$$P_{asy} = \frac{4870e^{-0.36E}}{1 + 4870e^{-0.36E}}. \quad (86)$$

Table 6: $C(Z)$ and $A_0(Z)$ values used in GEM2

Z	$C(Z)$	$A_0(Z)$
89	0.23000	219.40
90	0.23300	226.90
91	0.12225	229.75
92	0.14727	234.04
93	0.13559	238.88
94	0.15735	241.34
95	0.16597	243.04
96	0.17589	245.52
97	0.18018	246.84
98	0.19568	250.18
99	0.16313	254.00
100	0.17123	257.80
101	0.17123	261.30
102	0.17123	264.80
103	0.17123	268.30
104	0.17123	271.80
105	0.17123	275.30
106	0.17123	278.80

Asymmetric fission. For asymmetric fission, the mass of one of the post-fission fragments A_1 is selected from a Gaussian distribution of mean $A_f = 140$ and width $\sigma_M = 6.5$. The mass of the second fragment is $A_2 = A_i - A_1$.

Symmetric fission. For symmetric fission, A_1 is selected from a Gaussian distribution of mean $A_f = A_i/2$ and two options for the width σ_M as described below.

The first option for choosing σ_M is the original Atchison approximation:

$$\sigma_M = \begin{cases} 3.97 + 0.425(E - B_f) - 0.00212(E - B_f)^2, \\ 25.27, \end{cases} \quad (87)$$

for $(E - B_f)$ below or above 100 MeV, respectively. In this expression all values are in MeV and the fission barriers B_f are calculated according to Eq. (84) for nuclei with $Z_i \leq 88$. For nuclei with $Z_i > 88$, the expression by Neuzil and Fairhall [124] is used:

$$B_f = C - 0.36(Z_i^2/A_i), \quad (88)$$

where $C = 18.8, 18.1, 18.1,$ and 18.5 [MeV] for odd-odd, even-odd, odd-even, and even-even nuclei, respectively.

The second option in GEM2 for σ_M (used in CEM03.03 and LAQGSM03.03) was found by Furihata [99, 100] as:

$$\sigma_M = C_3(Z_i^2/A_i)^2 + C_4(Z_i^2/A_i) + C_5(E - B_f) + C_6. \quad (89)$$

The constants $C_3 = 0.122$, $C_4 = -7.77$, $C_5 = 3.32 \times 10^{-2}$, and $C_6 = 134.0$ were obtained by fitting with GEM2 the recent Russian collection of experimental fission-fragment mass distributions [125]. In this expression, the fission barriers B_f by Myers and Swiatecki [126] are used. More details may be found in Ref. [100].

5.1.3 Charge Distribution

The charge distribution of fission fragments is assumed to be a Gaussian distribution of mean Z_f and width σ_Z . Z_f is expressed as

$$Z_f = \frac{Z_i + Z'_1 - Z'_2}{2}, \quad (90)$$

where

$$Z'_l = \frac{65.5A_l}{131 + A_l^{2/3}}, l = 1 \text{ or } 2. \quad (91)$$

The original Atchison model uses $\sigma_Z = 2.0$. An investigation by Furihata [100] suggests that $\sigma_Z = 0.75$ provides a better agreement with data; therefore $\sigma_Z = 0.75$ is used in GEM2 and in MCNP6.

5.1.4 Kinetic Energy Distribution

The kinetic energy of fission fragments [MeV] is determined by a Gaussian distribution with mean ϵ_f and width σ_{ϵ_f} .

The original parameters in the Atchison model are:

$$\begin{aligned}\epsilon_f &= 0.133Z_i^2/A_i^{1/3} - 11.4, \\ \sigma_{\epsilon_f} &= 0.084\epsilon_f.\end{aligned}$$

Furihata's parameters in the GEM, used by default in MCNP6, are:

$$\epsilon_f = \begin{cases} 0.131Z_i^2/A_i^{1/3}, \\ 0.104Z_i^2/A_i^{1/3} + 24.3, \end{cases} \quad (92)$$

for $Z_i^2/A_i^{1/3} \leq 900$ and $900 < Z_i^2/A_i^{1/3} \leq 1800$, respectively, according to Rusanov *et al.* [125]. By fitting the experimental data by Itkis *et al.* [127], Furihata found the following expression for σ_{ϵ_f}

$$\sigma_{\epsilon_f} = \begin{cases} C_1(Z_i^2/A_i^{1/3} - 1000) + C_2, \\ C_2, \end{cases} \quad (93)$$

for $Z_i^2/A_i^{1/3}$ above and below 1000, respectively, and the values of the fitted constants are $C_1 = 5.70 \times 10^{-4}$ and $C_2 = 86.5$. The experimental data used by Furihata for fitting are the values extrapolated to the nuclear temperature 1.5 MeV by Itkis *et al.* [127]. More details may be found in [100].

We note that Atchison has also modified his original version using recent data and published [128] improved (and more complicated) parameterizations for many quantities and distributions in his model, but these modifications [128] have not been included either in LAHET or in GEM2 and are not used by MCNP6.

5.1.5 Modifications to GEM2 in CEM03.03 and LAQGSM03.03

First, for CEM and LAQGSM, several observed uncertainties and small errors in the 2002 version of GEM2 received from Dr. Furihata were fixed. Then, GEM2 was extended to describe fission of lighter nuclei, down to $Z \geq 65$, and was modified [129] so that it provides a good description of fission cross sections when it is used after the INC and preequilibrium stages of CEM and LAQGSM.

If GEM2 would be merged with the INC and preequilibrium-decay modules of CEM or of LAQGSM without any modifications, the new code would not describe correctly fission cross sections (and the yields of fission fragments). This is because Atchison fitted the parameters of his RAL fission model when it followed the Bertini INC [8] which differs from the ones of CEM and LAQGSM. In addition, Atchison did not model preequilibrium emission. Therefore, the distributions of fissioning nuclei in A , Z , and excitation energy E^* simulated by Atchison differ significantly from the distributions got with CEM and LAQGSM; as a consequence, all the fission characteristics are also different. Furihata used GEM2 coupled either with the Bertini INC [8] or with the ISABEL [9] INC code, which also differs from the INC of CEM and LAQGSM, and did not include preequilibrium particle emission. Therefore the

distributions of fissioning nuclei simulated by Furihata differ from those in CEM/LAQGSM simulations, so the parameters adjusted by Furihata to work well with her INC are not appropriate for CEM/LAQGSM. To get a good description of fission cross sections (and fission-fragment yields) in CEM03.03 and LAQGSM03.03, at least two parameters in GEM2 had to be modified (see more details in [3, 91, 129, 130]).

The main parameters that determine the fission cross sections calculated by GEM2 are the level-density parameter in the fission channel, a_f (or more exactly, the ratio a_f/a_n as calculated by Eq. (83)) for preactinides, and parameter $C(Z)$ in Eq. (85) for actinides. The sensitivity of results to these parameters is much higher than to either the fission-barrier heights used in a calculation or other parameters of the model. Therefore in Ref. [129] was chosen to adjust only these two parameters in the CEM/LAQGSM+GEM2 merged codes. The form of systematics (83) and (85) derived by Atchison were not changed in Ref. [129]. Only additional coefficients both to a_f and $C(Z)$ have been introduced, replacing $a_f \rightarrow C_a \times a_f$ in Eq. (83) and $C(Z_i) \rightarrow C_c \times C(Z_i)$ in Eq. (85); C_a and C_c were fitted to experimental proton-induced fission cross sections covered by Prokofiev's systematics [131] for both CEM and LAQGSM. No other parameters in GEM2 have been changed. For preactinides, only C_a was fitted. The values of C_a found in such a fit to Prokofiev's systematics are close to one and vary smoothly with the proton energy and the charge or mass number of the target. This result provides some confidence in such a procedure, and allows to interpolate the values of C_a for nuclei and incident proton energies not analyzed by Prokofiev. For actinides, as described in [91, 130], both C_a and C_c have to be fitted. The values of C_a were found to be also very close to one, while the values of C_c are more varied, but both of them change smoothly with the proton energy and Z or A of the target, which again allows to interpolate them for nuclei and energies outside Prokofiev's systematics.

The fitted values of C_a and C_c were fixed in data blocks in the CEM/LAQGSM codes and routines **fitafpa** and **fitafac** are used to interpolate to nuclei not covered by Prokofiev's systematics. It is believed that such a procedure provides a reasonably accurate fission cross-section calculation, at least for proton energies and target nuclei not too far from the ones covered by the systematics.

It should be mention that the situation with the fitting procedure of parameters C_a and C_c is quite tricky, as it should be redone after all major improvements of other parts of the codes describing INC, preequilibrium, or evaporation. This is a major minus of such types of models like GEM2 that are based mostly on systematics of available experimental data rather than on fundamental physics. (This was the main reason why development of new improved evaporation and fission models for CEM and LAQGSM codes have been started in Ref. [130], that would describe experimental data not worse than GEM2 but would be based more on physics rather than on systematics of available data; this work is waiting for funding and was not completed yet; so CEM and LAQGSM have to use still GEM2 at present.) Indeed, after making the major improvements to the INC and preequilibrium parts of CEM and LAQGSM as described above, the mean values of the mass and charge numbers, A and Z of the excited compound nuclei produced after the preequilibrium stage of nuclear reactions and their mean excitation energy E^* have changed slightly, which affects the probability of heavy compound nuclei (especially preactinides) to fission. This means that the procedure of fitting the C_a and C_c parameters which was performed in Ref [129] to provide the best description by CEM2k and LAQGSM of fission cross sections was no longer

correct. For the latest versions of CEM03.03 and LAQGSM03.03, a new similar fitting had to be performed, ensuring that they describe as well as possible fission cross sections from various reactions.

5.2 Fission Reactions Simulated with the Bertini INC and ISABEL

When using the Bertini INC [8] or ISABEL [9], MCNP6 employs at the evaporation stages of reactions, simulated usually with EVAP [14]-[17], either the RAL fission model (works only for $Z > 70$) [20] or the ORNL fission model (works only for $Z \geq 91$) [19, 132].

As mentioned above in the Evaporation section, Bertini INC and ISABEL can be also used in MCNP6 with the ABLA evaporation model [7], if users chose $ievap = 2$ on the 7th entry of the **LEA** MCNP6 input card. In this case, the fission model from ABLA will be used (works only for $Z \geq 70$). However, this option is not used often, ABLA is merged by default in MCNP6 with INCL4.2 [6]; the fission model from ABLA is discussed separately, in the next subsection.)

Note that the EVAP model invoking either RAL or the ORNL fission model can be used also in the case of incident protons with energies below or of the order of only several tens of MeV, when the MCNP6 users do not like to use data libraries (*e.g.*, when the 3rd entry on the **phys:h** MCNP6 input card is set to 0, *i.e.*, requiring to use data libraries at energies up to 0 MeV, that is, to not use at all data libraries).

Below, both the RAL and the ORNL fission models are briefly reviewed.

5.2.1 The RAL Fission Model

The RAL fission model [20] was developed by Dr. Francis Atchison when he was working at the Rutherford Appleton Laboratory (RAL). The model is often referred to in the literature by various names, “Rutherford laboratory,” “Dresner-Atchison,” “LAHET-Bertini,” “Atchison” and others.

MCNP6 uses the old, “standard” version of the RAL model, as developed originally by Atchison in Ref. [20] and implemented by Prael in LAHET [18]. It was described in good detail in the previous subsection, when discussing the the fission model from the GEM2 code by Furihata [99]–[101] adopted with some further modifications by CEM03.03 and LAQGSM03.03, therefore this is not repeated here.

However, the main physical assumptions of the RAL model are listed below, following mainly Ref. [122].

The logical flow of the overall particle-nucleus interaction with fission is shown in Fig. 13. To calculate a fission reaction with RAL, two things have to be known:

- 1) the fission probability, P_f , given by Eq. (79), and
- 2) the post-scission fragment nuclear state: charge, mass, and excitation and recoil energies (Z , A , E^* , and T_{rec}).

The most important assumptions of RAL are:

- Fission competes at all stages of de-excitation (evaporation).
- Fission width depends only on the state of the nucleus and not on how it arrived there.

- Only binary fission is accounted. In term of the calculational flow (see Fig. 13), this means that fission is locked-off for the fission fragments.
- The mass split is always complete. The two fission fragments will conserve baryons and charge. This means that “fission” neutrons come from either evaporation prior to fission or from the evaporation from fission fragments.
- Fission for nuclei with $Z < 70$ is not considered.

More details on the RAL fission model used in MCNP6 can be found in the previous subsection dedicated to fission by CEM03.03 and LAQGSM03.03 and in Refs. [20, 52, 122, 133].

5.2.2 The ORNL Fission Model

The ORNL fission model [19, 132] was developed at Oak Ridge National Laboratory to describe fission of only heavy nuclei with $Z \geq 91$ in competition with evaporation of particles calculated by the Dresner code EVAP [14].

Just like in case of other fission models used by MCNP6, the fundamental basis of the ORNL fission model is the statistical model of fission developed by Fong [134]. Basically, the assumption is that the fission process is “slow” (*i.e.*, the nucleus exists in an equilibrium state at any time), so the probability of a particular fission mode (state of the fission fragments) is proportional to the density of quantum states at the time of splitting. From the Fong theory, the fission mode probability is expressed as a function of eleven variables: $N(A_1, A_2, Z_1, Z_2, C, D, k, E, E_1, j_1, j_2,)$, where the subscripts denote the fission fragments; A , Z , and j denote mass number, charge number, and angular momentum; and the remaining are energy variables (C , Coulomb; D , deformation; k , translational; E , total; and E_1 , excitation).

Different high-energy fission models differ in the approximations made in arriving at a practical implementation of the above general expression and in the physical data used. To a large extent the physical data that occur in the statistical model used by the ORNL fission model have been derived from the experimental measurements of Epperson [135].

Following the work by Hahn and Bertini [136], the ORNL fission model uses an empirical relation derived by Sikkeland et al. [137] to estimate the fission probability:

$$\log_{10}\left(\frac{\Gamma_n}{\Gamma_f}\right) = -0.276Z + \begin{cases} 5.46 + 0.14N & \text{for } N \leq 153, \\ 19.23 + 0.05N & \text{for } N > 153. \end{cases} \quad (94)$$

For odd- Z nuclei, 0.12 is added to this equation. It is also assumed that fission may be neglected in nuclei with atomic numbers $Z < 91$ and that no fission occurs for excitation energies $E_f < 4$ MeV.

The values of the relative kinetic energy of fission fragments and their mass numbers are found from experimental and the Fong model considerations (see Ref. [132] for more details). The angular distribution of fission fragments is assumed to be isotropic in the center-of-mass (CM) system. The partition of the excitation energy between the two fission fragments is determined using the Fong statistical model [134].

The level density parameter used by the ORNL fission model in the evaporation and in the fission process is based on formulation by LeCouteur and Lang [138] and is given as:

$$a_i = \frac{A_i}{B_0} [1 + y_0(A_i - Z_i)^2/A_i^2] , \quad (95)$$

where B_0 and y_0 are constants, taken to be independent of the deformation or excitation energy. Their exact values are not known, developers of the ORNL fission model tried different options for them (see, *e.g.* [19, 132, 139]); their “optimal” values were found to be $B_0 = 10$ and $y_0 = 1.5$.

At the end of this subsection let us mention that because the RAL and the ORNL fission models are different and use different values for the level density parameters, the multiplicity of neutrons calculated by these models for a target, *e.g.*, of ^{238}U bombarded with protons of intermediate energy of ~ 1 GeV is also significantly different: It was found [139] that the ORNL model predicts about 20% more neutrons than does RAL. This is a big difference and it may be of importance for some applications on spallation neutron sources. Users of MCNP6 should keep this in mind when choosing between the RAL and the ORNL models for such applications.

More details on the ORNL fission model used in MCNP6 can be found in Refs. [19, 132, 139].

5.3 Fission Reactions Simulated with INCL4.2

As mentioned above, INCL4.2 is merged in MCNP6 only with the ABLA evaporation/fission model. The fission model from ABLA is sometimes referred to in the literature as “Karl-Hans Schmidt” (KHS), or “Schmidt”, or PROFI model. Many details on how the fission channel is treated in ABLA including the influence of dissipative effects on fission at high excitation energies can be found in Ref. [140, 141]. Here we recall only the main ideas of the model following mainly [140, 141].

The asymptotic level-density parameter \tilde{a} is calculated according to Ignatyuk et al. [86]. For the saddle-point deformation, the asymptotic level-density parameter \tilde{a}_f is approximately 4-5 (2-3) percent larger than \tilde{a}_n , at the ground-state deformation for nuclei with mass number $A \approx 200$ (230).

The fission barriers are calculated in a macroscopic-microscopic approach. The macroscopic part is calculated from the rotating finite-range liquid-drop model [142]. The ground-state shell effects are calculated as the difference between the calculated ground-state atomic mass excess and the corresponding macroscopic value from the finite-range liquid-drop model [88]. The macroscopic part of the fission barrier is obtained by adding the ground-state shell effect to the total fission barriers. Any shell effects at the saddle point are assumed to be small and negligible.

The collective enhancement of the level density is calculated according to Eq. (76), with rotational enhancement defined by Eq. (77) and vibrational enhancement, by Eq. (78).

At low excitation energies, ABLA calculates the fission width using the known expression proposed by Bohr and Wheeler [84] written in a simplified version [143] as:

$$\Gamma_f^{BW} = \frac{1}{2\pi\rho_c(E)} T_f \rho_f(E - B_f) , \quad (96)$$

where ρ_f is the level density of transition states of the fissioning nucleus in the saddle configuration (above the fission barrier), B_f is the height of the fission barrier and T_f is the corresponding nuclear temperature.

However, during the last decades it was recognized that the description of the fission probability for high excitation energies requires some essential modifications of the Bohr-Wheeler approach. An appropriate way to account for the fission dynamics begins with viewing fission as a diffusion process over the fission barrier, which is described by the corresponding Fokker-Planck equation. In the quasi-stationary approximation Kramers obtained the following equation for the fission width [144]:

$$\Gamma_f^K = \Gamma_f^{BW} \left\{ \left[1 + \left(\frac{\beta}{2\omega_0} \right)^2 \right]^{1/2} - \frac{\beta}{2\omega_0} \right\} = \Gamma_f^{BW} f \left(\frac{\beta}{2\omega_0} \right), \quad (97)$$

where β is the reduced dissipation coefficient and ω_0 is the frequency of the effective harmonic-oscillator potential that osculates the fission barrier at the saddle point. In Kramers' picture, β corresponds to "the resistance to which the vibration of the nucleus is subject as a consequence of the viscosity of nuclear matter" [144].

The formation of any large-amplitude collective motion similar to the fission process requires some finite time. The dependence of this transient time τ on the dissipation coefficient can be derived from two analytical solutions of the time-dependent Fokker-Planck equation for the under-damped and the over-damped regimes, respectively:

$$\tau_{\text{under}} \simeq \beta^{-1} \ln \frac{10B_f}{T} \quad \text{for } \frac{\beta}{2\omega_1} \gg 1, \quad (98)$$

$$\tau_{\text{over}} \simeq \frac{\beta}{2\omega_1^2} \ln \frac{10B_f}{T} \quad \text{for } \frac{\beta}{2\omega_1} \ll 1. \quad (99)$$

Here ω_1 is the frequency of the harmonic-oscillator potential osculating the potential energy at the ground-state deformation.

Taking into account the transient time, the ratio of the widths for fission and neutron emission may be written as:

$$\frac{\Gamma_f}{\Gamma_n} = \frac{\Gamma_f^{BW}}{\Gamma_n} \left\{ \left[1 + \left(\frac{\beta}{2\omega_0} \right)^2 \right]^{1/2} - \frac{\beta}{2\omega_0} \right\} \exp \left(-\frac{\tau(\beta)}{\tau_\nu} \right), \quad (100)$$

where $\tau_\nu = \hbar/\Gamma_\nu$ is the mean life-time against neutron emission. If emission of protons and α -particles is included as well, as is in the version of ABLA used by MCNP6, the corresponding mean life-time for particle emission is defined as

$$\tau_\nu = \frac{1}{1/\tau_n + 1/\tau_p + 1/\tau_\alpha}. \quad (101)$$

Properties of fission fragments, *i.e.* masses, atomic numbers, excitation and kinetic energies, are calculated in ABLA based on a macro-microscopic approach and the separability of compound-nucleus and fragment properties on the fission path. The original description of the fragment-formation model – PROFI – was published in Refs. [141, 145, 146]. Bellow we provide only the main ideas of PROFI, following mainly Ref. [141].

The population of the fission channels is assumed to be basically determined by the statistical weight of transition states above the potential-energy landscape near the fission barrier. PROFI assumes that the mass-asymmetric degree of freedom at the fission barrier is on average uniquely related to the neutron number N of the fission fragments. The numbers of protons and neutrons are considered to be strictly correlated.

For a given excitation energy E , the yield $Y(E, N)$ of fission fragments with neutron number N is calculated by the statistical weight of transition states above the conditional potential barrier:

$$Y(E, N) = \frac{\int_0^{E-V(N)} \rho_N(U) dU}{\sum_{N=0}^{N_{CN}} \int_0^{E-V(N)} \rho_N(U) dU}, \quad (102)$$

where $V(N)$ is the height of the conditional potential barrier for a given mass-asymmetric deformation, ρ_N is the level density for an energy U above this potential and N_{CN} is the neutron number of the fissioning (compound) nucleus.

Yields of fission fragments with neutron number N corresponding to the symmetric and asymmetric fission channels can be obtained from the expressions:

$$Y_{mac}(E_0^*, N) \approx \exp\left(2\sqrt{\tilde{a}E_{mac}(E_0^*, N)}\right), \quad (103)$$

$$Y_{sh,i}(E_0^*, N) \approx \exp\left(2\sqrt{\tilde{a}E_{sh,i}(E_0^*, N)}\right) - Y_{mac}(E_0^*, N), \quad (104)$$

where E_0^* is the excitation energy above the macroscopic potential at symmetry ($N_{CN}/2$) and Y_{mac} stands for the symmetric channel and $Y_{sh,i}$ for one of the asymmetric channels. In Eq. (104) the contribution of the symmetric channel is subtracted in order to avoid double counting. The asymptotic level-density parameter is calculated as $\tilde{a} = A/8$.

The effective excitation energies above the macroscopic potential (E_{mac}) and above the shell-corrected potential ($E_{sh,i}$) to be inserted in Eqs. (103) and (104) are calculated as:

$$E_{mac}(E_0^*, N) = E_0^* - C_{mac}(N_{CN}/2 - N)^2, \quad (105)$$

$$E_{sh,i}(E_0^*, N) = E_{mac}(E_0^*, N) - \delta U_i(E_0^*, N). \quad (106)$$

In these expressions $\delta U_i(E_0^*, N)$ is the value of the shell-correction-parabolic function parameterized in Ref [141]. The energy dependence of this shell correction is described according to the analytical description of Ref. [147].

$$\delta U_i(E_0^*, N) = (\delta U_i + C_{sh,i}(N_{sh,i} - N)^2) \exp(-\gamma\epsilon). \quad (107)$$

The curvatures, $2C_{mac}$ and $2C_{sh,i}$, are calculated as described in Ref. [141]. The factor γ is calculated as $\tilde{a}/(0.4A_{CN}^{4/3})$ as proposed in Ref. [148] and $\epsilon = E_{mac} + C_{sh,i}(N_{sh,i} - N)^2 + \delta U_i$.

Expanding expressions (103) and (104), we obtain in a first approximation that the neutron-dependent statistical weight of each fission channel can be expressed as a Gaussian function:

$$Y_{mac}(E_0^*, N) \approx \exp(S_{mac}) \exp\left(\frac{-(N_{CN}/2 - N)^2}{\sigma_{mac}^2}\right), \quad (108)$$

$$Y_{sh,i}(E_0^*, N) \approx \exp(S_{sh,i}) \exp\left(\frac{-(N_{sh,i} - N)^2}{\sigma_{sh,i}^2}\right) - Y_{mac}(E_0^*, N) , \quad (109)$$

with

$$S_{mac} = 2\sqrt{\tilde{a}E_0^*} , \quad (110)$$

$$S_{sh,i} = 2\sqrt{\tilde{a}[E_{mac}(E_0^*, N) - \delta U_i(E_0^*, N)]} , \quad (111)$$

and the widths of these Gaussian functions are given by:

$$\sigma_{mac}^2 = \frac{1}{2} \frac{\sqrt{E_0^*}}{\sqrt{\tilde{a}}C_{mac}} , \quad (112)$$

$$\sigma_{sh,i}^2 = \frac{1}{2} \frac{\sqrt{E_{mac}(E_0^*, N) - \delta U_i(E_0^*, N)}}{\sqrt{\tilde{a}}C_{sh,i} \exp(-\gamma\epsilon)} . \quad (113)$$

The neutron-to-proton ratio is assumed to be given by the unchanged charge density (UCD) of the fissioning nucleus. For the asymmetric channels, a polarization of $|\Delta Z| = 0.5$ is included to approximately reproduce the measured neutron-to-proton ratio:

$$Z(N) = N \frac{Z_{CN}}{N_{CN}} \pm \Delta Z , \quad (114)$$

where the different signs correspond to the light (+) and the heavy (-) fragment. The width in proton number for fixed neutron number $\sigma_{Z|N}$ is calculated by using the following formula:

$$\sigma_{Z|N}^2 = \frac{1}{2} \frac{\sqrt{E_{mac}(E_0^*, N)}}{\sqrt{\tilde{A}}C_{Z|N}} + \sigma_0^2 , \quad (115)$$

where the term $\sigma_0 = 0.4$ is used to take into account the influence of quantum fluctuations not considered in the statistical picture, and the curvature $2C_{Z|N}$ is calculated in a touching-sphere configuration for a symmetric split as:

$$\begin{aligned} C_{Z|N} = \frac{d^2V}{dZ^2} \Big|_N &= B(Z+1, N) + B(Z-1, N) - 2B(Z, N) \\ &- \frac{e^2}{r_0^2} \left[\frac{(Z+1)(Z-1)}{(A+1)^{1/3} + (A-1)^{1/3}} - \frac{Z^2}{2A^{1/3}} \right] , \end{aligned} \quad (116)$$

with e the electron charge, $r_0 = 1.22$ fm the radius parameter, and $B(Z, N)$ representing the macroscopic binding energy of a nucleus with Z protons and N neutrons. The element yields are modulated by an even-odd effect with the variation of this effect as a function of the fissility parameter is given by:

$$\delta_p = \exp(29.86 - 0.74Z_{CN}^2/A_{CN}) , \quad (117)$$

and the energy dependence is obtained as:

$$\delta_p(E) = \begin{cases} \delta_p & \text{if } 0 \ll E \ll E_1 , \\ \delta_p \exp\left(-\frac{E-E_1}{T}\right) & \text{if } E > E_1 , \end{cases} \quad (118)$$

where $T = 1$ MeV and $E_1 = V_B + 2\Delta$, with V_B the height of the fission saddle point and Δ the pairing gap calculated as $\Delta = 12/\sqrt{A_{CN}}$.

Consecutive evaporation from the excited fission fragments is included, too. The excitation energy of the fragments is taken as the sum of the excitation energy above the barrier and the intrinsic excitation energy E_{dis} on the way from the fission barrier to scission. The latter is parameterized in the following way:

$$E_{dis} = 3.53(Z_{CN}^2/A_{CN} - 34.25) . \quad (119)$$

The final excitation energy is attributed to the fission fragments proportionally to their mass values.

More details about the fission model used in MCNP6 by the ABLA evaporation/fission code can be found in publications [7, 52, 116, 140, 141, 145, 146] and references therein.

6 Fermi Break-up Reactions

As a rule, after the fast INC stage of nuclear reactions, a much slower evaporation/fission stage follows, with or without taking into account an intermediate preequilibrium stage between the INC and the evaporation/fission. Such a picture is well grounded in cases of heavy nuclei, as both evaporation and fission models are based on statistical assumptions, requiring a large number of nucleons. Naturally, in case of light nuclei with only a few nucleons, statistical models are much less justified. The nature of light nuclei is such that their unique nuclear structure must be taken into account in any model calculation, as the effects of their structures are not masked by the statistical behavior caused by a large number of nucleons. In addition, such light nuclei like carbon and oxygen exhibit considerable alpha-particle clustering, not accounted by evaporation/fission models. This is why in the case of light excited nuclei, their deexcitation is often calculated using the so called ‘‘Fermi breakup’’ model, suggested initially by Fermi [21], and subsequently used by, among other, Zhdanov and Fedotov [149] and Gradsztajn et al. [150].

MCNP6 uses two versions of the Fermi breakup model, both discussed briefly below.

6.1 Fermi Breakup Reactions in CEM03.03 and LAQGSM03.03

After calculating the coalescence stage of a reaction, CEM03.03 and LAQGSM03.03 move to the description of the last slower stages of the interaction, namely to preequilibrium decay and evaporation, with a possible competition of fission for nuclei with $Z \geq 65$. But if the residual nuclei have atomic numbers with $A < 13$, CEM03.03 and LAQGSM03.03 use the Fermi breakup model [21] to calculate their further disintegration instead of using the preequilibrium and evaporation models. CEM03.03 and LAQGSM03.03 use the Fermi breakup model also during the preequilibrium and/or evaporation stages of reactions, when the residual nucleus gets an atomic number with $A < 13$ after the emission of several particles or/and light fragments.

Finally, CEM03.03 and LAQGSM03.03 use the Fermi breakup model also to disintegrate the unstable fission fragments with $A < 13$ that can be produced in very rare cases of very asymmetric fission.

All formulas and details of the algorithms of the version of the Fermi breakup model used in CEM and LAQGSM, as developed in the former group of Prof. Barashenkov at the Joint Institute for Nuclear Research (JINR), Dubna, Russia can be found in Ref. [151].

All the information needed to calculate the breakup of an excited nucleus is its excitation energy U and the mass and charge numbers A and Z . The total energy of the nucleus in the rest frame will be $E = U + M(A, Z)$, where M is the mass of the nucleus. The total probability per unit time for a nucleus to break up into n components in the final state (*e.g.*, a possible residual nucleus, nucleons, deuterons, tritons, alphas, *etc.*) is given by

$$W(E, n) = (V/\Omega)^{n-1} \rho_n(E), \quad (120)$$

where ρ_n is the density of final states, V is the volume of the decaying system and $\Omega = (2\pi\hbar)^3$ is the normalization volume. The density $\rho_n(E)$ can be defined as a product of three factors:

$$\rho_n(E) = M_n(E) S_n G_n. \quad (121)$$

The first one is the phase space factor defined as

$$M_n(E) = \int_{-\infty}^{+\infty} \cdots \int_{-\infty}^{+\infty} \delta \left(\sum_{b=1}^n \vec{p}_b \right) \delta \left(E - \sum_{b=1}^n \sqrt{p^2 + m_b^2} \right) \prod_{b=1}^n d^3 p_b, \quad (122)$$

where \vec{p}_b are fragment momenta. The second one is the spin factor

$$S_n = \prod_{b=1}^n (2s_b + 1), \quad (123)$$

which gives the number of states with different spin orientations. The last one is the permutation factor

$$G_n = \prod_{j=1}^k \frac{1}{n_j!}, \quad (124)$$

which takes into account identical particles in the final state (n_j is the number of components of j -type particles and k is defined by $n = \sum_{j=1}^k n_j$). For example, if we have in the final state six particles ($n = 6$) and two of them are alphas, three are nucleons, and one is a deuteron, then $G_6 = 1/(2!3!1!) = 1/12$. For the non-relativistic case, the integration in Eq. (122) can be evaluated analytically (see, *e.g.*, Ref. [151]) and the probability for a nucleus to disintegrate into n fragments with masses m_b , where $b = 1, 2, 3, \dots, n$ is

$$W(E, n) = S_n G_n \left(\frac{V}{\Omega} \right)^{n-1} \left(\frac{1}{\sum_{b=1}^n m_b} \prod_{b=1}^n m_b \right)^{3/2} \frac{(2\pi)^{3(n-1)/2}}{\Gamma(3(n-1)/2)} E^{(3n-5)/2}, \quad (125)$$

where $\Gamma(x)$ is the gamma function.

The angular distribution of n emitted fragments is assumed to be isotropic in the c.m. system of the disintegrating nucleus and their kinetic energies are calculated from momentum-energy conservation. The Monte-Carlo method is used to randomly select the decay channel

according to probabilities defined by Eq. (125). Then, for a given channel, the code calculates kinematic quantities for each fragment according to the n -body phase space distribution using the Kopylov's method [152]. Generally, the Fermi breakup model considers formation of fragments only in their ground and those low-lying states which are stable for nucleon emission. However, several unstable fragments with large lifetimes: ${}^5\text{He}$, ${}^5\text{Li}$, ${}^8\text{Be}$, ${}^9\text{B}$, *etc.* were considered as well by the initial version of the Fermi breakup model code as described in Ref. [151]. The randomly chosen channel will be allowed to decay only if the total kinetic energy E_{kin} of all fragments at the moment of breakup is positive, otherwise a new simulation will be performed and a new channel will be selected. The total kinetic energy E_{kin} can be calculated according to the equation:

$$E_{kin} = U + M(A, Z) - E_{Coulomb} - \sum_{b=1}^n (m_b + \epsilon_b), \quad (126)$$

where m_b and ϵ_b are masses and excitation energies of the fragments, respectively, and $E_{Coulomb}$ is the Coulomb barrier for the given channel. It is approximated by

$$E_{Coulomb} = \frac{3}{5} \frac{e^2}{r_0} \left(1 + \frac{V}{V_0}\right)^{-1/3} \left(\frac{Z^2}{A^{1/3}} - \sum_{b=1}^n \frac{Z_b^2}{A_b^{1/3}}\right), \quad (127)$$

where A_b and Z_b are the mass number and the charge of the b -th particle of a given channel, respectively. V_0 is the volume of the system corresponding to normal nuclear density and $V = kV_0$ is the decaying system volume ($k = 1$ is assumed in the CEM/LAQGSM codes).

Thus, the Fermi breakup model we use has only one free parameter, V or V_0 , the volume of the decaying system, which is estimated as follows:

$$V = 4\pi R^3/3 = 4\pi r_0^3 A/3, \quad (128)$$

where $r_0 = 1.4$ fm.

There is no limitation on the number n of fragments a nucleus may break up into in this version of the breakup model, in contrast to implementations in other codes, such as $n \leq 7$ in LAHET [18] discussed in the next subsection.

In comparison with its initial version as described in [151], the Fermi breakup model used in CEM03.02 and LAQGSM03.02 has been modified [153] to decay the unstable light fragments that were produced by the original code. As mentioned above, the initial routines that describe the Fermi breakup model were written more than twenty years ago in the group of Prof. Barashenkov at JINR, Dubna, and unfortunately had some problems. First, those routines allowed in rare cases production of some light unstable fragments like ${}^5\text{He}$, ${}^5\text{Li}$, ${}^8\text{Be}$, ${}^9\text{B}$, *etc.* as a result of a breakup of some light excited nuclei. Second, they allowed very rarely even production of “neutron stars” (or “proton stars”), *i.e.*, residual “nuclei” produced via Fermi breakup that consist of only neutrons (or only protons). Lastly, those routines could even crash the code, due to very rare cases of division by 0. All these problems of the Fermi breakup model routines were addressed and solved in CEM03.02 [153]; the changes were then put in LAQGSM03.02 [153]. Several observed bugs were also fixed. However, even after solving these problems and after implementing the improved Fermi breakup model into CEM03.02 and LAQGSM03.02 [153], these event generators still could produce some unstable

products via very asymmetric fission, when the excitation energies of those fragments were below 3 MeV so they were not checked and disintegrated with the Fermi breakup model. The analysis performed in Ref. [5] had shown that such events could occur very rarely, in less than 0.0006% of all simulated events, so that production of such unstable nuclides affects by less than 0.0006% the other correct cross sections calculated by CEM03.02 and LAQGSM03.02. However, these unstable nuclides are not physical and should be eliminated. This was the reason why a universal checking of all unstable light products has been incorporated into the following generation of CEM and LAQGSM models, CEM03.03 and LAQGSM03.03. Such unstable products are forced to disintegrate via Fermi breakup independently of their excitation energy. The latest versions of the CEM03.03 and LAQGSM03.03 event generators do not produce any such unstable products.

Examples of results by CEM03.03 and LAQGSM03.03 for different nuclear reactions where the Fermi breakup mechanism is important and simulated, together with more relevant details and references can be found in Refs. [1, 3, 5].

6.2 Fermi Breakup Reactions Simulated with the Bertini INC, ISABEL, or INCL4.2

The version of the Fermi breakup model used in MCNP6 with the Bertini INC, ISABEL, or INCL4.2 originates from LAHET [18] and is described briefly in Refs. [154, 155, 156, 158, 159].

The general physics ideas of this modification of the Fermi breakup model are the same or very similar to the version of the model used by CEM03.03 and LAQGSM03.03 discussed in the previous subsection, therefore this is not repeated here. However, this version of the Fermi breakup model differs in several important features and implementations from the one used by CEM03.03 and LAQGSM03.03, like:

1) Perhaps the most significant feature of this version of the Fermi breakup model is that particle-unstable states are allowed as intermediate states, thus permitting sequential decay processes.

2) Two-body breakup channels use a Coulomb barrier penetration factor approximated from Coulomb wave functions, while multi-particle modes use a breakup threshold adjusted for Coulomb energy.

3) Two-body breakup of levels with known spin and parity are restricted to conserve parity and isospin and are inhibited by neutral particle angular momentum barrier penetration factors.

4) Only up to seven-body breakup modes are allowed.

Experimental data are used for mass excesses and for the excitation energies, spins, and isospins, and parities of nuclear levels.

The real employment of this version of the Fermi breakup model in MCNP6 also differ from the one used with CEM03.03 and LAQGSM03.03: By default, MCNP6 uses it with the Bertini INC, ISABEL, or INCL4.2 when the atomic mass of excited nuclei, A , is $A \leq 13$, and also for $14 \leq A \leq 20$ in cases when the excitation energy is below 44 MeV. But MCNP6 users can change this default option with the 5th entry on the **LCA** MCNP6 input card, *ifbrk*: If to use *ifbrk* = 0, Fermi breakup model will be used only for nuclei with $A \leq 5$.

More details about this version of the Fermi breakup model can be found in Refs. [154, 155, 156, 158, 159].

7 Coalescence Reactions

The coalescence model is used in MCNP6 only with the CEM03.03 and LAQGSM03.03 event generators. Its aim is to describe production of very energetic light fragments that would not come from other reaction mechanisms. In addition, the coalescence mechanism of nuclear reactions contributes also to some production of intermediate-, and even low-energy light fragments, improving the general predictive power of the CEM and LAQGSM models accounting for such reactions.

When the cascade stage of a reaction is completed, CEM03.03 and LAQGSM03.03 use the coalescence model described in Refs. [22, 41] to “create” high-energy d , t , ${}^3\text{He}$, and ${}^4\text{He}$ by final-state interactions among emitted cascade nucleons, already outside of the target nucleus. In contrast to most other coalescence models for heavy-ion-induced reactions, where complex-particle spectra are estimated simply by convolving the measured or calculated inclusive spectra of nucleons with corresponding fitted coefficients, CEM03.03 and LAQGSM03.03 use in their simulations of particle coalescence real information about all emitted cascade nucleons and do not use integrated spectra. These models assume that all the cascade nucleons having differences in their momenta smaller than p_c and the correct isotopic content form an appropriate composite particle. This means that the formation probability for, *e.g.* a deuteron is

$$W_d(\vec{p}, b) = \int \int d\vec{p}_p d\vec{p}_n \rho^C(\vec{p}_p, b) \rho^C(\vec{p}_n, b) \delta(\vec{p}_p + \vec{p}_n - \vec{p}) \Theta(p_c - |\vec{p}_p - \vec{p}_n|), \quad (129)$$

where the particle density in momentum space is related to the one-particle distribution function f by

$$\rho^C(\vec{p}, b) = \int d\vec{r} f^C(\vec{r}, \vec{p}, b). \quad (130)$$

Here, b is the impact parameter for the projectile interacting with the target nucleus and the superscript index C shows that only cascade nucleons are taken into account for the coalescence process. The coalescence radii p_c were fitted for each composite particle in Ref. [41] to describe available data for the reaction Ne+U at 1.04 GeV/nucleon, but the fitted values turned out to be quite universal and were subsequently found to satisfactorily describe high-energy complex-particle production for a variety of reactions induced both by particles and nuclei at incident energies up to about 200 GeV/nucleon, when describing nuclear reactions with different versions of LAQGSM [4, 5, 153] or with its predecessor, the Quark-Gluon String Model (QGSM) [42]. These parameters are:

$$p_c(d) = 90 \text{ MeV}/c; \quad p_c(t) = p_c({}^3\text{He}) = 108 \text{ MeV}/c; \quad p_c({}^4\text{He}) = 115 \text{ MeV}/c. \quad (131)$$

As the INC of CEM is different from those of LAQGSM or QGSM, it is natural to expect different best values for p_c as well. Recent studies have shown (see *e.g.*, Refs. [1, 3] and references therein) that the values of parameters p_c defined by Eq. (131) are also good for

CEM03.03 for projectile particles with kinetic energies T_0 lower than 300 MeV and equal to or above 1 GeV. For incident energies in the interval $300 \text{ MeV} < T_0 \leq 1 \text{ GeV}$, a better overall agreement with the available experimental data is obtained by using values of p_c equal to 150, 175, and 175 MeV/c for d , $t(^3\text{He})$, and ^4He , respectively. These values of p_c are fixed as defaults in CEM03.03. If several cascade nucleons are chosen to coalesce into composite particles, they are removed from the distributions of nucleons and do not contribute further to such nucleon characteristics as spectra, multiplicities, *etc.*

In comparison with the initial version [22, 41], in CEM03.03 and LAQGSM03.03, several coalescence routines have been changed and have been tested against a large variety of measured data on nucleon- and nucleus-induced reactions at different incident energies. Many examples with results by CEM03.03 and LAQGSM03.03 for reactions where the contribution from the coalescence mechanism is important and can be easily seen may be found in Refs. [3, 40, 47].

Note that the latest versions of the INCL code, *e.g.*, INCL4.3 [160], INCL4.4 [70], and INCL++ [161], also consider (in different ways) the coalescence of nucleons in the very outskirts of the nuclear surface into light fragments during the INC stages of reactions. MCNP6 does not have yet these latest versions of INCL implemented into the code, therefore details of their coalescence model are not discussed here.

References

- [1] Stepan G. Mashnik and Arnold J. Sierk, “CEM03.03 User Manual,” LANL Report LA-UR-12-01364, Los Alamos, 2012; RSICC Code Package <http://www-rsicc.ornl.gov/codes/psr/psr5/psr-532.html>; <http://www.oecd-neutrona.org/tools/abstract/detail/psr-0532/>.
- [2] K. K. Gudima, S. G. Mashnik, and V. D. Toneev, “Cascade-Exciton Model of Nuclear Reactions,” Nucl. Phys. **A401** (1983) 329–361.
- [3] S. G. Mashnik, K. K. Gudima, R. E. Prael, A. J. Sierk, M. I. Baznat, and N. V. Mokhov, “CEM03.03 and LAQGSM03.03 Event Generators for the MCNP6, MCNPX, and MARS15 Transport Codes,” Invited lectures presented at the Joint ICTP-IAEA Advanced Workshop on Model Codes for Spallation Reactions, February 4–8, 2008, ICTP, Trieste, Italy, LANL Report LA-UR-08-2931, Los Alamos, 2008; E-print: arXiv:0805.0751.
- [4] K. K. Gudima, S. G. Mashnik, and A. J. Sierk, “User Manual for the Code LAQGSM,” LANL Report LA-UR-01-6804, Los Alamos, 2001.
- [5] S. G. Mashnik, K. K. Gudima, N. V. Mokhov, and R. E. Prael, “LAQGSM03.03 Upgrade and Its Validation,” LANL Report LA-UR-07-6198, Los Alamos, 2007; E-print: arXiv:0709.173.
- [6] A. Boudard, J. Cugnon, S. Leray, and C. Volant, “Intranuclear Cascade Model for a Comprehensive Description of Spallation Reaction Data,” Phys. Rev. C **66** (2002) 044615.
- [7] A. R. Junghans, M. de Jong, H.-G. Clerc, A.V. Ignatyuk, G. A. Kudyaev, and K.-H. Schmidt, “Projectile-Fragment Yields as a Probe for the Collective Enhancement in

- the Nuclear Level Density,” Nucl. Phys. **A629** (1998) 635–655; J.-J. Gaimard and K.-H. Schmidt, “A Reexamination of the Abrasion-Ablation Model for the Description of the Nuclear Fragmentation Reaction,” Nucl. Phys. **A531** (1991) 709–745.
- [8] Hugo W. Bertini, “Low-Energy Intranuclear Cascade Calculation,” Phys. Rev. **131** (1963) 1801–1871; “Intranuclear Cascade Calculation of the Secondary Nucleon Spectra from Nucleon-Nucleus Interactions in the Energy Range 340 to 2900 MeV and Comparison with Experiment,” Phys. Rev. **188** (1969) 1711–1730.
- [9] Y. Yariv and Z. Frankel, “Intranuclear Cascade Calculation of High-Energy Heavy-Ion Interactions,” Phys. Rev. C **20** (1979) 2227–2243.
- [10] K. K. Gudima, G. A. Ososkov, and V. D. Toneev, “Model for Pre-Equilibrium Decay of Excited Nuclei,” Yad. Fiz. **21** (1975) 260–272 [Sov. J. Nucl. Phys. **21** (1975) 138–143].
- [11] S. G. Mashnik and V. D. Toneev, “MODEX—the Program for Calculation of the Energy Spectra of Particles Emitted in the Reactions of Pre-Equilibrium and Equilibrium Statistical Decays,” JINR Communication P4-8417, Dubna, 1974.
- [12] R. E. Prael and M. Bozoian, “Adaption of the Multistage Preequilibrium Model for the Monte Carlo Method,” LANL Report LA-UR-88-3238, Los Alamos, 1988.
- [13] I. Dostrovsky, Z. Frankel, and G. Friedlander, “Monte Carlo Calculations of Nuclear Evaporation Processes. III. Application to Low-Energy Reactions,” Phys. Rev. **116** (1959) 683–702; I. Dostrovsky, P. Rabinowitz, and R. Bivins, “Monte Carlo Calculations of High-Energy Nuclear Interactions. I. Systematics of Nuclear Evaporation,” Phys. Rev. **111** (1958) 1659–1676.
- [14] L. Dresner, “EVAP – A Fortran Program for Calculation the Evaporation of Various Particles from Excited Compound Nuclei”, ORNL-TM-196, Oak Ridge National Laboratory, 1962.
- [15] M. P. Guthrie, “EVAP-2 and EVAP-3 – Modifications of a Code to Calculate Particle Evaporation from Excited Compound Nuclei,” ORNL-TM-4379, Oak Ridge National Laboratory, 1969; “Corrections in the DRES Subroutine of the EVAP Codes,” 1971.
- [16] M. P. Guthrie, “Another Modification of a Code to Calculate Particle Evaporation from Excited Compound Nuclei,” ORNL-TM-3119, Oak Ridge National Laboratory, 1970.
- [17] P. Cloth, D. Filges, R. D. Neef, G. Sterzenbach, T. W. Armstrong, B. L. Colborn, H. Brueckmann, and B. Anders, “HERMES, A Monte Carlo Program System for Beam-Materials Interaction Studies,” Jülich GmbH, JUL-2203, Jülich, Germany, 1988.
- [18] R. E. Prael and H. Lichtenstein, “User guide to LCS: The LAHET Code System,” LANL Report LA-UR-89-3014, Los Alamos, 1989.
- [19] J. Barish, T. A. Gabriel, F. S. Alsmiller, and R. G. Alsmiller, Jr., “HETFIS High-Energy Nucleon Meson Transport Code with Fission,” ORNL/TM-7882, Oak Ridge National Laboratory, 1981; F. S. Alsmiller, R. G. Alsmiller, Jr., T. A. Gabriel, R. A. Lillie, and J. Barish, “A Phenomenological Model for Particle Production from the Collisions of Nucleons and Pions with Fissile Elements at Medium Energies,” Nucl. Sci. Eng. **79** (1981) 147–161.

- [20] F. Atchison, “Spallation and Fission in Heavy Metal Nuclei under Medium Energy Proton Bombardment,” in Proc. Meeting on Targets for Neutron Beam Spallation Source, Jülich, June 11–12, 1979, pp. 17–46, G. S. Bauer, Ed., Jül-Conf-34, Kernforschungsanlage Jülich GmbH, Germany (1980); F. Atchison, “A Treatment of Medium-Energy Particle Induced Fission for Spallation-Systems’ Calculations,” Nucl. Instrum. Methods B **259** (2007) 909–932.
- [21] E. Fermi, “High Energy Nuclear Events”, Prog. Theor. Phys. **5** (1950) 570–583.
- [22] K. K. Gudima, G. Röpke, H. Schulz, and V. D. Toneev, “The Coalescence Model and Pauli Quenching in High-Energy Heavy-Ion Collisions,” JINR Preprint JINR-E2-83-101, Dubna, 1983; H. Schulz, G. Röpke, K. K. Gudima, and V. D. Toneev, “The Coalescence Phenomenon and the Pauli Quenching in High-Energy Heavy-Ion Collisions,” Phys. Lett. B **124** (1983) 458–460.
- [23] V. S. Barashenkov and V. D. Toneev, *Interaction of High Energy Particle and Nuclei with Atomic Nuclei*, Atomizdat, Moscow (1972).
- [24] V. S. Barashenkov, A. S. Iljinov, N. M. Sobolevskii, and V. D. Toneev, “Interaction of Particles and Nuclei of High and Ultrahigh Energy with Nuclei,” Usp. Fiz. Nauk **109** (1973) 91–136 [Sov. Phys. Usp. **16** (1973) 31–52].
- [25] M. L. Goldberger, “The Interaction of High Energy Neutrons and Heavy Nuclei,” Phys. Rev. **74** (1948) 1269–1277.
- [26] R. Serber, “Nuclear Reactions at High Energies,” Phys. Rev. **72** (1947) 1114–1115.
- [27] V. S. Barashenkov, K. K. Gudima, and V. D. Toneev, “Intranuclear Cascade Calculation Scheme,” [in Russian] JINR Communication P2-4065, Dubna, 1968.
- [28] V. S. Barashenkov, K. K. Gudima, and V. D. Toneev, “Statistical Calculation of Inelastic Collisions of Fast Particles with Intranuclear Nucleons,” [in Russian] JINR Communication P2-4066, Dubna, 1968; Acta Physica Polonica **36** (1969) 415–432.
- [29] S. G. Mashnik, M. I. Baznat, K. K. Gudima, A. J. Sierk, and R. E. Prael, “Extension of the CEM2k and LAQGSM Codes to Describe Photo-Nuclear Reactions,” LANL Report LA-UR-05-2013, Los Alamos (2005), E-print: nucl-th/0503061; “CEM03 and LAQGSM03: Extension of the CEM2k+GEM2 and LAQGSM Codes to Describe Photo-Nuclear Reactions at Intermediate Energies (30 MeV to 1.5 GeV),” J. Nucl. Radiochem. Sci. **6** (2005) A1–A19.
- [30] K. K. Gudima, A. S. Iljinov, and V. D. Toneev, “A Cascade Model for Photonuclear Reactions,” [in Russian] JINR Communication P2-4661, Dubna, 1969.
- [31] V. S. Barashenkov, F. G. Gegeri, A. S. Iljinov, G. G. Jonsson, and V. D. Toneev, “A Cascade-Evaporation Model for Photonuclear Reactions,” Nucl. Phys. **A231** (1974) 462–476.
- [32] J. S. Levinger, “The High Energy Nuclear Photoeffect,” Phys. Rev. **84** (1951) 43–51.
- [33] W. O. Lock and D. F. Measday, *Intermediate Energy Nuclear Physics*, London, Methuen; [Distributed in the U.S.A. by Barnes and Noble, 1970].

- [34] S. G. Mashnik, *User Manual for the Code CEM95*, 1995, Bogoliubov Laboratory of Theoretical Physics, Joint Institute for Nuclear Research, Dubna, Russia; OECD Nuclear Energy Agency Data Bank, Le Seine Saint-Germain 12, Boulevard des Iles, F-92130 Issy-les-Moulineaux, Paris, France <http://www.nea.fr/abs/html/iaea1247.html>; Radiation Safety Information Computational Center (RSICC), Oak Ridge, USA, <http://www-rsicc.ornl.gov/codes/psr/psr3/psr-357.html>.
- [35] S. G. Mashnik and A. J. Sierk, “Improved Cascade-Exciton Model of Nuclear Reactions,” LANL Report LA-UR-98-5999, Los Alamos, 1998; E-print: nucl-th/9812069; Proc. SARE-4, Knoxville, TN, September 13–16, 1998, edited by Tony A. Gabriel (ORNL, 1999), pp. 29–51.
- [36] H. Duarte, “An Intranuclear Cascade Model for High Energy Transport Codes,” Proc. Int. Conf. on Accelerator-Driven Transmutation Technologies and Applications (ADTT’99), Praha, Czech Republic, June 7–11, 1999, paper Mo–O–C17 on the Conference CD–ROM and Web page http://fjfi.cvut.cz/con_adtt99; “Particle Production in Nucleon Induced Reactions Above 14 MeV with an Intranuclear Cascade Model,” Phys. Rev. C **75** (2007) 024611.
- [37] S. G. Mashnik, K. K. Gudima, A. J. Sierk, and R. E. Prael, “Improved Intranuclear Cascade Models for the Codes CEM2k and LAQGSM,” LA-UR-05-0711, Los Alamos, 2005; E-print: nucl-th/0502019; Proc. ND2004, September 26–October 1, 2004, Santa Fe, NM, USA, edited by R. C. Haight, M. B. Chadwick, T. Kawano, and P. Talou, (AIP Conf. Proc. **769**, Melville, New York, 2005), pp. 1188–1192.
- [38] A. S. Iljinov, I. A. Pshenichnov, N. Bianchi, E. De Sanctis, V. Muccifora, M. Mirazita, and P. Rossi, “Extension of the Intranuclear Cascade Model for Photonuclear Reactions at Energies up to 10 GeV,” Nucl. Phys. **A616** (1997) 575–605.
- [39] S. J. Lindenbaum and R. M. Sternheimer, “Isobaric Nucleon Model for Pion Production in Nucleon-Nucleon Collisions,” Phys. Rev. **105** (1957) 1874–1899; “Pion Production in Pion-Nucleon Collisions,” Phys. Rev. **109** (1958) 1723–1733; “Extension of the Isobaric Nucleon Model for Pion Production in Pion-Nucleon, Nucleon-Nucleon, and Antinucleon-Nucleon Interactions,” Phys. Rev. **123** (1958) 333–376.
- [40] K. K. Gudima and S. G. Mashnik, “Extension of the LAQGSM03 Code to Describe Photo-Nuclear Reactions up to Tens of GeV,” Proc. 11th Internat. Conf. on Nuclear Reaction Mechanisms, Varenna, Italy, June 12–16, 2006, edited by E. Gadioli (2006) pp. 525–534; E-print: nucl-th/0607007.
- [41] V. D. Toneev and K. K. Gudima, “Particle Emission in Light and Heavy-Ion Reactions,” Nucl. Phys. **A400** (1983) 173c–190c.
- [42] N. S. Amelin and V. S. Barashenkov, “Intranuclear Cascade with Quark-Gluon Strings,” (in Russian) JINR Preprint P2-83-770, Dubna, 1983; N. S. Amelin, K. K. Gudima, and V. D. Toneev, “The Quark-Gluon String Model and Ultrarelativistic Heavy-Ion Collisions,” Yad. Fiz. **51** (1990) 512–523 [Sov. J. Nucl. Phys. **51** (1990) 327–333]; N. S. Amelin, K. K. Gudima, and V. D. Toneev, “Further Development of the Model of Quark-Gluon Strings for the Description of High-Energy Collisions with a Target Nucleus,” Yad. Fiz. **52** (1990) 272–282 [Sov. J. Nucl. Phys. **52** (1990) 172–178].

- [43] N. S. Amelin, “Simulation of Nuclear Collisions at High Energy in the Framework of the Quark-Gluon String Model,” JINR Communication JINR-86-802, Dubna, 1986.
- [44] A. B. Kaidalov, “Quark and Diquark Fragmentation Functions in the Model of Quark-Gluon Strings,” *Yad. Fiz.* **45** (1987) 1452–1461 [*Sov. J. Nucl. Phys.* **45** (1987) 902–907].
- [45] N. S. Amelin, V. S. Barashenkov, and N. V. Slavin, “Monte-Carlo Simulation of Multi-particle Production in High-Energy Collisions of Hadrons,” *Yad. Fiz.* **40** (1984) 1560–1569 [*Sov. J. Nucl. Phys.* **40** (1984) 991–996].
- [46] S. S. Adler *et al.* [PHENIX Collaboration], “Nuclear Effects on Hadron Production in d+Au and $p + p$ Collisions at $\sqrt{s_{NN}} = 200$ GeV Revealed by Comparison with $p + p$ Data” *Phys. Rev. C* **74**, (2006) 024904; tabulated values of data are available at: http://www.phenix.bnl.gov/phenix/WWW/info/data/ppg030/ppg030_data.txt.
- [47] Stepan G. Mashnik, “Validation and Verification of MCNP6 Against Intermediate and High-Energy Experimental Data and Results by Other Codes,” LANL Report LA-UR-10-07847, Los Alamos, 2010; arXiv:1011.4978; *Eur. Phys. J. Plus* (2011) **126**: 49.
- [48] Stepan G. Mashnik, “Validation and Verification of MCNP6 Against High-Energy Experimental Data and Calculations by Other Codes. I. The CEM Testing Primer,” LANL Report LA-UR-11-05129, Los Alamos, 2011.
- [49] Stepan G. Mashnik, “Validation and Verification of MCNP6 against High-Energy Experimental Data and Calculations by other Codes. II. The LAQGSM Testing Primer,” LANL Report LA-UR-11-05627, Los Alamos, 2011.
- [50] Stepan G. Mashnik, “Validation and Verification of MCNP6 Against High-Energy Experimental Data and Calculations by Other Codes. III. The MPI Testing Primer,” LANL Report LA-UR-13-26944, Los Alamos, 2013.
- [51] Stepan G. Mashnik, “V&V of MCNP 6.1.1 Beta Against Intermediate and High-Energy Experimental Data,” LANL Report LA-UR-14-27018, Los Alamos, 2014.
- [52] Detlef Filges and Frank Goldenbaum, *Handbook of Spallation Research: Theory, Experiments and Applications*, WILEY-VCH Verlag GmbH & Co., 2009.
- [53] D. H. Wright and M. H. Kelsey, for the GEANT4 Hadronics Working Group, “The Geant4 Bertini Cascade,” *Nucl. Instrum. Methods A* **804** (2015) 175–188.
- [54] H. Grady Hughes, R. E. Prael, and R. C. Little, “MCNPX - The LAHET/MCNP Code Merger,” LANL Report LA-UR-97-4891, Los Alamos, 1997; Denise B. Pelowitz, Joe W. Durkee, Jay S. Elson, Michael L. Fensin, John S. Hendricks, Michael R. James, Russell C. Johns, Gregg W. McKinney, Stepan G. Mashnik, Jerome M. Verbeke, Laurie S. Waters, and Trevor A. Wilcox, “MCNPX 2.7.0 Extensions,” LANL Report LA-UR-11-02295, Los Alamos, 2011 and references therein; <https://mcnpx.lanl.gov/>.
- [55] H. W. Bertini, M. P. Guthrie, and O. W. Hermann, “Instructions for the Operation of Codes Associated with MECC-7, A Preliminary Version of an Intranuclear-Cascade Calculation for Nuclear Reactions.” ORNL-4564, 1971, (updated code version 1973).
- [56] Computer program CCC-0156 MECC-7, MECC-7, Medium-Energy Intranuclear Cascade Code System, Nuclear Energy Agency, Organisation for Economic Cooperation and Development (NEA OECD), Paris, France, <http://www.oecd-nea.org/tools/abstract/detail/ccc-0156/>.

- [57] T. W. Armstrong and K. C. Chandler, “HETC — A High Energy Transport Code,” *Nucl. Sci. and Engr.* **49** (1972) 110–111; Tony W. Armstrong, “Lecture 23: The HETC Hadronic Cascade Code,” p. 373 in: *Computer Techniques in Radiation Transport and Dosimetry* W. R. Nelson et al. (eds.), Plenum Press, New York 1980.
- [58] Hugo W. Bertini and Miriam P. Guthrie, “New Item Results from Medium-Energy Intranuclear-Cascade Calculation,” *Nucl. Phys.* **A169** (1971) 670–672.
- [59] Hugo W. Bertini, “Nonelastic Interactions of Nucleons and π Mesons with Complex Nuclei at Energies Below 3 GeV,” *Phys. Rev. C* **6** (1972) 631–659.
- [60] V. S. Barashenkov, H. W. Bertini, K. Chen, G. Friedlander, G. D. Harp, A. S. Iljinov, J. M. Miller, and V. D. Toneev, “Medium Energy Intranuclear Cascade Calculations: A Comparative Study,” *Nucl. Phys.* **A187** (1972) 531–544.
- [61] Y. Yariv, “ISABEL — INC Model for High-Energy Hadron-Nucleus Reactions,” pp. 15–28 in: *Joint ICTP-IAEA Advanced Workshop on Model Codes for Spallation Reactions*, International Centre for Theoretical Physics Trieste, Italy, 4 – 8 February 2008, prepared by D. Filges, S. Leray, Y. Yariv, A. Mengoni, A. Stanculescu, and G. Mank, IAEA Nuclear Data Section, Wagramer Strasse 5, A-1400 Vienna, Austria, INDC(NDS)-0530, August 2008.
- [62] K. Chen, Z. Fraenkel, G. Friedlander, J. R. Grover, J. M. Miller, and Y. Shimamoto, “VEGAS: A Monte Carlo Simulation of Intranuclear Cascades,” *Phys. Rev.* **166** (1968) 949–967.
- [63] Y. Yariv and Z. Frankel, “Inclusive Cascade Calculation of High Energy Heavy Ion Collisions: Effect of Interactions between Cascade Particles,” *Phys. Rev. C* **24** (1981) 488–494.
- [64] M. R. Clover, R. M. DeVries, N. J. DiGiacomo, and Y. Yariv, “Low Energy Antiproton-Nucleus Interactions,” *Phys. Rev. C* **26** (1982) 2138–2151.
- [65] G. D. Harp, K. Chen, G. Friedlander, Z. Fraenkel, and J. M. Miller, “Intranuclear Cascade Studies of Low-Energy Pion-Induced Nuclear Reactions: Possible Effects of the Finite Lifetime of the (3,3) Isobar,” *Phys. Rev. C* **8** (1973) 581–593; G. D. Harp, “Extension of the Isobar MKodel for Intranuclear Cascades to 1 GeV,” *Phys. Rev. C* **10** (1973) 2387–2396.
- [66] J. N. Ginocchio “Deep Inelastic Pion-Induced Nuclear Reactions in the Isobar Model,” *Phys. Rev. C* **17** (1978) 195–214.
- [67] T. P. Clements and L. Winsberg, “Polynomial Fits of Nucleon-Nucleon Scattering Data,” Lawrence Radiation Laboratory Report UCRL-9043 (1960).
- [68] Zeev Fraenkel “Pion Capture in Complex Nuclei,” *Phys. Rev.* **130** (1963) 2407–2416; Z. Fraenkel, “The Interactions of Unstable Particles,” *Nuovo Cimento* **30** (1963) 512–521.
- [69] G. Giacomelli, P. Pini, and S. Stagni, “Compilation of Pion-Nucleon Scattering Data,” Report CERN-HERA 69-1, Geneva, Switzerland, 1969.
- [70] A. Boudard and J. Cugnon, “INCL4 — The Liège INC Model for High-Energy Hadron-Nucleus Reactions. A Short Description of the INCL4.2 and INCL4.4 Versions,” pp.

- 29-50 in: *Joint ICTP-IAEA Advanced Workshop on Model Codes for Spallation Reactions*, International Centre for Theoretical Physics Trieste, Italy, 4 – 8 February 2008, prepared by D. Filges, S. Leray, Y. Yariv, A. Mengoni, A. Stanculescu, and G. Mank, IAEA Nuclear Data Section, Wagramer Strasse 5, A-1400 Vienna, Austria, INDC(NDS)-0530, August 2008.
- [71] J. Cugnon, D. L'Hôte, and J. Vandermeulen, "Simple Parametrization of Cross-Sections for Nuclear Transport Studies up to the GeV Range," *Nucl. Instrum. Methods B* **111** (1996) 215–220.
- [72] E. Gadioli and P. E. Hodgson, *Pre-Equilibrium Nuclear Reactions*, Oxford University Press, New York (1992).
- [73] F. A. Zhivopistsev, E. I. Kebin, and V. G. Sukharevskii, *Pre-Equilibrium Nuclear Reactions*, (in Russian) Moscow State University, Moscow, Part I (1984) and Part II (1985); see also F. A. Zhivopistsev, E. I. Kebin, and V. G. Sukharevskii, *Pre-Equilibrium Nuclear Reaction Models*, (in Russian) Moscow State University, Moscow (1987).
- [74] M. BLANN, "Preequilibrium Decay," *Annu. Rev. Nucl. Sci.* **25** (1975) 123–166.
- [75] K. Seidel, D. Seeliger, R. Reif, and V. D. Toneev, "Pre-Equilibrium Decay in Nuclear Reactions," *Fiz. Elem. Chast. i Atom. Yad. [Sov. J. Part. Phys.]* **7** (1976) 499–522.
- [76] T. Ericson, "The Statistical Model and Nuclear Level Densities," *Adv. in Physics* **9** (1960) 425–511.
- [77] F. C. Williams Jr., "Intermediate State Transition Rates in the Griffin Model," *Phys. Lett. B* **31** (1970) 184–186.
- [78] F. C. Williams Jr., "Particle-Hole State Density in the Uniform Spacing Model," *Nucl. Phys.* **A161** (1971) 231–240.
- [79] I. Ribansky, P. Oblozinsky, and E. Betak, "Pre-Equilibrium Decay and the Exciton Model," *Nucl. Phys.* **A205** (1973) 545–560.
- [80] N. Metropolis, R. Bivins, M. Storm, A. Turkevich, J. M. Miller, and G. Friedlander, "Monte Carlo Calculations on Intranuclear Cascades. I. Low-Energy Studies," *Phys. Rev.* **110** (1958) 185–203.
- [81] G. Mantzouranis, H. A. Weidenmüller, and D. Agassi, "Generalized Exciton Model for the Description of Preequilibrium Angular Distributions," *Z. Phys. A* **276** (1976) 145–154.
- [82] C. Kalbach, "Systematics of Continuum Angular Distributions: Extensions to Higher Energies," LANL Report LA-UR-87-4139, Los Alamos, 1987; *Phys. Rev. C* **37** (1988) 2350–2370.
- [83] V. F. Weisskopf, "Statistics and Nuclear Reactions," *Phys. Rev.* **52** (1937) 295–303; V. F. Weisskopf and D. H. Ewing, "On the Yield of Nuclear Reactions with Heavy Elements," *Phys. Rev.* **57** (1940) 472–483.
- [84] N. Bohr and J. A. Wheeler, "The Mechanism of Nuclear Fission," *Phys. Rev.* **56** (1939) 426–450.

- [85] A. J. Sierk and S. G. Mashnik, “Modeling Fission in the Cascade-Exciton Model,” LANL Report LA-UR-98-5998, 1998; E-print: nucl-th/9812070; Proc. SARE-4, Knoxville, TN, September 13–16, 1998, edited by Tony A. Gabriel (ORNL, 1999), pp. 53–67.
- [86] A. V. Ignatyuk, G. N. Smirenkin, and A. S. Tishin, “Phenomenological Description of the Energy Dependence of the Level Density Parameter,” *Yad. Fiz.* **21** (1975) 485–490 [*Sov. J. Nucl. Phys.* **21** (1975) 255–257]; A. V. Ignatyuk, M. G. Itkis, V. N. Okolovich, G. N. Smirenkin, and A. S. Tishin, “Fission of Pre-Actinide Nuclei. Excitation Functions for the (α, f) Reactions,” *Yad. Fiz.* **21** (1975) 1185–1205 [*Sov. J. Nucl. Phys.* **21** (1975) 612–621].
- [87] A. S. Iljinov, M. V. Mebel, N. Bianchi, E. De Sanctis, C. Guaraldo, V. Lucherini, V. Muccifora, E. Polli, A. R. Reolon, and P. Rossi, “Phenomenological Statistical Analysis of Level Densities, Decay Width and Lifetimes of Excited Nuclei,” *Nucl. Phys.* **A543** (1992) 517–557.
- [88] P. Möller, J. R. Nix, W. D. Myers, and W. J. Swiatecki, “Nuclear Ground-States Masses and Deformations,” *Atomic Data and Nuclear Data Tables*, **59** (1995) 185–381.
- [89] P. Möller, J. R. Nix, and K.-L. Kratz, “Nuclear Properties for Astrophysical and Radioactive-Ion-Beam Application,” *Atomic Data and Nuclear Data Tables*, **66** (1997) 131–343.
- [90] S. G. Mashnik and A. J. Sierk, “CEM2k—Recent Developments in CEM,” LANL Report LA-UR-00-5437, Los Alamos, 2000; E-print: nucl-th/0011064; Proc. AccApp00, November 12–16, 2000, Washington, DC (USA), ANS, La Grange Park, IL, 2001, pp. 328–341.
- [91] S. G. Mashnik, K. K. Gudima, and A. J. Sierk, “Merging the CEM2k and LAQGSM Codes with GEM2 to Describe Fission and Light-Fragment Production,” LANL Report LA-UR-03-2261, Los Alamos, 2003; E-print: nucl-th/0304012; Proc. SATIF-6, April 10–12, 2002, Stanford Linear Accelerator Center, CA 94025, USA, (NEA/OECD, Paris, France, 2004), pp. 337–366.
- [92] M. Veselský, “Production Mechanism of Hot Nuclei in Violent Collisions in the Fermi Energy Domain,” *Nucl Phys.* **A705** (2002) 193–222; M. Veselský, Š. Šáro, F. P. Heßberger, V. Ninov, S. Hofmann, and D. Ackermann, “Production of Fast Evaporation Residues by the Reaction $^{20}\text{Ne} + ^{208}\text{Pb}$ at Projectile Energies of 8.6, 11.4 and 14.9 A MeV,” *Z. Phys. A* **356** (1997) 403–410.
- [93] E. D. Arthur, “The GNASH Preequilibrium-Statistical Model Code,” LANL Report LA-UR-88-382, Los Alamos, 1988; P. G. Young, E. D. Arthur, and M. B. Chadwick “Comprehensive Nuclear Model Calculations: Introduction to the Theory and Use of the GNASH Code,” LANL Report LA-12343-MS, Los Alamos, 1992.
- [94] C. Kalbach, “PRECO-D2: Program for Calculating Preequilibrium and Direct Reaction Double Differential Cross Sections,” LANL Report LA-10248-MS, Los Alamos, 1985.
- [95] H. Gruppelaar and J. M. Akkermans, “The GRAPE Code System for the Calculation of Precompound and Compound Nuclear Reactions — GRYPHON Code Description and Manual,” ECN-164, Netherlands Energy Research Foundation ECN, 1985.

- [96] <http://www.fluka.org/fluka.php>.
- [97] A. Gilbert and A. G. W. Cameron, “A Composite Nuclear-Level Density Formula with Shell Corrections,” *Can. J. Phys.* **43** (1965) 1446–1496.
- [98] P. Cloth, D. Filges, G. Sterzenbach, T. W. Armstrong and B. L. Colborn, “The KFA-Version of the High-Energy Transport Code HETC and the Generalized Evaluation Code SIMPEL”, Kernforschungsanlage Jülich Report Jül-Spez-196, 1983.
- [99] S. Furihata, “Statistical Analysis of Light Fragment Production from Medium Energy Proton-Induced Reactions,” *Nucl. Instr. Meth. B* **171** (2000) 252–258; “The Gem Code — the Generalized Evaporation Model and the Fission Model,” Proc. MC2000, Lisbon, Portugal, 2000, edited by A. Kling, F. J. C. Barão, M. Nakagawa, L. Távora, and P. Vaz, Springer, Berlin, (2001), pp. 1045–1050; *The Gem Code Version 2 Users Manual*, Mitsubishi Research Institute, Inc., Tokyo, Japan (November 8, 2001).
- [100] S. Furihata, K. Niita, S. Meigo, Y. Ikeda, and F. Maekawa, “The Gem Code—a Simulation Program for the Evaporation and Fission process of an Excited Nucleus,” JAERI-Data/Code 2001-015, JAERI, Tokai-mura, Naka-gam, Ibaraki-ken, Japan, 2001.
- [101] S. Furihata, *Development of a Generalized Evaporation Model and Study of Residual nuclei Production*, Ph.D. thesis, Tohoku University, March, 2003; S. Furihata and T. Nakamura, “Calculation of Nuclide Production from Proton Induced Reactions on heavy Targets with INC/GEM,” *J. Nucl. Sci. Technol. Suppl.* **2** (2002) 758–761.
- [102] G. Audi and A. H. Wapstra, “The 1995 Update to the Atomic Mass Evaluation,” *Nucl. Phys.* **A595** (1995) 409–480.
- [103] P. E. Haustein, “An Overview of the 1986–1987 Atomic Mass Predictions,” *Atomic Data and Nuclear Data Tables* **39** (1988) 185–393.
- [104] A. G. W. Cameron, “A Revised Semiempirical Atomic Mass Formula,” *Can. J. Phys.* **35** (1957) 1021–1032.
- [105] T. Matsuse, A. Arima, and S. M. Lee, “Critical Distance in Fusion Reactions,” *Phys. Rev. C* **26** (1982) 2338–2341.
- [106] A. S. Botvina, A. S. Iljinov, I. N. Mishustin, J. P. Bondorf, R. Donangelo, and K. Snappen, “Statistical Simulation of the Break-up of Highly Excited Nuclei,” *Nucl. Phys.* **A475** (1987) 663–686.
- [107] J. L. Cook, H. Ferguson, and A. R. del Musgrove, “Nuclear Level Densities in Intermediate and Heavy Nuclei,” *Australian Journal of Physics* **20** (1967) 477–487.
- [108] W. A. Friedman and W. G. Lynch, “Statistical Formalism for Particle Emission,” *Phys. Rev. C* **28** (1983) 16–23.
- [109] The Evaluated Nuclear Structure Data File (ENSDF) maintained by the National Nuclear Data Center (NNDC), Brookhaven National Laboratory, <http://www.nndc.bnl.gov/>.
- [110] S. G. Mashnik, K. K. Gudima, R. E. Prael, and A. J. Sierk, “Analysis of the GSI A+p and A+A Spallation, Fission, and Fragmentation Measurements with the LANL CEM2k and LAQGSM Codes,” in Proc. TRAMU@GSI, Darmstadt, Germany, 2003, Eds. A. Kelic and K.-H. Schmidt, ISBN 3-00-012276-1, <http://ww-wnt.gsi.de/tramu>; E-print: nucl-th/0404018.

- [111] A. H. Wapstra and K. Bos, “The 1977 Atomic Mass Evaluation: in Four Parts,” *Atomic Data and Nuclear Data Tables* **19** (1977) 175–297.
- [112] R. W. Peelle and P. M. Aebbersold, “Energy Parameters for the Light Nuclides in Monte Carlo Nuclear Evaporation Programs Based on EVAP,” ORNL-TM-1538, Oar Ridge National Laboratory, 1966.
- [113] K.-H. Schmidt, H. Delagrange, J. P. Dufour, N. Cârjan, and A. Fleury, “Influence of Shell Structure and Pairing Correlations on the Nuclear State Density,” *Z. Phys. A* **308** (1982) 215–225.
- [114] W. D. Myers and W. J. Swiatecki, “The Nuclear Droplet Model for Arbitrary Shapes,” *Ann. Phys.* **84** (1974) 186–210.
- [115] Stanley Cohen and Wladyslaw J. Swiatecki, “The Deformation Energy of a Charged Drop: Part V: Results of Electronic Computer Studies,” *Ann. Phys.* **22** (1962) 406–437.
- [116] A. Kelić, M. V. Ricciardi, and K.-H. Schmidt, “ABLA07 - Towards a Complete Description of the Decay Channels of a Nuclear System from Spontaneous Fission to Multifragmentation,” pp. 181–221 in: *Joint ICTP-IAEA Advanced Workshop on Model Codes for Spallation Reactions*, International Centre for Theoretical Physics Trieste, Italy, 4 – 8 February 2008, prepared by D. Filges, S. Leray, Y. Yariv, A. Mengoni, A. Stanculescu, and G. Mank, IAEA Nuclear Data Section, Wagramer Strasse 5, A-1400 Vienna, Austria, INDC(NDS)-0530, August 2008; arXiv:0906.4193.
- [117] Franz X. Gallmeier, “Implementation of the CEM-Code into the MCNPX-Code,” Proc. Forth Int. Workshop on Simulating Accelerator Radiation Environments (SARE-4), Knoxville, TN, September 13-16, 1998, ORNL, 1999, edited by Tony A. Gabriel, pp. 131-139.
- [118] R. J. Howerton, “ENSL82 and CDRL82: the 1982 Version of Evaluated Nuclear Structure Libraries ENSL and CDRL,” Reports UCRL-50400-Vol.23 and UCRL-50400-Vol.23-Add, Lawrence Livermore National Laboratory, CA, USA, 1983.
- [119] V. F. Weisskopf, “Radiative Transition Probability in Nuclei,” *Phys. Rev.* **83** (1951) 1073–1073.
- [120] J. M. Blatt and V. F. Weisskopf, *Theoretical Nuclear Physics*, John Wiley, New York, 1952.
- [121] E. S. Troubetzkoy, “Statistical Theory of Gamma-Ray Spectra Following Nuclear Reactions,” *Phys. Rev.* **122** (1961) 212–217.
- [122] F. Atchison, “A Treatment of Fission for HETC,” pp. 199–218 in *Intermediate Energy Nuclear Data: Models and Codes*, Proc. of a Specialists’s Meeting, May 30–June 1, 1994, Issy-Les-Moulineaux, France, OECD, Paris, France (1994).
- [123] R. Vandenbosch and J. R. Huizenga, *Nuclear Fission*, Academic Press, New York, 1973.
- [124] E. F. Neuzil and A. W. Fairhall, “Fission Product Yields in Helium Ion-Induced Fission of Au¹⁹⁷, Pb²⁰⁴, and Pb²⁰⁶ Targets,” *Phys. Rev.* **129** (1963) 2705–2710.

- [125] A. Ya. Rusanov, M. G. Itkis, and V. N. Okolovich, “Features of Mass Distributions of Hot Rotating Nuclei,” *Yad. Fiz.* **60** (1997) 773–803 [*Phys. At. Nucl.* **60** (1997) 683–712]; M. G. Itkis, Yu. A. Muzychka, Yu. Ts. Oganessian, V. N. Okolovich, V. V. Pashkevich, A. Ya. Rusanov, V. S. Salamatin, G. N. Smirenkin, and G. G. Chubaryan, “Fission of Excited Nuclei with $Z^2/A = 20\text{--}33$: Mass-Energy Distributions of Fragments, Angular Momentum, and Liquid-Drop Model,” *Yad. Fiz.* **58** (1995) 2140–2165 [*Phys. At. Nucl.* **58** (1995) 2026–2051].
- [126] W. D. Myers and W. J. Swiatecki, “Thomas-Fermi Fission Barriers,” *Phys. Rev. C* **60** (1999) 014606.
- [127] M. G. Itkis, S. M. Luk’yanov, V. N. Okolovich, Yu. E. Penionzhkevich, A. Ya. Rusanov, V. S. Salamatin, G. N. Smirenkin, and G. G. Chubaryan, “Experimental Study of the Mass and Energy Distributions of Fragments from Fission,” *Ya. Fiz.* **52** (1990) 23–35 [*Sov. J. Nucl. Phys.* **52** (1990) 15–22].
- [128] F. Atchison, “A Revised Computational Model for Fission,” Paul Scherrer Insitutut Report No. 98-12, Villigen PSI, Switzerland, 1998.
- [129] M. Baznat, K. Gudima, and S. Mashnik, “Proton-Induced Fission Cross Section Calculation with the LANL Codes CEM2k+GEM2 and LAQGSM+GEM2,” LANL Report LA-UR-03-3750, Los Alamos, 2003; Proc. AccApp03, San Diego, California, June 1–5, 2003, (ANS, La Grange Park, IL 60526, USA, 2004), pp. 976–985; E-print: nucl-th/0307014.
- [130] S. G. Mashnik, A. J. Sierk, and K. K. Gudima, “Complex Particle and Light Fragment Emission in the Cascade-Exciton Model of Nuclear Reactions,” LANL Report LA-UR-02-5185, Los Alamos, 2002; E-print: nucl-th/0208048.
- [131] A. V. Prokofiev, “Compilation and Systematics of Proton-Induced Fission Cross-Section Data,” *Nucl. Instr. Meth. A* **463** (2001) 557–575; A. V. Prokofiev, S. G. Mashnik, and W. B. Wilson, “Systematics of Proton-Induced Fission Cross Sections for Intermediate Energy Applications,” LANL Report LA-UR-02-5837, Los Alamos, 2002; E-print: nucl-th/0210071.
- [132] F. S. Alsmiller, R. G. Alsmiller, Jr., T. A. Gabriel, R. A. Lillie, and J. Barish, “A Phenomenological Model for Particle Production from the Collisions of Nucleons and Pions with Fissile Elements at Medium Energies,” ORNL/TM-7528, Oar Ridge National Laboratory, 1980; *Nucl. Sci. Eng.* **79** (1981) 147-161.
- [133] F. Atchison, “A Treatment of Medium-Energy Particle Induced Fission for Spallation-Systems’ Calculations,” *Nucl. Instrum. Methods B* **259** (2007) 909–932.
- [134] P. Fong, *Statistical Theory of Nuclear Fission*, Gordon and Beach Publishers, New York, 1969.
- [135] D. H. Epperson, “Systematics of Mass Yield Distributions for Nuclear Fission of Neptunium,” Dissertation, Dep. of Physics, Duke University, 1978.
- [136] R. L. Hahn and H. W. Bertini, “Calculations of Spallation-Fission Competition in the Reactions of Protons with Heavy Elements at Energies ≤ 3 GeV,” *Phys. Rev. C* **6** (1972) 660–669.

- [137] Torbjorn Sikkeland, Albert Ghiorso, and Matti J. Nurmi, “Analysis of Excitation Functions in Cm(C,xn)No Reactions,” *Phys. Rev.* **172** (1972) 1232–1238.
- [138] K.J. Le Couteur and D.W. Lang, “Neutron Evaporation and Level Densities in Excited Nuclei,” *Nucl. Phys.* **13** (1959) 32–52.
- [139] T. W. Armutrongt and D. Filges, “A Comparison of High-Energy Fission Models for the HETC Transport Code – Part I: Thin Target,” pp. 281–298 in: *Proc. of the 5th Meeting of International Collaboration on Advanced Neutron Sources (ICANS-V)*, Jülich, Germany, June 22-26, 1981, Jül-Conf-45, edited by G. S. Bauer and D. Filges, 1981.
- [140] A. V. Ignatyuk, G. A. Kudyaev, A. Junghans, M. de Jong, H.-G. Clerc, and K.-H. Schmidt, “Analysis of Dissipative Effects in Nuclear Fission Observed in the Fragmentation of ^{238}U Projectiles,” *Nucl. Phys.* **A593** (1995) 519–534.
- [141] J. Benlliure, A. Grewe, M. de Jong, K.-H. Schmidt, and S. Zhdanov, “Calculated Nuclide Production Yields in Relativistic Collisions of Fissile Nuclei,” *Nucl. Phys.* **A628** (1998) 458–478.
- [142] Arnold J. Sierk, “Macroscopic Model of Rotating Nuclei,” *Phys. Rev. C* **33** 2039–2053.
- [143] L. Moretto, “Fission Probabilities in Lighter Nuclei: A Theoretical and Experimental Investigation of the Shell and Pairing Effects in Fissioning Nuclei,” *Proc. Third IAEA Symp. on the Physics and Chemistry of Fission*, Rochester, NY, 13–17 August 1973, vol. 1, (IAEA, Vienna, 1974), pp. 329–365 (IAEA-SM-174/204).
- [144] H. A. Kramers, “Brownian Motion in a Field of Force and the Diffusion Model of Chemical Reactions,” *Physica* **7** (1940) 284–360.
- [145] S. I. Mulgin, K.-H. Schmidt, A. Grewe, and S. V. Zhdanov, “Shell Effects in the Symmetric-Modal Fission of Pre-Actinide Nuclei,” *Nucl. Phys.* **A640** (1998) 375–388.
- [146] K. Kruglov, A. Andreyev, B. Bruyneel, S. Dean, S. Franchoo, M. Górska, K. Helariutta, M. Huyse, Yu. Kudryavtsev, W. F. Mueller, N. V. S. V. Prasad, R. Raabe, K.-H. Schmidt, P. Van Duppen, J. Van Roosbroeck, K. Van de Vel, and L. Weissman, “Yields of Neutron-Rich Isotopes Around $Z = 28$ Produced in 30 MeV Proton-Induced Fission of ^{238}U ,” *Eur. Phys. J.* **A14** (2002) 365–370.
- [147] A. V. Ignatyuk, K. K. Istekov, and G. N. Smirenkin, “The Role of Collective Effects in the Systematics of Nuclear Level Densities,” *Yad. Fiz.* **29** (1979) 875–883 [*Sov. J. Nucl. Phys.* **29** (1979) 450–454].
- [148] K.-H. Schmidt, H. Delagrange, J. P. Dufour, N. Cârjan, and A. Fleury, “Influence of Shell Structure and Pairing Correlations on the Nuclear State Density,” *Z. Phys.* **A308** (1982) 215–225.
- [149] A. P. Zdanov and P. I. Fedotov, “Decay of Residual Nuclei Produced in the Interaction of 660-MeV Protons with Carbon Nuclei,” *Zh. Eksperim. i Teor. Fiz.* **45** (1963) 455–459 (in Russian) [*Soviet Phys. JETP* **18** (1964) 313–315].
- [150] E. Gradsztajn, F. Yiou, R. Klapisch, and R. Bernas, “Intranuclear Cascade and Fermi-Model Breakup Calculations on the Production of Li, Be, and B Isotopes in C^{12} by 156-MeV Protons,” *Phys. Rev. Lett.* **14** (1965) 436–439.

- [151] N. Amelin, *Physics and Algorithms of the Hadronic Monte-Carlo Event Generators. Notes for a Developer*, CERN/IT/ASD Report CERN/IT/99/6, Geneva, Switzerland and JINR LHE, Dubna, Russia; http://wwwinfo.cern.ch/asd/geant/geant4_public/G4UsersDocuments/Overview/html/index.html/.
- [152] G. I. Kopylov, *Principles of Resonance Kinematics*, Moscow, Nauka, 1970 [in Russian].
- [153] S. G. Mashnik, R. E. Prael, and K. K. Gudima, “Implementation of CEM03.01 into MCNP6 and its Verification and Validation Running through MCNP6. CEM03.02 Upgrade,” LANL Report LA-UR-06-8652, Los Alamos, 2007.
- [154] D. J. Brenner, R. E. Prael, J. F. Dicello, and M. Zaider, “Improved Calculations of Energy Deposition from Fast Neutrons,” Proc. 4th Symposium on Neutron Dosimetry, June 1981, Neuhererg/Munich, Germany, LANL Report LA-UR-81-1694, Los Alamos, 1981.
- [155] D. J. Brenner and R. E. Prael, “Non-Elastic Cross Sections for Neutron Interactions with Carbon and Oxygen Above 14 MeV,” Proc. IAEA Advisory Group Meeting on Nuclear and Atomic Data for Radiotherapy and Radiobiology (IAEA Panel Proceedings SerieS), Sept. 16–20, Radiobiological Institute, T. N. O. Rijswijk, The Netherlands, LANL Report LA-UR-85-4056, Los Alamos, 1985.
- [156] T. S. Subramanian, J. L. Romero, F. P. Brady, J. W. Watson, D. H. Fitzgerald, R. Garrett, G. A. Needham, J. L. Ullmann, C. I. Zanelli, D. J. Brenner, and R. E. Prael, “Double Differential Inclusive Hydrogen and Helium Spectra from Neutron-Induced Reactions on Carbon at 27.4, 39.7, and 60.7 MeV,” *Phys. Rev. C* **28** (1983) 521–528.
- [157] T. S. Subramanian, J. L. Romero, F. P. Brady, D. H. Fitzgerald, R. Garrett, G. A. Needham, J. L. Ullmann, J. W. Watson, C. I. Zanelli, D. J. Brenner, and R. E. Prael, “Double-Differential Inclusive Hydrogen and Helium Spectra from Neutron-Induced Reactions at 27.4, 39.7, and 60.7 MeV: Oxygen and Nitrogen,” *Phys. Rev. C* **34** (1986) 1580–1587.
- [158] R. E. Prael, “Approximations for Coulomb Barrier Transmission Probability in HETC and Related Codes,” LANL Report LA-UR-88-3141, Los Alamos, 1988.
- [159] D. J. Brenner and R. E. Prael, “Calculated Differential Secondary-Particle Production Cross Sections After Nonelastic Neutron Interactions with Carbon and Oxygen between 15 and 60 MeV,” *At. Data Nucl. Data Tables* **41** (1989) 71–130.
- [160] A. Boudard, J. Cugnon, S. Leray, and C Volant, “A New Model for Production of Fast Light Clusters in Spallation Reactions,” *Nucl. Phys.* **A740** (2004) 195–210.
- [161] Davide Mancusi, Alain Boudard, Joseph Cugnon, Jean-Christophe David, Pekka Kaitaniemi, and Sylvie Leray, “Extension of the Liège Intranuclear-Cascade Model to Reactions Induced by Light Nuclei,” *Phys. Rev. C* **90** (2014) 054602.

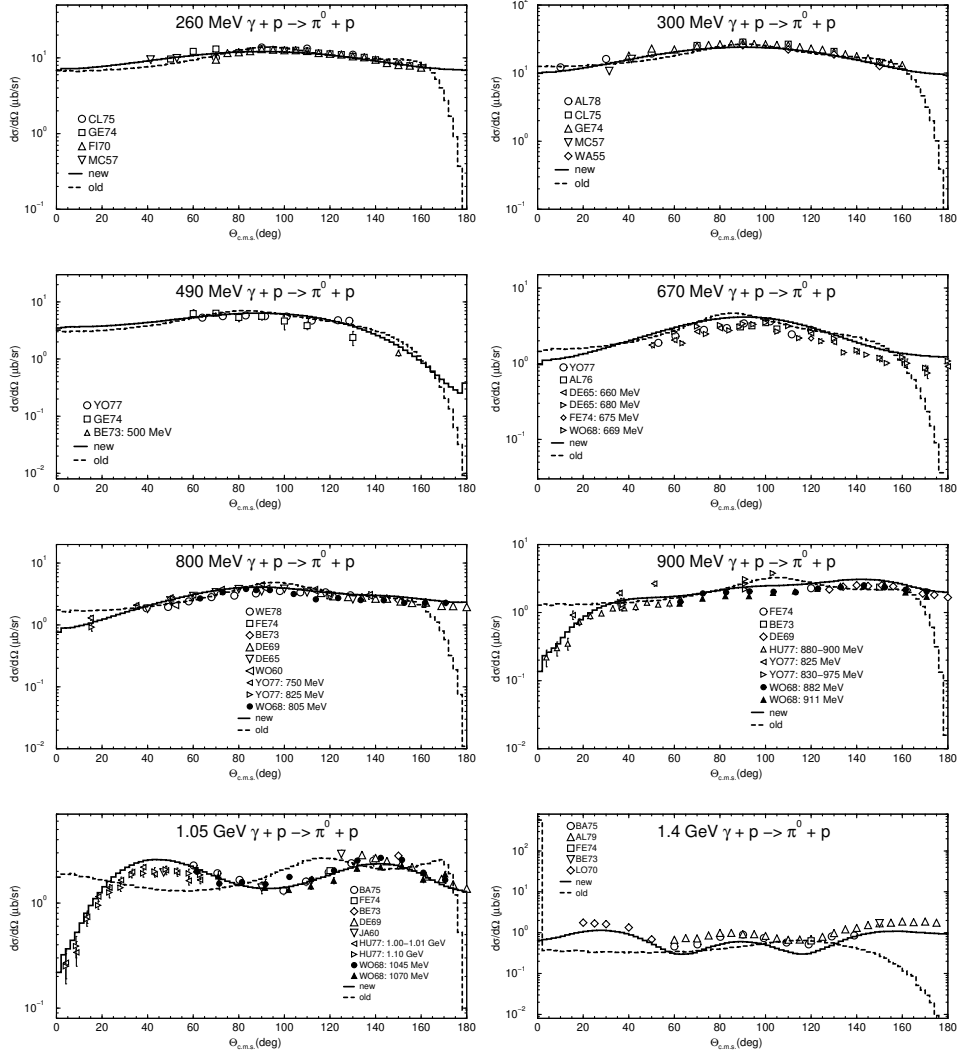


Figure 6: Example of eight angular distributions of π^0 from $\gamma p \rightarrow \pi^0 p$ as functions of $\Theta_{c.m.s.}^\pi$ at photon energies from 260 MeV to 1.4 GeV. The dashed lines show the old approximations of the Dubna INC [30] while the solid lines are the new approximations incorporated into LAQGSM03.03 (and into CEM03.03). References to experimental data shown by different symbols may be found in Ref. [29].

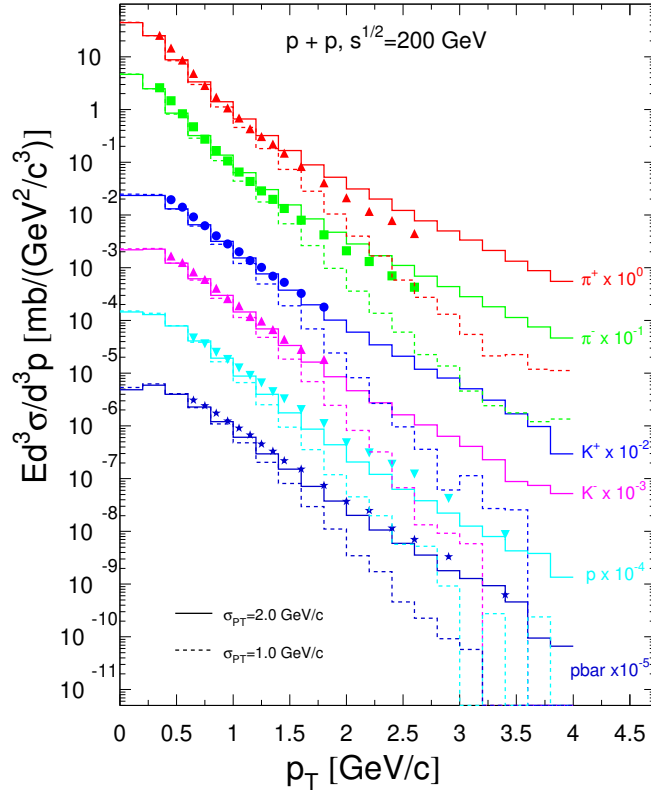


Figure 7: Mid-rapidity spectra of π^+ , π^- , K^+ , K^- , p , and \bar{p} produced in ultra-relativistic $p + p$ interactions at $\sqrt{s} = 200$ GeV ($T_p = 21314$ GeV) calculated with values of the parameter $\sigma_{\perp} = 2.0$ GeV/c (solid histograms) and $\sigma_{\perp} = 1.0$ GeV/c (dashed histograms) in the transverse momentum distribution of the constituent quarks of the QGSM compared with the recent RHIC data [46] (symbols).

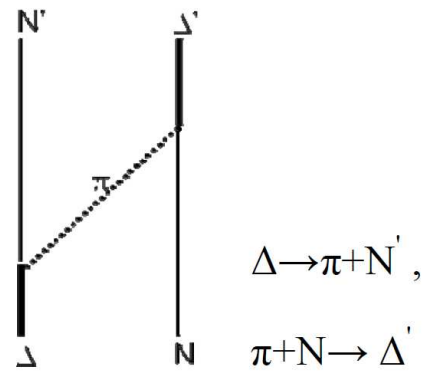


Figure 8: “ Δ ” charge exchange in ISABEL (adopted from Ref. [61].)

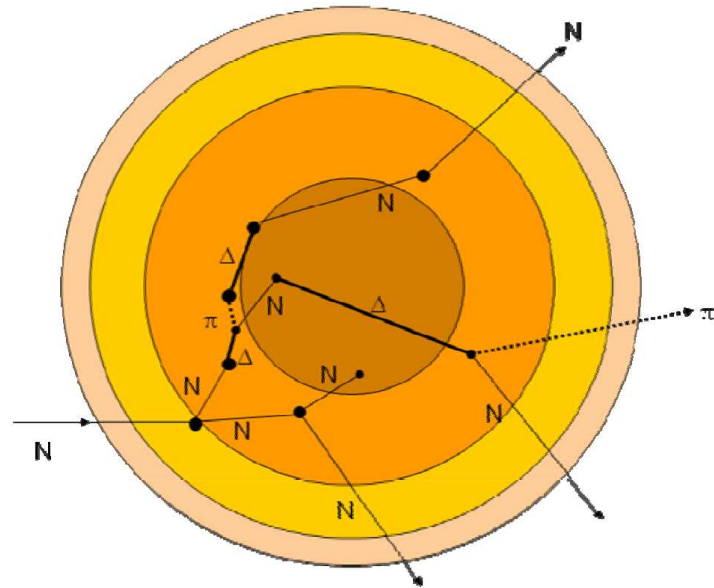


Figure 9: An example of ISABEL event (adopted from Ref. [61].)

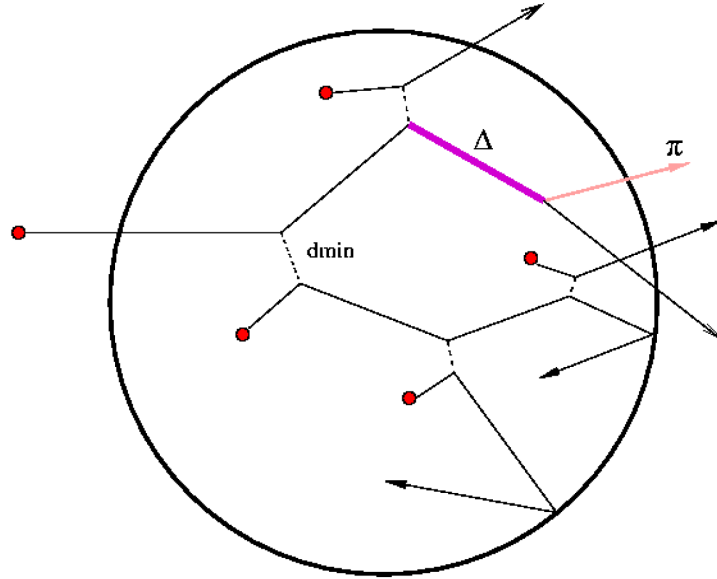


Figure 10: Schematic illustration of the main features of the INCL4.2 model (adopted from Ref. [70].)

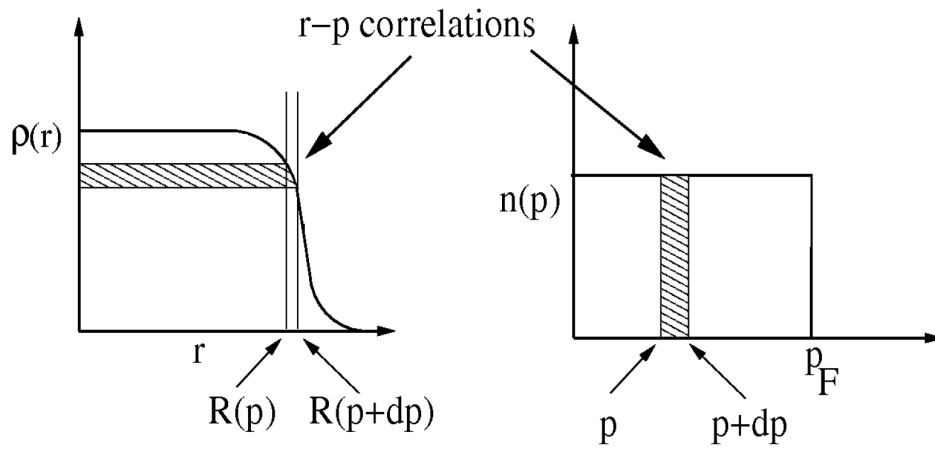


Figure 11: Illustration of the $r - p$ correlations introduced in the generation of the target initial state in INCL4.2 (adopted from Ref. [70].)

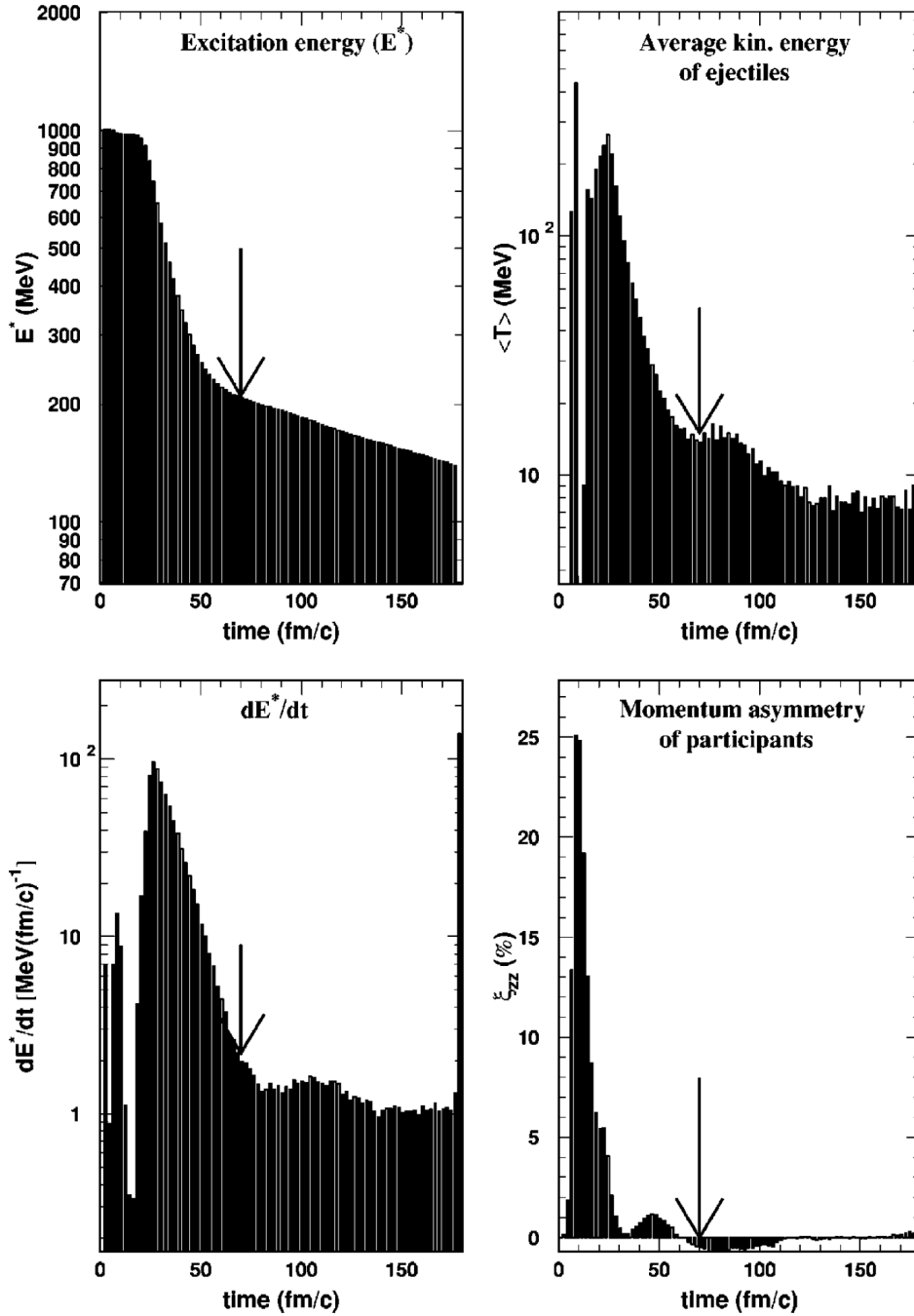


Figure 12: Time variation of the average value of a few physical quantities, within the INCL4.2 model. The panels refer, in a clockwise order, starting from the upper left, to the excitation energy, the average kinetic energy of the ejectiles, the asymmetry of the participant momentum distribution, and the time derivative of the excitation energy, respectively. The results correspond to collisions of 1-GeV protons with Pb nuclei with an impact parameter of 4 fm. The arrows indicate the chosen stopping time. (Adopted from Ref. [6].)

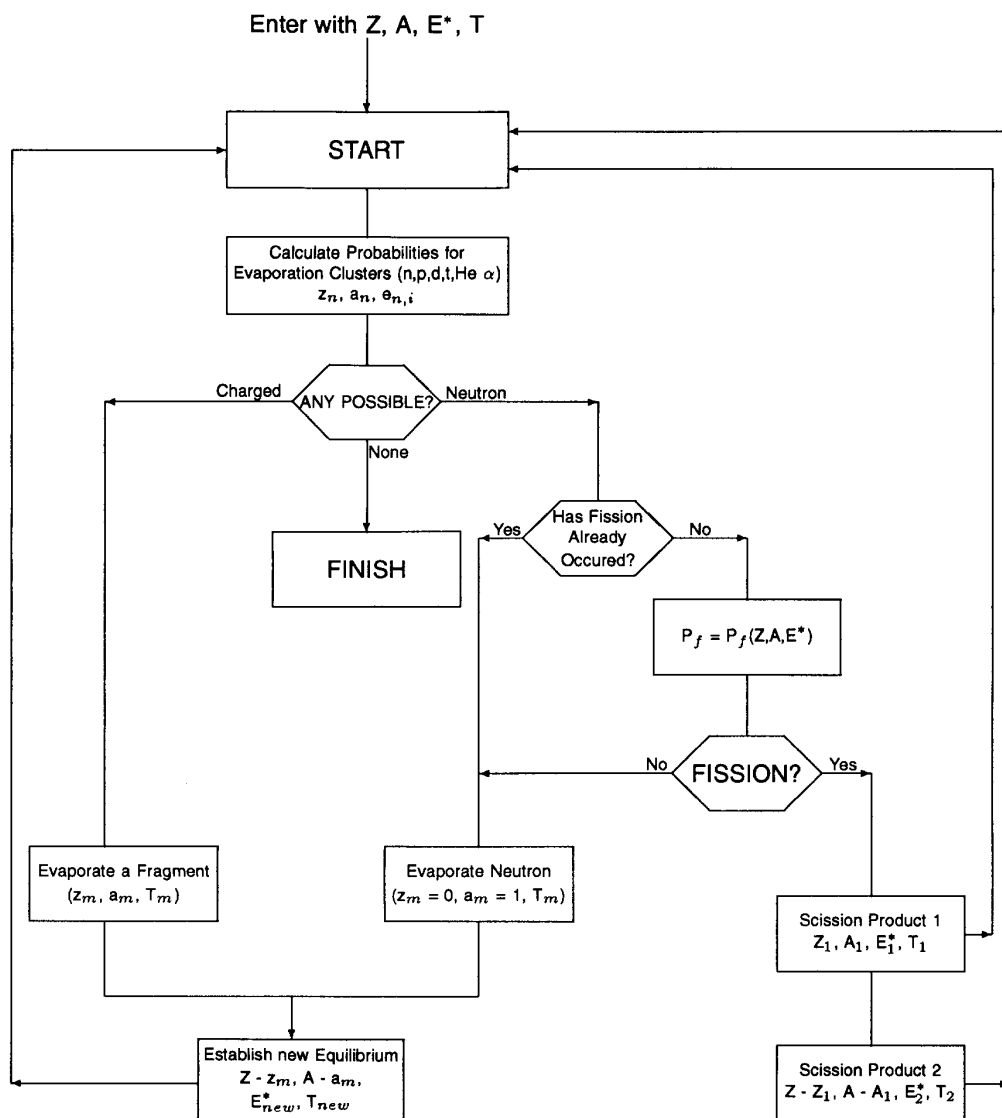


Figure 13: The logical flow for evaporation including fission in RAL. (Adopted from Ref. [122].)